Icarus 253 (2015) 66–98

Contents lists available at ScienceDirect

Icarus

journal homepage: www.elsevier.com/locate/icarus

Geological and hydrological histories of the Argyre province, Mars

J.M. Dohm [a,*], T.M. Hare [b], S.J. Robbins [c], J.-P. Williams [d], R.J. Soare [e], M.R. El-Maarry [f], S.J. Conway [g], D.L. Buczkowski [h], J.S. Kargel [i], M.E. Banks [j,k], A.G. Fairén [l,m], D. Schulze-Makuch [n], G. Komatsu [o], H. Miyamoto [a], R.C. Anderson [p], A.F. Davila [q], W.C. Mahaney [r], W. Fink [s], H.J. Cleaves [t,u], J. Yan [v], B. Hynek [w], S. Maruyama [t]

[a] The University Museum, The University of Tokyo, Hongo 7-3-1, Bunkyo-ku, Tokyo 113-0033, Japan
[b] U.S. Geological Survey, Flagstaff, AZ 86001, USA
[c] Southwest Research Institute, Boulder, CO 80302, USA
[d] Department of Earth, Planetary, and Space Sciences, University of California, Los Angeles, CA 90095, USA
[e] Department of Geography, Dawson College, 3040 Sherbrooke St. W., Montreal H3Z 1A4, Canada
[f] Physikalisches Institut, Bern Universität, Berne 3012, Switzerland
[g] Department of Physical Sciences, Open University, Milton Keynes MK7 6AA, UK
[h] Applied Physics Laboratory, Johns Hopkins University, Laurel, MD 20723, USA
[i] Department of Hydrology and Water Resources, University of Arizona, Tucson, AZ 85721, USA
[j] Smithsonian Institution, National Air and Space Museum, Center for Earth and Planetary Studies, Washington, DC 20013, USA
[k] Planetary Science Institute, Tucson, AZ 85719, USA
[l] Department of Planetology and Habitability, Centro de Astrobiología, Madrid 28850, Spain
[m] Department of Astronomy, Cornell University, Ithaca, NY 14853, USA
[n] Center of Astronomy and Astrophysics, Technical University Berlin, 10623 Berlin, Germany
[o] International Research School of Planetary Sciences, Università d'Annunzio, 65421 Pescara, Italy
[p] Jet Propulsion Laboratory, California Inst. of Technology, Pasadena, CA 91109, USA
[q] SETI Institute, Mountain View, CA 94043, USA
[r] Quaternary Surveys, 26 Thornhill Ave., Thornhill, ON L4J 1J4, Canada
[s] College of Engineering, Department of Electrical and Computer Engineering, University of Arizona, Tucson, AZ 85721, USA
[t] Earth-Life Science Institute, Tokyo Institute of Technology, Meguro, Tokyo 152-8551, Japan
[u] The Institute for Advanced Study, Princeton, NJ 08540, USA
[v] RISE Project Office, National Astronomical Observatory of Japan, Oshu 0230861, Japan
[w] Laboratory for Atmospheric and Space Physics and Geological Sciences, University of Colorado, CO 80309, USA

ARTICLE INFO

Article history:
Received 29 September 2014
Revised 31 January 2015
Accepted 16 February 2015
Available online 21 February 2015

Keywords:
Mars
Geological processes
Astrobiology
Tectonics

ABSTRACT

The geologic history of the multi-ringed Argyre impact basin and surroundings has been reconstructed on the basis of geologic mapping and relative-age dating of rock materials and structures. The impact formed a primary basin, rim materials, and a complex basement structural fabric including faults and valleys that are radial and concentric about the primary basin, as well as structurally-controlled local basins. Since its formation, the basin has been a regional catchment for volatiles and sedimentary materials as well as a dominant influence on the flow of surface ice, debris flows, and groundwater through and over its basement structures. The basin is interpreted to have been occupied by lakes, including a possible Mediterranean-sized sea that formed in the aftermath of the Argyre impact event. The hypothesized lakes froze and diminished through time, though liquid water may have remained beneath the ice cover and sedimentation may have continued for some time. At its deepest, the main Argyre lake may have taken more than a hundred thousand years to freeze to the bottom even absent any heat source besides the Sun, but with impact-induced hydrothermal heat, geothermal heat flow due to long-lived radioactivities in early martian history, and concentration of solutes in sub-ice brine, liquid water may have persisted beneath thick ice for many millions of years. Existence of an ice-covered sea perhaps was long enough for life to originate and evolve with gradually colder and more hypersaline conditions. The Argyre rock materials, diverse in origin and emplacement mechanisms, have been modified by impact, magmatic, eolian, fluvial, lacustrine, glacial, periglacial, alluvial, colluvial, and tectonic processes.

Post-impact adjustment of part of the impact-generated basement structural fabric such as concentric faults is apparent. Distinct basin-stratigraphic units are interpreted to be linked to large-scale geologic

* Corresponding author.
E-mail address: jmd@um.u-tokyo.ac.jp (J.M. Dohm).

http://dx.doi.org/10.1016/j.icarus.2015.02.017

activity far from the basin, including growth of the Tharsis magmatic–tectonic complex and the growth into southern middle latitudes of south polar ice sheets. Along with the migration of surface and sub-surface volatiles towards the central part of the primary basin, the substantial difference in elevation with respect to the surrounding highlands and Tharsis and the Thaumasia highlands result in the trapping of atmospheric volatiles within the basin in the form of fog and regional or local precipitation, even today. In addition, the impact event caused long-term (millions of years) hydrothermal activity, as well as deep-seated basement structures that have tapped the internal heat of Mars, as conduits, for far greater time, possibly even today. This possibility is raised by the observation of putative open-system pingos and nearby gullies that occur in linear depressions with accompanying systems of faults and fractures. Long-term water and heat energy enrichment, complemented by the interaction of the nutrient-enriched primordial crustal and mantle materials favorable to life excavated to the surface and near-surface environs through the Argyre impact event, has not only resulted in distinct geomorphology, but also makes the Argyre basin a potential site of exceptional astrobiological significance.

1. Introduction

A detailed reconstruction of the geologic history of the Argyre impact basin and surroundings (30–65°S, 290–340.0°E; Figs. 1 and 2), referred to hereafter as the Argyre province, is presented through a preliminary United States Geological Survey (USGS) map based on stratigraphic, structural, and geomorphic mapping using Viking Orbiter, Mars Global Surveyor (MGS), Mars Odyssey (ODY), and Mars Reconnaissance Orbiter (MRO) data (Fig. 3). The Argyre province includes the primary impact basin, basin floor and rim materials, the transition zone (region between the Thaumasia highlands mountain range and the Argyre basin and rim materials), and the southeastern margin of the Thaumasia plateau (Figs. 1 and 2). The large impact event resulted in the construction of the primary Argyre basin and the uplift of a mountainous rim. It also produced deep-seated and shallow basement structures such as radial structurally-controlled valleys and concentric ring scarps, as well as local (i.e., secondary) basins occurring among the rim materials and away from the primary basin and rim materials; impact-related deformation occurred as much as 2000 km away from the impact site (Dohm et al., 2001a) (Fig. 2).

Since the formation of the impact basin, erosional and depositional processes have substantially modified the Argyre basin and rim materials, including the emplacement of five major and distinct basin-stratigraphic units (units NAb1, NAb2, NAb3, ANb4b, HAb4a, which are detailed in Section 3.1 and in Fig. 3 and Tables 1–3). As shown below, the Argye impact event has been a significant influence on the geologic and hydrologic history of the region

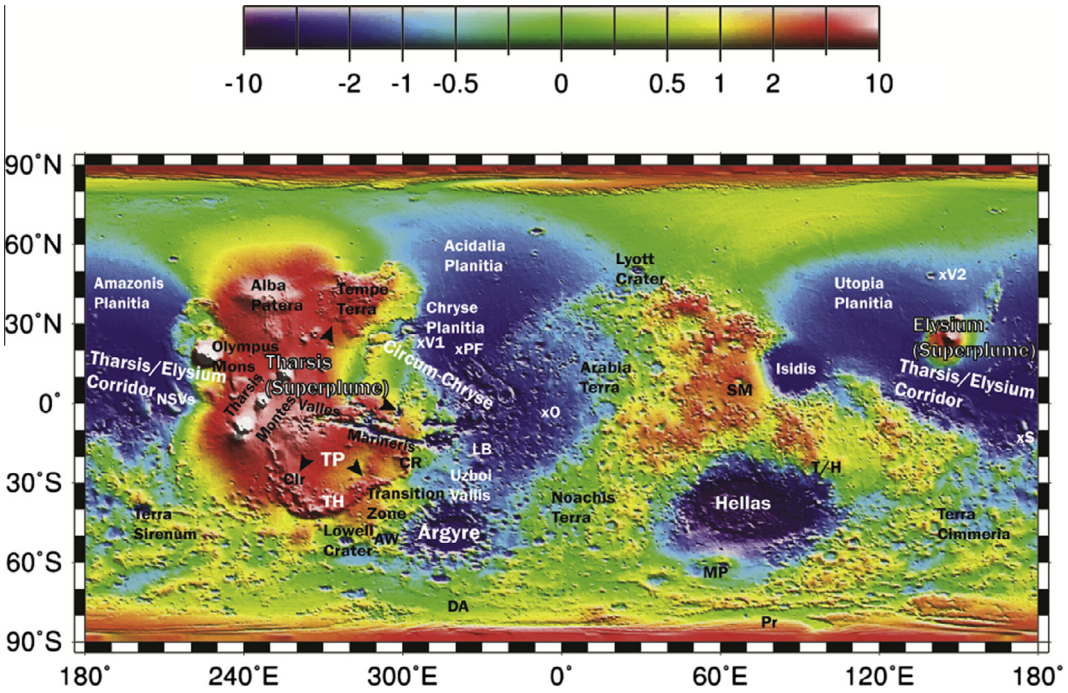

Fig. 1. Mars Orbiter Laser Altimeter Map showing the planet shape with the zonal spherical harmonic degree 1 removed (Smith et al., 1999) and nomenclature and general locations of features of interest, including Argyre basin, Tharsis and Elysium, both interpreted here as superplumes, Uzboi Vallis, the Argyre western-margin-paleolake basin (AW), Thaumasia plateau (TP), Thaumasia highlands mountain range (TH), Coprates rise mountain range (CR), Claritas Rise (Clr), Prometheus crater (Pr), Dorsa Argentea (DA), Ladon basin (LB), the northwestern slope valleys (NSVs), the ancient Europe-size drainage basin which may have contributed floodwaters to the circum-Chryse outflow channel system (black arrowheads pointing to the northern, eastern, southern, and western margins), Malea Planum volcanic province (MP), Tyrrhenus/Hadriacus volcanic province (T/H), Syrtis Major volcanic province (SM), Pathfinder landing site (xPF), Viking 1 landing site (xV1), Viking 2 landing site (xV2), Spirit landing site (xS), and Opportunity landing site (xO). Note that this geologic investigation points to the dark blue patches in the Argyre province (see Fig. 2 for outline of province), representative of relatively low topography, being inundated by water directly following the Argyre impact event (please also compare with Fig. 9). Also note the southeastern margin of the Thaumasia plateau paralleling the multi-ring structure of the Agyre impact, and as such, one of the many pieces of evidence of the influence that Tharsis and Argyre had on one another (also see Fig. 2). (For interpretation of the references to color in this figure legend, the reader is referred to the web version of this article.)

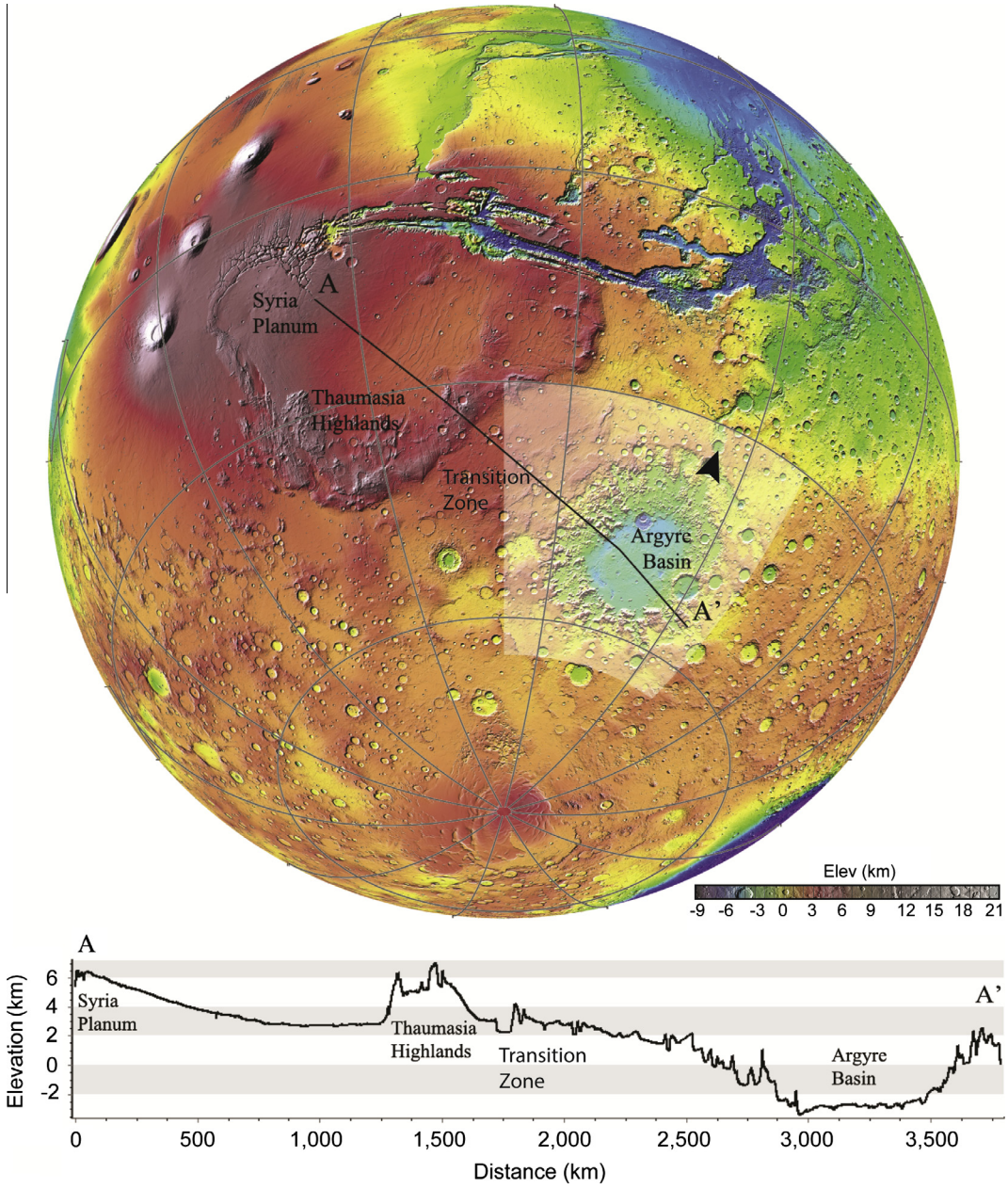

Fig. 2. MOLA map (top) with transect line of corresponding topographic profile (bottom) through Syria Planum (i.e., a shield complex and one of the major components of Tharsis), Thaumasia highlands (i.e., mountain range with a length nearing 2400 km, or approximating that of the Himalayas), transition zone, and the Argyre basin. The Argyre province is also highlighted at top (transparent box). Also shown is the possible headwaters of Uzboi Vallis (arrow). Note the rugged topography in the Argyre province resulting from the giant impact event including mountainous rim materials and structurally-controlled basins, including the deep primary basin. Both Tharsis and Argyre had a major influence on one another. For example, Tharsis magmatic-driven hydrological cycling included floods and associated inundations in the northern plains and associated precipitation in and surrounding the Argyre basin to form lakes and grow glaciers, as well as groundwater activity along Argyre impact-induced basement structures, which includes the possible migration at great distances (e.g., thousands of kilometers from Tharsis through the ancient Thaumasia highlands mountain range and eventually into the deep Argyre basin). Other diverse climatic and hydrologic phenomena may include fog in the Argyre basin and local precipitation due to the regional topographic variation. Yin (2012a) proposed an oblique impact event to help explain the distinct topography to the northwest of the Argyre basin, and the development of Tharsis, while other hypotheses for the origin of Tharsis include focused subduction of hydrated crustal materials through an ancient phase of plate tectonism (Baker et al., 2007).

from when the basin formed until now. Unraveling the history of the Argyre province is important to understanding the overall influence of the Argyre impact event on the regional and local geology and hydrology. Being one of the largest impact basins on Mars, it also offers a unique opportunity to peer deep into the crust and upper mantle and to discern hydrological processes and depositional surface environments across a span of billions of years.

Previous geologic mapping investigations of all or parts of the Argyre province, which involved data from the Mariner and Viking missions, resulted in: (1) maps of Coprates (McCauley, 1978), Magaritifer Sinus (Saunders, 1979), Argyre (Hodges, 1980), Thaumasia (McGill, 1978), and Mare Australe (Condit, 1978) quadrangles at 1:5,000,000-scale based mainly on Mariner 9 images; (2) the global map of Mars at 1:25,000,000 scale (Scott and Carr, 1978) compiled largely from the 1:5,000,000-scale geologic maps; (3) maps of the western equatorial and south polar regions of Mars at 1:15,000,000-scale based on Viking images (Scott et al., 1986–1987); and (4) the Viking-based map of the Thaumasia region at 1:5,000,000 scale, which covers the extreme northwestern part of the Argyre basin (Dohm et al., 2001a).

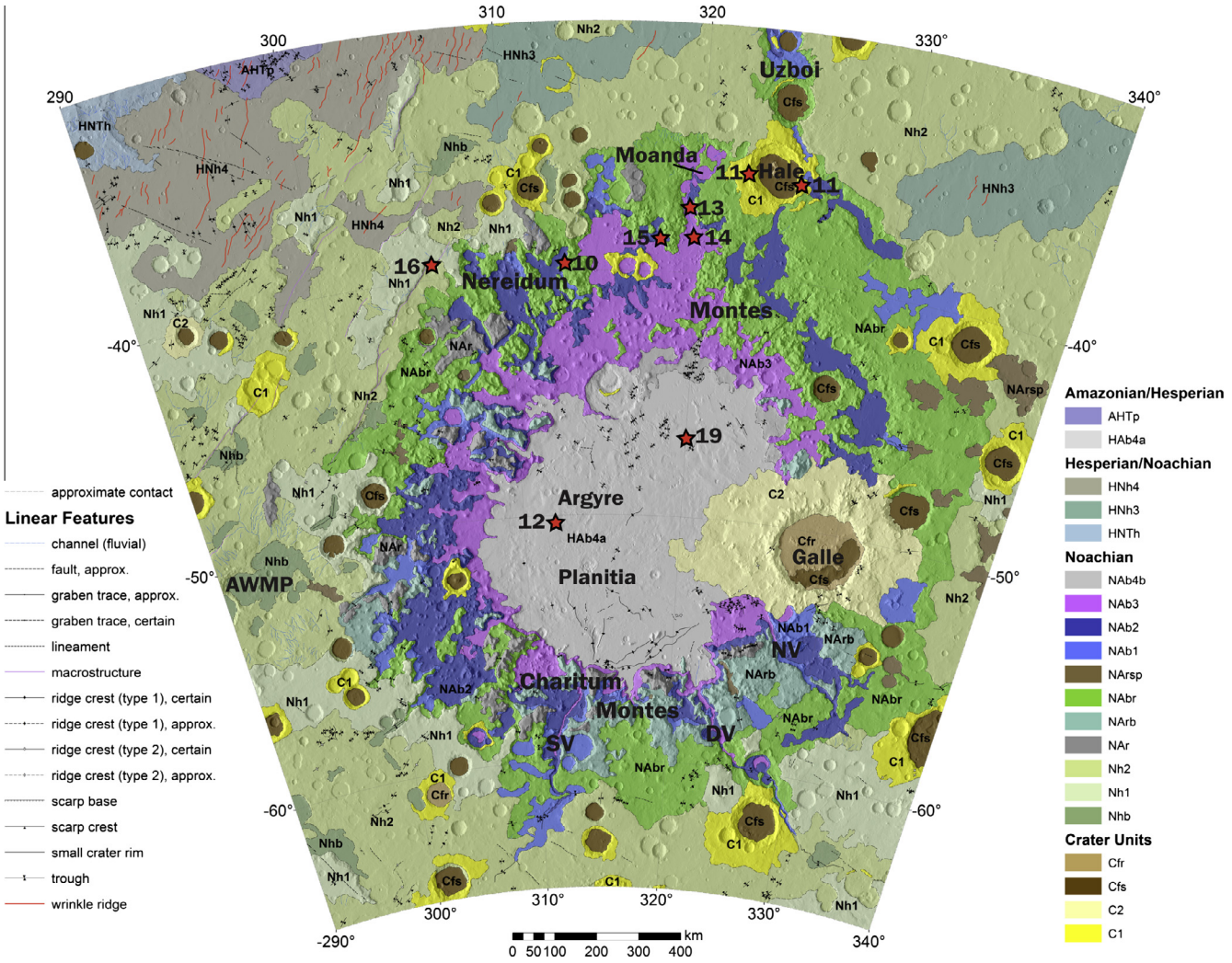

Fig. 3. Geologic map of the Argyre and surrounding region of Mars showing stratigraphy and structure (Dohm et al., USGS map in preparation). Map units are detailed in Tables 1–3. Also highlighted are the major valley systems, Uzboi Vallis (Uzboi), Surius Vallis (SV), Dzigai Vallis (DV), and Nia Vallis (NV), the Argyre western-margin-paleolake basin (AWMP), and locations of Figs. 10–16 and 19.

Study of the hydrogeologic evolution of the Argyre province through Viking Orbiter data (images at resolutions ranging from ~50 to 150 m/pixel) indicated that post-impact basin development has been heavily influenced by lacustrine, fluvial, and glacial processes (Parker, 1985, 1989, 1994; Parker and Gorsline, 1991, 1992, 1993; Kargel and Strom, 1992; Parker et al., 2000; Dohm et al., 2001a; Kargel, 2004). These investigations revealed evidence of a broad integration of hydrogeologic activity within the basin extending to headwaters in the highlands south and east of the basin. In particular, the multiple Parker et al. (Parker, 1985, 1989, 1994; Parker and Gorsline, 1991, 1992, 1993; Parker et al., 2000) found evidence for deep water ponding in the basin and water drainage northward both into Argyre from the south and from Argyre through Uzboi Vallis into the northern plains; this included basin filling to a spillpoint (refer to Figs. 1–3 for locations of highlighted features of interest). In addition, Kargel and Strom (1992) detailed a role of wet-based alpine and continental scale glaciation in southern Argyre and adjoining highlands, with the glacial system extending as far as the south polar region and eastward halfway to Hellas. Baker et al. (1991) suggested a latitude limit of south polar glaciation having been roughly halfway through the Argyre basin, making the southern part glaciated and the northern part unglaciated.

Subsequent to these Mariner- and Viking-era mapping investigations, using image data at what is now considered low resolutions, there has not been a new, detailed geologic map produced of the Argyre province using more recently available higher resolution data (e.g. images acquired by the High Resolution Imaging Science Experiment (HiRISE), on MRO, with a scale as small as 0.25 m/pixel). Post-Viking-era topographic, geomorphologic, and spectroscopic investigations (e.g., Hiesinger and Head, 2002; Kargel, 2004; Buczkowski et al., 2008a,b, 2010; Banks et al., 2008, 2009; Jones et al., 2011) have provided helpful information for this investigation.

Here, we discuss the results of our systematic geologic mapping of the Argyre province (Figs. 1–3). This work will be portrayed in a USGS geologic map product at 1:5,000,000 scale in both digital and print formats (Dohm et al., USGS map, in preparation). Although earlier geologic maps include all or parts of the Argyre province, none focuses on understanding the geologic and hydrologic histories of the province using post-Viking-era data. Additionally, detailed studies that did make use of post-Viking-era data did not make use of a systematic map-based approach and did not encompass the breadth of landscapes mapped in this geologic mapping investigation. We present the stratigraphic, hydrologic, and tectonic histories of the Argyre province as reconstructed from our geologic mapping, with particular focus on: (1) whether the Argyre basin contained lakes; (2) the extent of flooding and glaciation; (3) the origin of the narrow ridges located in the southeastern

Table 1
Unit symbols, unit names, and unit areas (see corresponding geologic map shown in Fig. 3). Interpreted sedimentary deposits include aeolian, lacustrine, glacial, periglacial, fluvial, alluvial, and colluvial deposits. Magmatic includes both intrusive (exposed through differential erosion and impact excavation) and volcanic. The primary basin materials (members NAb1, NAb2, NAb3, NAb4b, HAb4a) occur at distinct elevation ranges (see Figs. 3, 5, and 6 and Sections 4.2 and 4.3.1). See Table 2 for description and interpretation and Table 3 for relative age information through comprehensive crater statistics. Not shown below are the older impact crater materials (unit C1), younger impact crater materials (unit C2), smooth impact crater materials (unit Cfs), and rough crater floor materials (unit Cfr). Note that the Argyre rim materials are diverse in stratigraphy, topography, and morphology, as thus separated into Argyre rim (unit NAr; mainly rim materials), Argyre rim and basin (Unit NArb; majority being rim materials with interspersed basin (including valley) deposits), Argyre basin and rim (unit NAbr; majority being basin infill deposits with intervening rim materials in the form of knobs and mesas), Argyre rim smooth plains (rim materials with large distinct patches of relatively smooth plains) materials.

Unit	Unit names	Area (km^2)	Brief interpretation (see Table 2 for greater details)
Nh1	Highlands member 1	327,794	Sedimentary; impact; magmatic
Nh2	Highlands member 2	1,096,085	Sedimentary; impact; magmatic
HNh3	Highlands member 3	168,887	Sedimentary; impact; magmatic
HNh4	Highlands member 4	262,637	Sedimentary; impact; magmatic
Nhb	Highland basin	67,049	Local basins infilled by sedimentary deposits
HNTh	Thaumasia highlands	28,531	Sedimentary; highly modified basement complex; magmatic; impact
AHTp	Thaumasia plateau	16,282	Magmatic (e.g., ignimbrites); sedimentary
NAr	Argyre rim	58,067	Mantle and lower crustal materials; basement complex; sedimentary; hydrothermal
NArb	Argyre rim and basin	109,274	Mantle and lower crustal materials; basement complex; sedimentary; hydrothermal
NAbr	Argyre basin and rim	577,012	Similar to unit Arb but more basin materials (sedimentary); hydrothermal
NArsp	Argyre rim smooth plains	38,939	Similar to Arb but plains-forming materials mostly sedimentary
NAb1	Argyre basin, member 1	100,203	Sedimentary deposits
NAb2	Argyre basin, member 2	209,887	Sedimentary deposits
NAb3	Argyre basin, member 3	208,086	Sedimentary deposits
HAb4a	Argyre basin, member 4a	341,499	Sedimentary deposits
NAb4b	Argyre basin, member 4b	18,541	Sedimentary deposits; basin marginal unit, which underlies unit Ab4a, is related to unit NAb3

part of the basin floor and how the ridges fit into the context of the geologic mapping results; (4) the extent of Argyre-related tectonism and its influence on the surrounding regions and conversely the role of tectonics in adjoining regions in affecting the Argyre basin and its deposits; and (5) possible very Late Amazonian modifications by periglacial (cold-climate and non-glacial) processes.

2. Geologic setting

The Argyre province (Figs. 1–3) is located in the southern cratered highlands, which occur across nearly half of Mars; the highlands comprise the majority of exposed ancient Noachian rocks (Scott et al., 1986–1987; Tanaka, 1986; Tanaka et al., 2014). The martian highlands also contain the Hellas basin and surroundings. Unlike the Argyre province, the latter has received significant attention and is mapped in great detail (e.g., Crown et al., 1992; Mest and Crown, 2001; Leonard and Tanaka, 2001; Moore and Wilhelms, 2007; Glamoclija et al., 2011).

The southern highlands display geologic terrains that involved high rates of geologic and hydrologic activity during the Noachian Period (e.g., Scott et al., 1986–1987; Tanaka, 1986; Tanaka et al., 1988, 2014; Dohm et al., 2001a, 2013; Hartmann and Neukum, 2001; Hynek et al., 2010). Dynamic activity, including mountain building, formation of structurally-controlled basins, and possible plate tectonism (Sleep, 1994; Maruyama et al., 2001a; Dohm et al., 2001c, 2002a, 2005, 2013; Anguita et al., 2001; Fairén et al., 2002; Baker et al., 2002, 2007; Fairén and Dohm, 2004; Connerney et al., 2005; Yin, 2012a,b), is pronounced prior to the incipient development of the Tharsis rise, a long-lived (nearly 4.0 Ga) magmatic complex (Dohm et al., 2001b; Anderson et al., 2001), interpreted here to be a superplume (Maruyama et al., 2001b, 2008; Dohm et al., 2001d, 2007a; Baker et al., 2002, 2007). This pre-Tharsis activity is also prominent before the Argyre, Hellas, and Isidis impact events (Dohm et al., 2002a,b, 2005, 2013; Baker et al., 2002). This dynamic activity was followed by sporadic magmatic, tectonic, climatic, and hydrologic activity driven mainly by endogenic activity from the growth of Tharsis superplume until present-day (Dohm et al., 2007a; Baker et al., 2007) (Fig. 4), but also by the giant impact events such as Argyre, and to the development of the Elysium superplume (Baker et al., 2007). Other influences including changes in the spin axis magnitude and precession and orbital eccentricity of Mars (Touma and Wisdom, 1993; Laskar et al., 2004), steadily brightening solar luminosity (Kasting et al., 1993), and volatile releases from other large impacts (Segura et al., 2002) also have contributed to climate change and the geomorphology and surficial deposits of Mars (Head et al., 2003; Kargel, 2004).

Dominant in the geologic, hydrologic, and climatic histories of Mars since its incipient development, Tharsis superplume locates to the northwest of and adjacent to the Argyre basin. Based on topographic, stratigraphic, paleoerosional, and paleotectonic information, Tharsis is interpreted to have recorded five major stages of magmatic-driven activity (Fig. 4) (for details on the major stages of development of Tharsis, please refer to Dohm et al. (2001b, 2007a, 2009a) and Anderson et al. (2001), and for general stratigraphic information and time-chronologic information of Tharsis and the rest of Mars, the new global map of Mars by Tanaka et al. (2014)). The five major stages of development and a representative features of each stage (from oldest to youngest with some overlap largely due to uncertainty in the crater statistics) include: Stage 1 (Early to Middle Noachian)—Tharsis basin with subsequent uplift of the Thaumasia Plateau and incipient development of Syria Planum; Stage 2 (Late Noachian to Early Hesperian)—opening of Valles Marines cutting the northern part of the Thaumasia Plateau, as well as major development of Syria Planum; Stage 3 (Early Hesperian)—early development of the prominent volcanoes of Tharsis Montes and Alba Mons; Stage 4 (Late Hesperian to Early Amazonian)—major magmatic outgassing of Tharsis, including related major growth of the Alba Mons, Olympus Mons, the Tharsis Montes, and associated major incisement of the circum-Chryse outflow channel system that began to form as early as and associated with major Stage 2 Tharsis activity; and Stage 5—(Amazonian) all of the components of Tharsis forged by this time with concentrated magmatic-driven tectonic activity in parts into the Late Amazonian.

These five major thermal pulses of Tharsis activity, which includes magmatism and associated release of volatiles, major outflows, inundations of the northern plains to form oceans, and hydrological cycles, have manifested themselves at regional and possibly global scales at least since the Middle Noachian epoch

Table 2
Description and interpretation of map units. For cumulative crater densities and estimated unit ages of the geologic units in the Argyre and surrounding region of Mars, see Table 3.

Unit name	Unit label	Description	Interpretation
Argyre basin sequence stratigraphy (units HAb4a, NAb4b, NAb3, NAb2, NAb1)			
Argyre basin member 4a	HAb4a	Younger Argyre plains-forming basin floor deposits marked by sinuous ridges, knobs, broken terrain, topographic depressions of varying geometric shapes, buried/subdued impact craters, and dune fields. The younger floor materials are approximately or gradationally in contact with either unit HAb4b or unit NAb3 materials	The upper most part of the Argyre basin infill floor materials representative of environmental change induced by Stage 4 (Late Hesperian; for Tharsis-Stage information see Section 2 and Fig. 4) Tharsis magmatic-driven activity with lesser activities including Elysium. This includes ice melt, spring-fed activity, flooding, gelifluction, and lake and glacier formation along its margin, with subsequent resurfacing, including aeolian, fluvial, volatile-release, glacial, alluvial, impact cratering including secondaries, and/or colluvial, some processes of which are active today; the lower parts (those underlying unit HAb4a materials with associated impact craters exposed at the surface or not totally buried by unit HAb4a) of the infill deposits (extending at depth to the ancient Argyre basin floor) were emplaced by earlier perturbations in climate/environmental conditions from Tharsis and less prominent activities such as Elysium volcanism. The relative timing of these activities are indicated by stratigraphy and impact crater densities (Table 3). The rock materials source from diverse provenances, including the Argyre rim and ejecta deposits (upper mantle materials and older primordial crustal materials excavated to and near the martian surface by the impact event and associated overturn and inversion of stratigraphy; materials also include hydrothermal deposits) and beyond, even including materials transported from as far north as Tharsis and the Thaumasia highlands and from as far south as the south pole. Therefore, the rock materials are considered to be diverse in both geochemistry and the mineralogic record, representative of diverse environmental conditions. The sinuous ridges located in the southeast part of the basin floor are eskers, associated with the latter stage of lake formation (margins of the lake were freezing) and marginal glaciers were connected to the lake. The subglacial rivers followed topography
Argyre basin member 4b	NAb4b	Older Argyre plains-forming basin floor deposits marked by flows, erosional scarps, systems of sinuous valleys, and highly degraded and subdued impact craters, which partly form the contact separating these deposits from the younger plains-forming basin floor deposits. These materials are buried and/or embayed by unit HAb4a materials and gradational with generally higher-standing unit NAb3 materials	Argyre basin floor materials representing older basin infill materials emplaced largely by early Tharsis magmatic-driven activity (e.g., Stages 1–2), which includes unit NAb3 materials with subsequent resurfacing, including aeolian, fluvial, volatile-release, glacial, alluvial, impact cratering, which includes secondaries, and/or colluvial. The rock materials source from diverse provenances, including the Argyre rim and ejecta deposits (upper mantle materials and older primordial crustal materials excavated to and near the martian surface by the impact event and associated overturn and inversion of stratigraphy; materials also include hydrothermal deposits) and beyond, even including materials transported from as far north as Tharsis and the Thaumasia highlands and from as far south as the south pole. Therefore, the rock materials are considered to be diverse in both geochemistry and the mineralogic record, representative of diverse environmental conditions (e.g., assortment of varying pressure, temperature, and volatile conditions)
Argyre basin member 3	NAb3	Deposits that are gradationally in contact with the younger and older plains-forming basin floor deposits, which are marked by flows, networking channel systems such as highlighted in the southeast part of the basin at the juncture of the floor and rim-associated slope (e.g., troughs delineated on the geologic map near the terminus of Nia Vallis; Fig. 3) and Moanda impact crater in the northeast part (Fig. 3), aprons along the margins of promontories and other flow-feature types, degraded and partly buried impact craters, knobs and other quasi-circular promontories with marginal aprons, erosional scarps, and irregular depressions. In addition, deposits which occur on the lower-most valley segment extending from the margin of the basin floor inset within the Argyre-impact-induced radial valleys, with distinct breaks in slope (including terrace-like topography in places) at the contact between these deposits and the older deposits of unit NAb2 at higher elevations along the valley floor, particularly distinct along the floors of the three valleys that debouch into the southern and southeast parts of the Argyre basin, Surius Vallis and Dzigai and Nia Valles, respectively (Figs. 1, 3, and 6)	Hillslope-forming materials in contact with the basin floor materials related to changes in environmental conditions/climate, as well as gravity-driven processes of ice-enriched rock materials through time. Major surface modification related to Tharsis-driven activity (e.g., Stages 1–3), indicated by stratigraphy and impact crater densities (Table 3), which includes hydrologic activity (ice melt, flooding, gelifluction, and lake formation, as well as incisement of the radial valleys related to a changing hydraulic head linked to the changing hydrologic system of groundwater, surface lakes, and glaciers), with subsequent surface modification including Tharsis- (Stages 4–5) and obliquity-driven, aeolian, fluvial, volatile-release, glacial, alluvial, impact cratering, which includes secondaries, and/or colluvial, some processes of which are active today. Wind and water (liquid and ice) activity has modified the landscape. The rock materials source from diverse provenances, including the Argyre rim and ejecta deposits (upper mantle materials and older primordial crustal materials excavated to and near the martian surface by the Argyre impact event and associated overturn and inversion of stratigraphy; materials also include hydrothermal deposits) and beyond, even including materials transported from as far north as Tharsis and the Thaumasia highlands and from as far south as the south pole. Therefore, the rock materials are considered to be diverse in both geochemistry

(*continued on next page*)

Table 2 (*continued*)

Unit name	Unit label	Description	Interpretation
			and the mineralogic record, representative of diverse environmental conditions (e.g., assortment of varying pressure, temperature, and volatile conditions). Argyre-impact-induced basement structures are conduits for the internal heat release of Mars and associated groundwater migration resulting in local geologic and hydrologic activity, including linear gullies with systems of faults and fractures and open-system pingos (Soare et al., 2014b)
Argyre basin member 2	NAb2	Deposits are gradationally in contact with rock materials of units NAb3 and Nab1 and Argyre rim materials such as unit NArb materials. The unit is marked by flows, aprons along the margins of promontories and other flow feature types, degraded and partly buried impact craters, knobs and other quasi-circular promontories with marginal aprons (more prevalent than the younger unit NAb3), erosional scarps, and irregular depressions. In addition, the deposits include valley fill extending through the rim materials; they are topographically between unit NAb3 and unit NAb1, separated by gradational contacts of which often are breaks in slope such as terraces, exemplified in the three valleys that debouch into the southern and southeast parts of the Argyre basin, Surius Vallis and Dzigai and Nia Valles, respectively (Figs. 1, 3, and 6)	Hillslope-forming materials associated with changes in environmental conditions/climate, as well as gravity-driven processes such as colluvial activity of ice-enriched rock materials through time. Major surface modification related to Tharsis-driven activity (e.g., Stages 1–3), indicated by stratigraphy and impact crater densities (Table 3), which includes hydrologic activity (ice melt, flooding, gelifluction, and lake formation, as well as incisement of the radial valleys related to a changing hydraulic head linked to the changing hydrologic system of groundwater, surface lakes, and glaciers), with subsequent surface modification including obliquity-driven, aeolian, fluvial, volatile-release, glacial, alluvial, impact cratering which includes secondary impacts, and/or colluvial. Wind and water (liquid and ice) activity has modified the landscape. The crater retention age of unit NAb2 is less than unit Nab3 due to higher energy conditions and activity at higher reaches, including those associated with the incisement of the valleys radial about the basin such as Surius Vallis and Dzigai and Nia Valles. The rock materials source from diverse provenances, including the Argyre rim and ejecta deposits (upper mantle materials and older primordial crustal materials excavated to and near the martian surface by the Argyre impact event and associated overturn and inversion of stratigraphy; materials also include hydrothermal deposits) and beyond, even including materials transported from as far north as Tharsis and the Thaumasia highlands and from as far south as the south pole. Therefore, the rock materials are considered to be diverse in both geochemistry and the mineralogic record, representative of diverse environmental conditions (e.g., assortment of varying pressure, temperature, and volatile conditions)
Argyre basin member 1	NAb1	Deposits are gradationally in contact with unit NAb2. The unit is marked by flows, aprons along the margins of promontories and other flow feature types, degraded and partly buried impact craters, knobs and other quasi-circular promontories with marginal aprons (more prevalent than the younger member NAb3), erosional scarps, and irregular depressions. In addition, the deposits include valley fill extending through the rim materials and onto the surrounding highlands; they are the elevationally highest occurring fill deposits in the valleys that debouch into the Argyre basin. Prime examples of the stratigraphy are observed in Surius and Dzigai Valles, which are the two southern most valley systems that debouch into the Argyre basin (Figs. 1, 3, and 6)	High-standing basin-fill deposits which were emplaced directly following the Argyre impact event, including ice melt at regional and possibly global scale and related hydrologic conditions, which includes the Mediterranean-size lake that sourced Uzboi Valles. The Argyre-induced lake formed several million years subsequent to the termination of the dynamo and a reported ancient phase of plate tectonism (Baker et al., 2007), as well as a once interacting atmosphere, ocean, and landmass (e.g., southern cratered highlands as a hypothesized supercontinent (Spagnuolo and Dohm, 2004)), referred to as Habitable-Trinity conditions (Dohm and Maruyama, 2014b). Through time, the deposits have largely diminished resulting from degradational processes related to subsequent climatic/environmental perturbations; though, in addition to materials related to Argyre-induced activity including lake formation which have been largely degrading through time, this unit also includes rock materials emplaced during subsequent activity such as related to the growth of the Tharsis superplume (e.g., the upper reaches of the Argyre-impact-controlled valleys). Deposits include channel and floodplain materials related to the initial formation of Uzboi Vallis. The rock materials source from diverse provenances, including the Argyre rim and ejecta deposits (upper mantle materials and older primordial crustal materials excavated to and near the martian surface by the Argyre impact event and associated overturn and inversion of stratigraphy; materials also include hydrothermal deposits) and beyond, even including materials transported from as far north as the Thaumasia highlands and from as far south as the south pole
Argyre rim materials (units NAr, NArb, NAbr, NArsp)			
Argyre rim materials	NAr	High-relief, heavily cratered massifs tens of kilometers across and intervening broad linear troughs and valleys. Massifs of varying geometric shapes display basins at distinct breaks in slope with the higher parts of the massifs, knife-like ridges, amphitheatre-like valley heads, pyramidal peaks, and u-shape valleys. The massifs display aprons along their flanks. Similar to some of the other Argyre rim and basin materials, but this particular unit is mostly composed of rim-related massifs, whereas the other units include a combination of massifs and valley and basin infill deposits. The impact retention ages	Argyre rim materials and ejecta deposits (upper mantle materials and older primordial crustal materials excavated to and near the martian surface by the impact event and associated overturn and inversion of stratigraphy; materials include hydrothermal deposits) and dissected by basin-related fault structures and erosional valleys, and degraded through time by wind-, water-, and gravity-driven processes. Glacial activity is prominent in the geologic and hydrologic records of the Argyre provinces, as highlighted by the tarns, aretes, cirques, horns, and U-shape valleys that mark the

Table 2 (*continued*)

Unit name	Unit label	Description	Interpretation
		reflect extremely ancient Argyre impact rim materials and ejecta deposits with a significant crater population being destroyed by processes such as glaciation along steep slopes of the rim massifs	prominent impact-crater massifs. The chiseled landscape records diverse geologic and hydrologic activity, including ice melt and associated hydrologic conditions following the giant Argyre impact event, including lake formation and subsequent perturbations to the climate and environmental conditions driven by Tharsis pulses and to a lesser extent Elysium and other volcanic provinces, subsequent impact events such as Lowell and Galle, and changes in obliquity and eccentricity
Argyre rim and basin materials	NArb	High-relief, heavily cratered massifs tens of kilometers across and intervening basins, broad linear troughs, and valleys. Massifs of varying geometric shapes display basins at distinct breaks in slope with the higher parts of the massifs, knife-like ridges, amphitheatre-like valley heads, pyramidal peaks, and u-shape valleys. The massifs display aprons along their flanks. Intervening basins display both relatively smooth plains-forming materials and massifs which occur isolated or in groups	Argyre rim materials and ejecta deposits (upper mantle materials and older primordial crustal materials excavated to and near the martian surface by the impact event and associated overturn and inversion of stratigraphy) and dissected by basin-related fault structures and erosional valleys, and degraded through time by wind-, water-, and gravity-driven processes. Glacial activity is prominent in the geologic and hydrologic records of the Argyre provinces, as highlighted by the tarns, aretes, cirques, horns, and -shape valleys. The chiseled landscape records diverse geologic and hydrologic activity, including ice melt and associated hydrologic conditions following the giant Argyre impact event, including lake formation and subsequent perturbations to the climate and environmental conditions driven by Tharsis pulses and to a lesser extent Elysium and other volcanic provinces, subsequent impact events such as Lowell, and changes in obliquity. These materials are similar to unit NAr but more degraded and thus basins, which partly mark inversion of topography due to the destruction of the rim materials through time, and massifs, with more isolated (i.e., individual) promontories when compared to unit NAr
Argyre basin and rim materials	NAbr	High-relief, heavily cratered and degraded massifs tens of kilometers across with intervening basins including valleys and broad linear troughs. Massifs of varying geometric shapes display basins at distinct breaks in slope with the higher parts of the massifs, knife-like ridges, amphitheatre-like valley heads, pyramidal peaks, and u-shape valleys. The massifs display aprons along their flanks. Intervening basins display both relatively smooth plains-forming materials and massifs which occur isolated or in groups. Similar to NArb but basins are more prevalent compared to the massifs, and the basins are not as distinct, large, and isolated as those associated with unit NArsp materials	Argyre rim materials and ejecta deposits (upper mantle materials and older primordial crustal materials excavated to and near the martian surface by the impact event and associated overturn and inversion of stratigraphy) and dissected by basin-related fault structures and erosional valleys, and degraded through time by wind-, water-, and gravity-driven processes; rock materials include those emplaced directly following the Argyre impact event, such as those associated with the formation of the Uzboi-sourcing lake, as well as those emplaced during subsequent activity, including major stages of activity of the Tharsis superplume (Fig. 4). Local basins which formed during and/or subsequent to the Argyre impact event. The basins have served as catchments for fluvial, lacustrine, glacial, periglacial, alluvial, and colluvial deposits. The knobs are markers of the major degradation of the rim materials which has resulted in an inversion of topography in places. Major degradation through processes including glacial have highly degraded the rim materials resulting in massifs and basins. This map unit generally marks a more significant degradational state when compared to unit NArb, and thus a greater amount of basin materials vs. rim massifs. The CRISM data corroborates the Argyre-rim materials in part being uplifted ancient upper mantle materials, and that the terrains, which are distinctly hydrologically modified, contain magnesian lithologies such as olivine-dominated rocks (Buczkowski et al., 2008a,b, 2010) (Fig. 10)
Argyre rim smooth plains materials	NArsp	Smooth plains-forming materials in basins among the Argyre rim materials, marked by knobs, valley networks, flows which include aprons along the flanks of knobs, and dune fields. These basins are generally more distinct and isolated than those of unit NAbr	Distinct local basins which formed during and/or subsequent to the Argyre impact event. The basins have served as catchments for fluvial, lacustrine, glacial, periglacial, alluvial, hydrothermal, and colluvial deposits. The knobs are markers of the major degradation of the rim materials
Highlands materials (units AHTp, NTh, HNh4, HNh3, Nhb, Nh2, Nh1)			
Thaumasia plateau SE	AHTp	Corresponds to unit HNplt of Dohm et al. (2001a). Uneven surface dissected by numerous networking large troughs along the south-eastern margin of the Thaumasia plateau; many troughs abruptly terminate on up-slope end at large graben and depressions. Marked in places by ridges	Easily eroded (i.e., friable) volcanic materials with morphologic expression appearing similar to dissected ignimbrites which occur along the margin of the Andes (Fig. 9 of Dohm et al. (2001a)). The troughs may have formed in part due to Tharsis-driven magmatism, such as related to the Thaumasia plateau, and associated ground-water conditions along the distinct break in slope (at the southeast part of the Thaumasia plateau where there appears to be a discontinuity between the Thaumasia highlands and Coprates rise mountain ranges)
Thaumasia highlands	HNTh	Corresponds to unit HNpld of Dohm et al. (2001a). Highly modified impact crater of the eastern part of the Thaumasia highlands mountain range, which is embayed and partly buried by unit HNh4 materials along its southern margin, at the juncture between the mountain range and the plains	Highly degraded ancient impact crater that impacted into the Thaumasia highlands mountain range; highly dissected and locally deformed. Materials include Thaumasia highlands mountain-building materials, therefore, the geochemical composition and environmental conditions of the rock materials are interpreted to be diverse and far-reaching both in time and space, which includes rocks ranging from basalt to felsic compositions, and rocks with

(*continued on next page*)

Table 2 (*continued*)

Unit name	Unit label	Description	Interpretation
			varying grades of metamorphism such as those associated with orogenic complexes of Earth (Maruyama, 1997; Maruyama et al., 1997, 2013, 2014; Dohm and Maruyama, 2014a; Dohm et al., 2014a,b)
Highlands member 4	HNh4	Moderately smooth plains-forming materials; wrinkle ridges, ridge crests, troughs, and lineaments in places	Undifferentiated impact, volcanic, aeolian, fluvial, alluvial, and colluvial materials; locally degraded and contractionally deformed. Materials include Argyre ejecta materials and materials shed from the Thaumasia plateau and the Thaumasia highlands mountain range. Thus, the geochemical composition and environmental records of the rock materials are interpreted to be diverse and far-reaching both in time and space, which includes rocks ranging from basalt to felsic compositions, and rocks with varying grades of metamorphism such as those associated with orogenic complexes of Earth (Maruyama, 1997; Maruyama et al., 1997). This unit includes phyllosilicate through analysis of CRISM data (Buczkowski et al., 2008a,b). This is consistent with the interpretation of resurfacing and weathering which includes aqueous processes as per above
Highlands member 3	HNh3	Moderately smooth plains-forming materials; wrinkle ridges and lineaments in places	Undifferentiated impact, volcanic, aeolian, fluvial, alluvial, and colluvial materials; locally degraded and contractionally deformed. Materials include Argyre ejecta materials and materials shed from the Thaumasia plateau and the Coprates rise mountain range. Similar to unit HNh4, the geochemical composition and environmental records of the rock materials are interpreted to be diverse and far-reaching both in time and space, which includes rocks ranging from basalt to felsic compositions, and rocks with varying grades of metamorphism such as those associated with orogenic complexes of Earth (Maruyama, 1997; Maruyama et al., 1997)
Highlands basin materials	Nhb	Relatively smooth plains-forming materials in basins located in the cratered highlands along the margin of and away from the Argyre rim materials. Several of the basins are elongated with linear margins and/or tectonic structures, including AWMP paleolake basin (Figs. 1, 7, and 8) on the west-central margin of the Argyre basin and rim materials. The basins are similar to those of unit NArsp, but many occur away from the rim materials, and many appear to have more numerous valley networks along their margins	Basins, many of which are controlled by Argyre-impact-derived basement structures. Many of the basins record changing environmental and hydrologic conditions, including those that were influenced by changing conditions with the Argyre basin. For example, AWMP was occupied by a lake at least at the zero datum, though there is evidence that the lake and associated hydraulic head could have reached at least 1 km above the martian datum. The basins also record glacial, periglacial, fluvial, aeolian, alluvial, colluvial, and/or hydrothermal activity, as well as groundwater activity along the basement structures possibly indicated by channels which occur along the structures (Figs. 15 and 16). Though, the channels could be structurally-controlled surface runoff. Many of the basins occur away from the rim materials and in many cases appear to have margins dissected by more numerous valley networks when compared to the basins of the unit NArsp. The distinct younger crater-retention age of unit Nhb when compared to unit NArsp (see Table 3) possibly reflects greater resurfacing of the former, in part due to possible enhanced geologic and hydrologic activity in the transition zone that connects the Thaumasia highlands and plateau with the Argyre rim and basin (Figs. 1–3). The basins contain sedimentary, lacustrine, evaporite, and hydrothermal deposits, as well as lower crustal materials and/or upper mantle materials largely related to the Argyre impact event and eolian deposits sourcing from nearby (rim materials) and distant provenances (e.g., Tharsis)
Highlands member 2	Nh2	Rolling topography marked by scarps, structurally-controlled basins, faults, troughs, channels, and ridges. Highly dissected in places such as along the margin of the unit Nhb materials which infill the AWMP paleolake basin (Figs. 1, 3, and 7)	Undifferentiated impact, volcanic, fluvial, lacustrine, alluvial, colluvial, and basin infill materials including sedimentary deposits, moderately to heavily degraded. This includes modified Argyre rim and ejecta deposits (upper mantle materials and older primordial crustal materials transferred at and near the martian surface by the impact event and associated overturn and inversion of stratigraphy). Materials also include those transported from as far north as Tharsis and the Thaumasia highlands, such as recorded in the outcrops in the transitional zone between the Thaumasia highlands and the Argyre basin and rim materials emplaced by fluvial, colluvial, alluvial, and glacial activities (Fig. 3), and from as far south as the south pole, as recorded in the outcrops which occur to the south of the Argyre basin and rim materials primarily by glacial and fluvial activities. The geochemical composition and environmental records of the rock materials are interpreted to be diverse and far-reaching both in time and space, which includes rocks ranging from basalt to felsic compositions, and rocks with varying grades of metamorphism such as those associated with orogenic complexes of Earth (Maruyama, 1997; Maruyama et al., 1997). For example, an Argyre-impact, structurally-controlled basin

Table 2 (*continued*)

Unit name	Unit label	Description	Interpretation
			with drainages along its margins (Fig. 16) are shown to include phyllosilicate (Buczkowski et al., 2008a,b). This is consistent with the interpretation of resurfacing and weathering which includes aqueous processes as per above
Highlands member 1	Nh1	High plateau-forming outcrops extending hundreds of kilometers, many controlled by basement structures related to the Argyre impact event. Densely cratered and valley networks and scarps mark the landscape	Extremely ancient crustal materials, which includes igneous, sedimentary, and metamorphic rocks, buried by Argyre impact ejecta deposits mixed through time due to impact cratering and water (liquid and ice), wind, and gravity-driven processes. The elongated and high-standing plateaus are in part due to the Argyre impact and other tectonism, including pre-Argyre basement structures. Elongated mesas have faults along their margins, and thus are structurally controlled
Impact crater materials post-dating the Argyre impact event (units C1, C2, Cfs, Cfr)			
Young crater materials	C2	Relatively pristine impact crater materials of the ~230-km-diameter Galle impact crater overly surrounding rock materials of various units, including younger smooth-plains-forming basin floor deposits	Stratigraphically-young, relatively large impact crater. The event contributed to major change in the topography/terrain of the east-central margin of the Argyre basin and rim materials. Compared to the ~200-km-diameter Lowell impact crater, which impacted into a relatively large basin located to the west of the Argyre province influenced by ancient tectonism and impact cratering, as well as triggered major ice melt and associated flooding and valley network formation (Lias et al., 1997; Dohm and Tanaka, 1999), Galle does not appear to have triggered major flood events. This might be explained by the impact occurring in the rim materials along the margin of the basin where there are massifs composed of upper mantle and ancient crustal materials with intervening water-enriched valleys and local basins (i.e., less volume of water). In addition there may have been ice melt in the basin, but due to the relatively low gradient, distinct valley networks did not develop. There are troughs, however, mapped along parts of the southern margin of the Galle ejecta blanket that could be the result of impact-generated flooding
Old crater materials	C1	Degraded impact crater rims and ejecta deposits	Most impact >50-km-diameter craters are highly degraded due to the subsequent impact events and diverse geologic and hydrologic activities in the Argyre province through time. In the case of Hale crater, CRISM-based identification of low- and high-calcium pyroxenes and prehnite and chlorite on the floor, the central peak, and the rim of Hale crater (Fig. 11) are consistent with Argyre-impact-modified terrain, including the excavation of relatively olivine-rich, deep mantle and/or primordial crustal materials transferred at or near the martian surface by the impact event and associated overturn and inversion of stratigraphy. In addition, the mineralogy is also consistent with hydrothermal activity possibly associated both with the initial Argyre impact event followed by the Hale impact event into a potentially water-enriched target materials associated with hydrologic conditions associated of the Uzboi-Vallis spillway
Smooth crater floor materials	Cfs	Smooth plains-forming materials in the highly degraded impact basins. Some basins display knobs	Impact basin infill deposits with remnants of rim materials and central peaks
Rough crater floor materials	Cfr	Occurrence only in few impact crater basins, including Galle impact crater. Irregular topography, including knobs, depressions, and scarps	Degradation of central peak materials, but also disruption of the terrain due to hydrologic conditions such as Galle-impact-driven following the impact cratering event

(Fig. 4). This includes the influence of the topography and stratigraphy of the northern plains (Tanaka et al., 2005), which correlate with the timing of the major pulses (Fairén et al., 2003). In the new global geologic map of Mars by Tanaka et al. (2014), the Hesperian and Noachian transition unit (unit HNt) links to Stages 1 and 2 (i.e., larger and older ocean; Fairén et al., 2003), the Early Hesperian transition unit (unit eHt) to Stages 2 and 3 (i.e., either the waning of the larger and older ocean, or possibly another ocean-inundation phase of the northern plains; Fairén et al., 2003), and the regional Late Hesperian lowland unit (unit lHl) and Late Hesperian transition unit (unit lHt) to Stages 4 and 5 (i.e., the smaller ocean inset within the larger older ocean; Fairén et al., 2003). Tharsis-driven activity has also been a major influence on the adjacent Argyre impact basin and surroundings as revealed in this geologic investigation.

The primary Argyre impact basin is more than 1200 km in diameter and more than 4 km in depth (Fig. 2). The basin formed during the Noachian Period, or an absolute age estimated to be ~3.93 Ga (Robbins and Hynek, 2012; Robbins et al., 2013); the upper terminus of the Noachian Period (see Tanaka et al. (2014) for details and references therein) is estimated to have started at about 3.85 Ga (Hartmann, 2005) or 3.83 Ga (Ivanov, 2001; Hartmann and Neukum, 2001). Argyre is the best preserved of the large multi-ringed impact basins on Mars, comparable to the ~327 km-diameter Orientale basin of the Moon when viewed at resolutions less than 1 km/pixel. The profound differences of the Argyre and Orientale basins due to pervasive post-impact modification of the former by geologic, hydrologic, and aeolian processes, are evident at higher resolutions. Unlike the Moon, there is no absolute radiometric chronology of Mars. However, a wide range of circumstantial evidence, including comprehensive impact crater statistics, points towards the formation of Argyre, and similar large martian basins (including Hellas and Isidis), at about the same time as large and distinct multi-ring impact basins on the

Table 3
Cumulative crater densities and unit ages of geologic units in the Argyre and surrounding region of Mars. Note that (1) average crater density $N(D)$ equals number of craters larger than diameter D per million square kilometers, (2) relative ages based on time-stratigraphic scale from Tanaka (1986), (3) "ALL" refers to both highly degraded and "Superposed" (pristine impact craters with distinct rims and ejecta blankets that are not visibly resurfaced). See Tables 1 and 2 for unit names, description, and interpretation. Estimated absolute ages are based on the Hartmann (2005) (referred to as Hartmann in column 2) and Neukum et al. (2001) (referred to as Neukum in column 2) chronology systems. These ages were assigned a range of chronostratigraphic epochs based on the boundaries defined in Neukum et al. (2001), Hartmann (2005), and Werner and Tanaka (2011), also compared with that shown in Tanaka et al. (2014). Epochs include Early Noachian (EN), Middle Noachian, (MN), Late Noachian (LN), Early Hesperian (EH), Late Hesperian (LH), Early Amazonian (EA), Middle Amazonian (MA), and Late Amazonian.

Unit symbol	Model	Area (km^2)	Total craters	$N(3)$ age, Ga	$N(5)$ age, Ga	$N(16)$ age, Ga	Isochron age, Ga/epoch	Estimated range of epochs
Highlands materials								
Nh1 All	Hartmann	327,794	290	3.63 ± 0.01	3.72 ± 0.02	3.89 ± 0.02	3.82 ± 0.03	LN–MN
Nh1 All	Neukum	327,794	290	3.88 ± 0.01	3.82 ± 0.01	3.95 ± 0.02	3.94 ± 0.02	MN–EN
Nh1 Superposed	Hartmann	327,794	71	2.25 ± 0.27	$2.94^{+0.26}_{-0.44}$	$3.39^{+0.14}_{-0.70}$	$3.17^{+0.20}_{-0.60}$	EA–LH
Nh1 Superposed	Neukum	327,794	71	3.61 ± 0.03	3.63 ± 0.04	$3.54^{+0.09}_{-0.23}$	$3.61^{+0.04}_{-0.06}$	LH–EH
Nh2 All	Hartmann	1,096,085	846	3.60 ± 0.01	3.71 ± 0.01	3.86 ± 0.01	3.78 ± 0.01	LN–MN
Nh2 All	Neukum	1,096,085	846	3.85 ± 0.01	3.90 ± 0.01	3.82 ± 0.01	3.90 ± 0.01	LN–MN
Nh2 Superposed	Hartmann	1,096,085	189	1.78 ± 0.13	$2.70^{+0.22}_{-0.25}$	$2.89^{+0.37}_{-0.72}$	$2.64^{+0.33}_{-0.37}$	EA
Nh2 Superposed	Neukum	1,096,085	189	3.54 ± 0.02	3.61 ± 0.03	$3.36^{+0.11}_{-0.33}$	3.56 ± 0.04	EA–LH
HNh3 All	Hartmann	168,887	108	3.55 ± 0.03	3.62 ± 0.04	3.75 ± 0.05	3.66 ± 0.07	EH–LN
HNh3 All	Neukum	168,887	108	3.82 ± 0.02	3.84 ± 0.02	3.82 ± 0.05	3.83 ± 0.04	LN–MN
HNh3 Superposed	Hartmann	168,887	39	2.41 ± 0.38	$3.22^{+0.15}_{-0.44}$	$2.87^{+0.56}_{-1.88}$	$3.11^{+0.25}_{-0.79}$	EA
HNh3 Superposed	Neukum	168,887	39	3.62 ± 0.04	3.67 ± 0.05	$3.36^{+0.20}_{-1.93}$	$3.62^{+0.05}_{-0.08}$	EA–EH
HNh4 All	Hartmann	262,637	129	3.46 ± 0.04	3.58 ± 0.04	$3.72^{+0.04}_{-0.06}$	3.63 ± 0.05	EH–LN
HNh4 All	Neukum	262,637	129	3.78 ± 0.02	3.81 ± 0.02	3.78 ± 0.05	3.80 ± 0.03	LN
HNh4 Superposed	Hartmann	262,637	81	$3.10^{+0.14}_{-0.25}$	$3.39^{+0.07}_{-0.11}$	$3.22^{+0.25}_{-1.39}$	$3.35^{+0.10}_{-0.22}$	EA–LH
HNh4 Superposed	Neukum	262,637	81	3.69 ± 0.03	3.72 ± 0.03	$3.46^{+0.13}_{-0.83}$	3.68 ± 0.04	LH–LN
Nhb All	Hartmann	67,049	44	3.58 ± 0.05	3.67 ± 0.05	$3.80^{+0.06}_{-0.09}$	$3.71^{+0.06}_{-0.09}$	LN
Nhb All	Neukum	67,049	44	3.84 ± 0.03	3.87 ± 0.04	$3.86^{+0.05}_{-0.09}$	$3.86^{+0.04}_{-0.06}$	MN
Nhb Superposed	Hartmann	67,049	12	$2.25^{+0.62}_{-0.65}$	$3.18^{+0.23}_{-0.92}$	$3.58^{+0.12}_{-1.09}$	$3.44^{+0.14}_{-1.01}$	EA–LN
Nhb Superposed	Neukum	67,049	12	$3.60^{+0.06}_{-0.10}$	$3.66^{+0.06}_{-0.10}$	$3.67^{+0.10}_{-0.43}$	$3.66^{+0.08}_{-0.16}$	LH–EH
HNTh All	Hartmann	28,531	19	$3.57^{+0.05}_{-0.08}$	$3.59^{+0.07}_{-0.13}$	$3.73^{+0.10}_{-0.38}$	$3.60^{+0.07}_{-0.14}$	LN
HNTh All	Neukum	28,531	19	$3.83^{+0.05}_{-0.03}$	$3.82^{+0.05}_{-0.07}$	$3.80^{+0.09}_{-0.28}$	$3.82^{+0.05}_{-0.07}$	LN
HNTh Superposed	Hartmann	28,531	13	$3.44^{+0.09}_{-0.23}$	$3.56^{+0.08}_{-0.18}$		$3.57^{+0.09}_{-0.28}$	EH–LN
HNTh Superposed	Neukum	28,531	13	$3.77^{+0.04}_{-0.06}$	$3.80^{+0.05}_{-0.08}$		$3.78^{+0.06}_{-0.11}$	LN
AHTp All	Hartmann	16,282	3	$2.88^{+0.54}_{-1.65}$	$2.29^{+1.07}_{-1.88}$		$2.29^{+1.06}_{-1.83}$	EA
AHTp All	Neukum	16,282	3	$3.66^{+0.09}_{-0.29}$	$3.56^{+0.14}_{-2.31}$		$3.57^{+0.13}_{-1.98}$	LH–EH
AHTp Superposed	Hartmann	16,282	3	$2.88^{+0.54}_{-1.65}$	$2.29^{+1.07}_{-1.88}$		$2.29^{+1.06}_{-1.83}$	EA
AHTp Superposed	Neukum	16,282	3	$3.66^{+0.09}_{-0.29}$	$3.56^{+0.14}_{-2.31}$		$3.57^{+0.13}_{-1.98}$	LH–EH
Argyre materials								
Rim materials								
NAr All	Hartmann	58,067	31	$0.50^{+0.05}_{-0.08}$	$3.63^{+0.05}_{-0.07}$	$3.78^{+0.06}_{-0.11}$	$3.71^{+0.06}_{-0.10}$	EH–LN
NAr All	Neukum	58,067	31	3.79 ± 0.04	3.84 ± 0.04	$3.84^{+0.06}_{-0.10}$	$3.84^{+0.05}_{-0.07}$	LN–MN
NAr Superposed	Hartmann	58,067	1					
NAr Superposed	Neukum	58,067	1					
NArb All	Hartmann	109,274	70	3.56 ± 0.04	3.66 ± 0.04	3.88 ± 0.04	$3.75^{+0.05}_{-0.07}$	EH–MN
NArb All	Neukum	109,274	70	3.83 ± 0.02	3.87 ± 0.03	3.94 ± 0.04	3.88 ± 0.05	LN–MN
NArb Superposed	Hartmann	109,274	8	1.06 ± 0.37	1.05 ± 0.50		0.92 ± 0.47	MA–EA
NArb Superposed	Neukum	109,274	8	$3.27^{+0.18}_{-0.88}$	$3.07^{+0.35}_{-1.40}$		$2.78^{+0.57}_{-1.36}$	EA–LN
NAbr All	Hartmann	577,012	432	3.60 ± 0.01	3.68 ± 0.01	3.89 ± 0.02	3.78 ± 0.02	LN–MN
NAbr All	Neukum	577,012	432	3.85 ± 0.01	3.88 ± 0.01	3.95 ± 0.02	3.90 ± 0.02	MN–EN
NAbr Superposed	Hartmann	577,012	50	0.91 ± 0.13	1.23 ± 0.24	$3.35^{+0.13}_{-0.50}$	1.54 ± 0.35	MA–LH
NAbr Superposed	Neukum	577,012	50	$3.13^{+0.15}_{-0.32}$	$3.28^{+0.12}_{-0.30}$	$3.51^{+0.08}_{-0.16}$	$3.30^{+0.12}_{-0.31}$	EA–LH
NArsp All	Hartmann	38,939	39	3.67 ± 0.04	3.75 ± 0.04	3.98 ± 0.05	3.93 ± 0.06	MN–EN
NArsp All	Neukum	38,939	39	3.90 ± 0.03	3.94 ± 0.04	4.04 ± 0.05	4.02 ± 0.05	MN–EN
NArsp Superposed	Hartmann	38,939	7	1.88 ± 0.71	$1.86^{+1.07}_{-1.11}$		$1.90^{+1.06}_{-1.11}$	EA
NArsp Superposed	Neukum	38,939	7	$3.56^{+0.08}_{-0.19}$	$3.50^{+0.13}_{-1.21}$		$3.51^{+0.12}_{-0.87}$	LH
Basin materials								
NAb1 All	Hartmann	100,203	42	$3.39^{+0.07}_{-0.12}$	$3.59^{+0.04}_{-0.06}$	3.91 ± 0.04	$3.95^{+0.05}_{-0.08}$	LH–MN
NAb1 All	Neukum	100,203	42	3.75 ± 0.03	3.82 ± 0.04	3.96 ± 0.04	$4.01^{+0.05}_{-0.09}$	LN–EN
NAb1 Superposed	Hartmann	100,203	6	0.66 ± 0.27	1.03 ± 0.51		0.91 ± 0.55	MA
NAb1 Superposed	Neukum	100,203	6	$2.38^{+0.77}_{-0.97}$	$3.03^{+0.39}_{-1.48}$		$2.57^{+0.77}_{-1.47}$	LN
NAb2 All	Hartmann	209,887	105	3.47 ± 0.05	3.57 ± 0.04	3.72 ± 0.06	3.63 ± 0.06	EH–LN
NAb2 All	Neukum	209,887	105	3.78 ± 0.02	3.81 ± 0.02	3.78 ± 0.05	3.80 ± 0.04	LN
NAb2 Superposed	Hartmann	209,887	15	0.80 ± 0.21	1.03 ± 0.36	$1.78^{+1.25}_{-1.33}$	1.12 ± 0.57	MA–EA
NAb2 Superposed	Neukum	209,887	15	$2.85^{+0.40}_{-0.72}$	$3.04^{+0.33}_{-0.99}$	$2.55^{+0.85}_{-1.91}$	$2.83^{+0.51}_{-1.21}$	EA
NAb3 All	Hartmann	208,086	127	3.54 ± 0.03	3.65 ± 0.03	3.79 ± 0.05	3.72 ± 0.05	EH–LN
NAb3 All	Neukum	208,086	127	3.81 ± 0.02	3.86 ± 0.02	3.85 ± 0.04	3.87 ± 0.04	LN–MN
NAb3 Superposed	Hartmann	208,086	18	0.98 ± 0.23	1.45 ± 0.42	$2.63^{+0.74}_{-1.63}$	1.76 ± 0.78	MA–EA
NAb3 Superposed	Neukum	208,086	18	$3.22^{+0.17}_{-0.53}$	$3.39^{+0.11}_{-0.36}$	$3.29^{+0.24}_{-1.85}$	$3.34^{+0.16}_{-0.87}$	EA–LH

Table 3 (*continued*)

Unit symbol	Model	Area (km^2)	Total craters	$N(3)$ age, Ga	$N(5)$ age, Ga	$N(16)$ age, Ga	Isochron age, Ga/epoch	Estimated range of epochs
HAb4a All	Hartmann	341,499	125	$3.31^{+0.06}_{-0.09}$	$3.45^{+0.05}_{-0.06}$	$3.55^{+0.07}_{-0.13}$	$3.46^{+0.06}_{-0.10}$	LH–EH
HAb4a All	Neukum	341,499	125	3.73 ± 0.02	$3.74^{+0.02}_{-0.03}$	$3.65^{+0.06}_{-0.09}$	3.72 ± 0.03	EH–LN
HAb4a Superposed	Hartmann	341,499	21	0.70 ± 0.15	1.11 ± 0.29	1.67 ± 1.02	1.29 ± 0.56	MA–EA
HAb4a Superposed	Neukum	341,499	21	$2.51^{+0.49}_{-0.55}$	$3.17^{+0.21}_{-0.67}$	$2.40^{+0.90}_{-1.46}$	$2.91^{+0.43}_{-1.07}$	EA
NAb4b All	Hartmann	18,541	11	$3.53^{+0.07}_{-0.15}$	$3.62^{+0.08}_{-0.16}$	$3.88^{+0.07}_{-0.15}$	$3.71^{+0.07}_{-0.14}$	EH–MN
NAb4b All	Neukum	18,541	11	$3.81^{+0.04}_{-0.06}$	$3.84^{+0.06}_{-0.09}$	$3.94^{+0.07}_{-0.14}$	$3.86^{+0.06}_{-0.10}$	LN–MN
NAb4b Superposed	Hartmann	18,541	1					
NAb4b Superposed	Neukum	18,541	1					

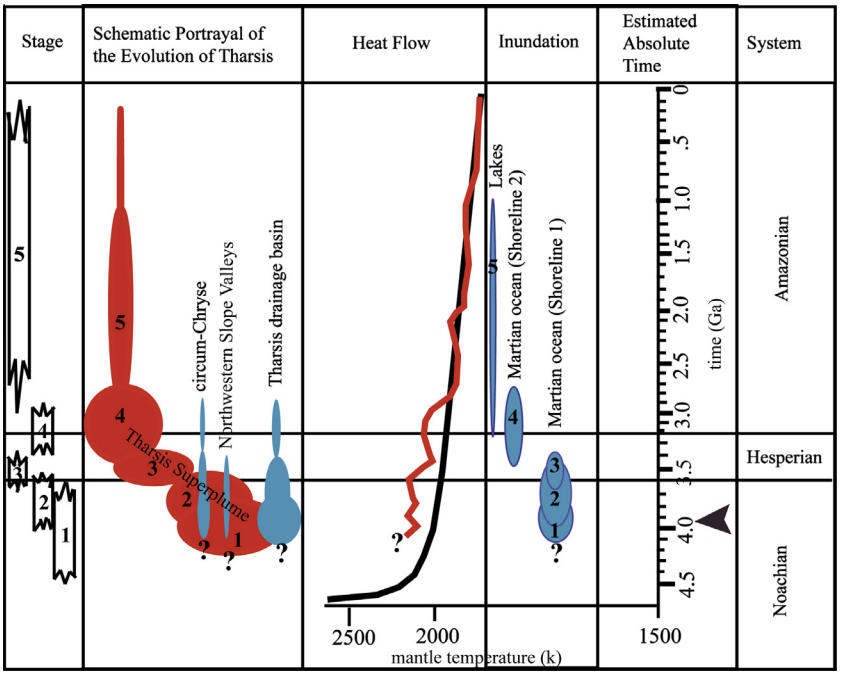

Fig. 4. Modified from Dohm et al. (2007a), chart comparing the major stages of the Tharsis superplume, which includes circum-Chryse, NSVs, and Tharsis drainage basin/aquifer system, with: (1) heat flow; note the maximum effective heat flow from the core to lithosphere in the Early and Middle Noachian (black line) and non-steady-state decline in subjective heat flow extending from part of the Early Noachian to present (red line) compared to proposed steady-state decline in mantle temperature with time (black line; Schubert et al., 1992) based on published geologic information (e.g., Dohm and Tanaka, 1999; Dohm et al., 2001a,b, 2007a, 2013; Anderson et al., 2001; Fairén et al., 2003; Baker et al., 2007), (2) hypothesized Tharsis-triggered inundations in the northern plains ranging from oceans to lakes (shorelines 1 and 2 as per Fairén et al. (2003)), (3) inferred absolute time (Hartmann, 2005), and (4) system information of Scott et al. (1986–1887). Sizes of solid areas are roughly proportional to degree of exposed activity. The estimated timing of the Argyre impact is also shown (black arrowhead), based on Robbins and Hynek (2012) and Robbins et al. (2013). The onset of Tharsis and other features are queried. Based on uncertainties in the unit age ranges and error in crater statistics, we conservatively show overlap among the stages with sawtooth lower and upper bounds of each column. Subjective heat flow greater than 4.0 Ga is queried, with consideration of a dynamo and plate tectonism reportedly active at that time (Baker et al., 2007; Dohm et al., 2013). (For interpretation of the references to color in this figure legend, the reader is referred to the web version of this article.)

Moon such as Oriental (i.e., somewhere between about 3.8–4.0 byr ago) (based on Wilhelms (1987) for the Moon and Robbins and Hynek (2012) and Robbins et al. (2013) for Mars).

Compared to the Hellas basin, which is estimated to have formed at about 4.0 Ga, the Argyre basin, occurring nearly 70 myr later than the Hellas impact event (both estimated ages based on Robbins et al. (2013)), is much more pristine than Hellas, including the impact-induced radial and concentric structures that can be more readily mapped and characterized (Dohm et al., 2002a). This difference in degradational state is interpreted to mark major changing planetary conditions at a time when the internal dynamo of Mars had shut down due to planetary cooling, putative plate tectonism was nearing its end, and the atmosphere was thinning (Baker et al., 2007).

Other basin examples, though much older than Hellas, include putative Utopia (e.g., McGill, 1989) and Arabia Terra (Dohm et al., 2007b) impact basins, largely subdued to the untrained eye. The putative Arabia Terra basin, for example, is not visible in present-day topography, but its hypothesized existence is supported by distinct characteristics such as stratigraphy, physiography, paleotectonism, and geomorphology, as well as notable structural, albedo, thermal inertia, gravity, magnetic, and elemental signatures (Dohm et al., 2007b). Similarly, ancient basins on Earth, particularly those tectonically-derived, that have been all but destroyed, are revealed through geologic investigation. Another example of an ancient, heavily eroded basin is the Chryse impact basin infilled by sediments derived from adjoining chaotic terrains and outflow channels (Rotto and Tanaka, 1995; Rodriguez et al., 2011). There are also relatively large features referred to as quasi-circular depressions interpreted to be impact in origin (Frey et al., 2002). Similar to Hellas, the younger Argyre impact event appears to have taken place after the shutdown of the planetary dynamo; the remanent magnetic anomalies (Acuña et al., 1999, 2001; Connerney et al., 1999, 2001; Arkani-Hamed, 2003, 2004; Roberts et al., 2009; Roberts and Arkani-Hamed, 2012), distinct in the extremely ancient geologic provinces of

Mars (e.g., Terra Cimmeria, Terra Sirenum, Arabia Terra, Xanthe Terra, and the Thaumasia highlands and Coprates rise mountain ranges), are not observed in and nearby the giant impact structure (Dohm et al., 2005, 2013). "Extremely ancient" refers to pre-Hellas Mars, or estimated to be >4.0 Ga (Robbins et al., 2013), equivalent to the Hadean of Earth, of which the rock record has been all but destroyed aside from traces, such as zircon grains in meta-sandstones (Harrison, 2009). There are other post-dynamo-shutdown geologic provinces such as Tharsis, Syrtis, Malea Planum, and Tyrrhena/Hadriaca volcanic provinces and the northern plains, which includes the Tharsis/Elysium corridor region (Dohm et al., 2008, 2013). The termination of the global magnetic field may have occurred between the formation of Ladon and Hellas impact basins (Lillis et al., 2008) and the formation of Ladon and Prometheus basins (Fig. 1), the latter of which is dated to be older than Hellas through comprehensive global crater statistics (Robbins et al., 2013).

The multi-ringed Argyre impact structure appears to have influenced the geophysical and geological development of a large part of Mars. This includes modification of the southeastern part of the Thaumasia plateau and control of the Uzboi drainage system and other systems of surface and subsurface movement of liquid water and water–ice (Parker and Gorsline, 1991, 1993; Kargel and Strom, 1990, 1992; Dohm et al., 2001a, 2011a; Kargel, 2004). The influence of the Argyre impact has even been proposed to have fixed the location of the Tharsis superplume through impact-induced subduction and slab rollback during an incipient plate tectonic period (Yin, 2012a). Though the onset and origin of Tharsis still remains in question according to various working hypotheses, such as focused subduction of hydrated crustal slab materials (Baker et al., 2007), the Argyre impact event and the development of the Tharsis superplume had an influence on one another. While the Argyre impact influenced the development of the southeast margin of the Thaumasia plateau, Tharsis-superplume-driven outgassing, flooding, and associated climate and environmental change significantly contributed to the modification of the Argyre basin (Figs. 2 and 4).

Impact-induced features such as rim-forming mountains (e.g., the Charitum and Nereidum Montes), local basins among the mountains, radial and concentric structures (including valleys), and the primary basin floor have all been altered by diverse processes since their formation both within and outside of the Argyre province. These include magmatic, impact cratering, tectonic (e.g., reactivated basement structures), eolian, fluvial, alluvial, colluvial, periglacial, glacial, and lacustrine (e.g., Parker, 1985, 1989, 1994; Scott et al., 1986–1987; Tanaka, 1986; Parker and Gorsline, 1991, 1992, 1993; Kargel and Strom, 1992; Dohm and Tanaka, 1999; Parker et al., 2000; Hiesinger and Head, 2002; Seibert and Kargel, 2001; Banks et al., 2008, 2009; Jones et al., 2011; Soare et al., 2012a, 2014a,b; El Maarry and Dohm, 2013; El Maarry et al., 2013). Geologically recent activity is highlighted by high-resolution data sets such as the Context Camera (CTX) at ~6 m/pixel and the High Resolution Imaging Science Experiment (HiRISE). It has involved liquid water, water–ice, and wind that suggest distinct and significant changes in regional environmental conditions (including both surface and near-surface modifications in temperature, moisture, hydrology, and surface morphology) generally in geologically recent time, including the very Late Amazonian (within the last roughly thousands of years) (e.g., El Maarry et al., 2013; Soare et al., 2014a,b).

Henceforth, "geologically recent activity" refers to Middle Amazonian and younger activity. This is in part based on the superposed crater counts (i.e., those impact craters which are superposed and pristine with distinct rims and ejecta blankets that are not visibly resurfaced) of many of the units in the Argyre province shown in Table 3, which give crater-retention ages of Late Hesperian and Early Amazonian epochs. This retention age is coeval with major Tharsis-driven activity during the Late Hesperian and Early Amazonian epochs (i.e., Stages 4 and 5; Fig. 4). In a marked shift from most Viking Orbiter-era geochronologies of Mars, in recent years it has been increasingly evident that intensive or widespread episodes of martian hydrogeologic activity took place at intervals throughout the Amazonian, even into the very Late Amazonian (Kargel et al., 1995; Head et al., 2003; Madeleine et al., 2009; Skinner et al., 2012; Rodriguez et al., 2014). Thus, "geologically recent" should be considered here as activity correlative in time with the latter part of Stage 5 Tharsis activity (schematically depicted in Fig. 4 through a narrowing of the solid area representative of decreased Stage-5 activity). Other processes documented during recent years include seasonal deposition and sublimation of a thin CO_2 ice cover and locally intense and frequent dust devils which distinctly leave their marks (Kargel, 2004). The rich and diverse history of the Argyre province, and its far-reaching record in terms of both time and space at local to regional and even global scales, is detailed below.

3. Mapping investigation

3.1. Mapping overview and data

Geologic units and tectonic and erosional structures primarily were identified and mapped using Odyssey Thermal Emission Imaging System (THEMIS) data (100 m/pixel near-infrared (IR) daytime and nighttime images and 18 m/pixel visible multi-band images) (Christensen et al., 2004), images from the HiRISE camera (McEwen et al., 2007) and CTX on MRO (Malin et al., 2007), and Viking Mars Digital Image Mosaic 2.1 information (generally 100 m–200 m/pixel) (e.g., Archinal et al., 2002, 2003).

The MGS Mars Orbiter Laser Altimeter (MOLA) has provided an unprecedented topographic information in the form of a digital-elevation model at 1/128° resolution (~460 m/pixel) (e.g., Smith et al., 1999). The MOLA data have helped: (1) define stratigraphic units; (2) determine the stratigraphic relations among the map units; (3) evaluate whether an impact crater or deposit was superposed or embayed or partly buried; and (4) assess spatial and temporal relations among map units, structures, terraces, valleys incised into existing valleys at distinct elevation ranges around parts of the basin, and possible equipotential surfaces.

Geologic information was assembled into a Geographic Information System (GIS) database, which enables the attribution of individual geologic features according to type and size, comparative analysis of the spatial and temporal relations among the rock outcrops and topography (Fig. 5), and area calculations of the map units for compiling crater statistics (Tables 1 and 3).

The materials of the Argyre province are divided into 20 distinct geologic units, as discussed in Section 4.2, shown in Fig. 3, and detailed in Tables 1–3. The map units are categorized into Argyre basin stratigraphic units (units HAb4a, NAb4b, NAb3, NAb2, and NAb1, in which H refers to the Hesperian Period, N—Noachian Period, Ab—Argyre basin materials divided into members 4a, 4b, 3, 2, and 1), Argyre rim materials (units NAr, NArb, NAbr, and NArsp, in which N refers to the Noachian Period, A—Argyre, r—rim, b—basin, and sp—smooth plains), highlands materials (units AHtp, HNTh, HNh4, HNh3, Nhb, Nh2, and Nh1, in which A refers to the Amazonian Period, H—Hesperian Period, N—Noachian Period, tp—Thaumasia plateau, Th—Thaumasia highlands, and h—highlands divided into members 4-1), and impact crater materials post-dating the Argyre impact event (units C1, C2, Cfs, and Cfr, in which C stands for crater, C1—older crater materials, C2—younger crater materials, Cfs—smooth crater floor materials, and Cfr—rough crater floor materials) (Fig. 3, Tables 1–3). The map units are

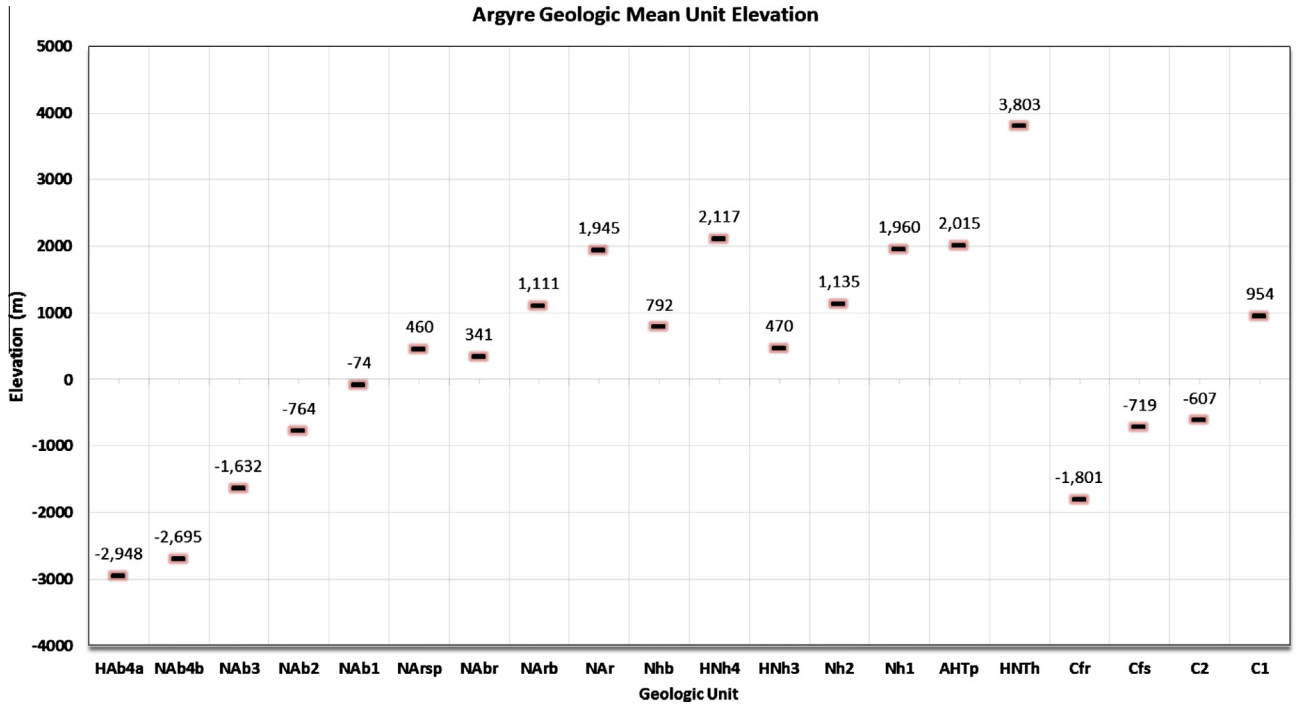

Fig. 5. Mean elevations for Argyre map units detailed in Tables 1–3. Note the distinct step-like mean elevation ranges of the basin units (NAb1, NAb2, NAb3, NAb4b, HAb4a) representative of distinct stratigraphy within the basin.

delineated based on stratigraphic relations, topography, and morphologic characteristics. Morphologic characteristics include albedo and bedform types such as valleys, terraces, knobs/massifs/plateaus, ridges, scarps, flow features, and pristine and highly degraded impact craters and other topographic lows such as Argyre-induced topographic basins.

By merging daytime THEMIS data and MOLA topography, distinct topographic levels with spatially associated bedforms were observed, aiding in the identification, characterization, and mapping of the basin units. The geologic contacts of the basin units are generally gradational due to major resurfacing through time, and have been delineated approximately on the geologic map. For example, there are distinct topographic levels evident where valleys incise into older valley segments often at terraces and erosional scarps. These topographic levels are particularly distinct along the floors of the three valleys that debouch into the southern and southeast parts of the Argyre basin; from west to east, they are: Surius Vallis, Dzigai Vallis, and Nia Valles, respectively (Figs. 3 and 6). These levels are interpreted to indicate changing hydraulic head (depth to the water table) and associated major changes in basin conditions.

The relative ages of rock materials were derived from stratigraphic and structural relations and crater densities. The formal stratigraphic systems (Noachian, Hesperian, and Amazonian) devised by Scott and Carr (1978) and the series (upper, middle, and lower divisions of systems) defined by Tanaka (1986) are used in this work.

The stratigraphic, hydrologic, and tectonic histories in the Argyre province, as discussed in Section 4, are based on stratigraphic and crosscutting relations among rock materials and structures (i.e., that are tectonic, erosional, and depositional in origin), and relative ages are further constrained through detailed impact crater investigations detailed in the following Section 3.2. We mapped the stratigraphy and structure including: channels, troughs, scarps, broad ridges, wrinkle ridges, crater rims, lineaments that may have a tectonic origin, graben, and faults. Mapped tectonic features with lengths ranging from hundreds of kilometers to more than a thousand kilometers are referred to as macrostructures and are interpreted to be major deep-seated (lower crust and possibly upper mantle) dislocations (faults) produced by the giant Argyre impact event and other dynamic geologic activity mostly prior to the development of Tharsis.

3.2. Impact crater dating

To evaluate the formation and modification ages of the Argyre rock units, crater statistics were compiled for 16 of the 20 units; this accounted for approximately 90% of the map region (Tables 1 and 3, and corresponding Fig. 3). Impact craters with diameters generally >50 km and their associated ejecta blankets were mapped, but crater statistics not tallied. This included units C1 (older crater materials), C2 (young crater materials), Cfr (rough crater floor materials), and smooth crater floor materials (Cfs). This age information was derived by counting all craters having rim diameters larger than or equal to 3 km and by calculating unit areas from our digital geologic map (Fig. 3). The crater populations were compiled using the global data base of Robbins and Hynek (2012). At the time of the compiling, the global data base was complete for impact craters with diameters down to 3 km. Thus, our counts included those craters with diameters $\geqslant$3 km.

Though crater statistics used in geologic investigations often include impact craters with $\geqslant$2 km (e.g., Scott et al., 1986–1987), we believe that $\geqslant$3 km-diameter craters are better for assessing the minimum relative ages of the rock materials. We have greater confidence using larger diameter craters for determining the minimum relative ages of the rock materials due to the major resurfacing reported here for the Argyre province; i.e., part of the crater populations have been destroyed by magmatic-, tectonic-, water-, wind-, gravity- (e.g., colluvial deposition), and/or subsequent impact-driven resurfacing especially at smaller diameters. Results of Irwin et al. (2013) point to major resurfacing and destruction of crater populations on Mars during the Noachian Period, highlighted through stratigraphy and impact crater statistics; this geologic investigation of the Argyre province shows that the Argyre

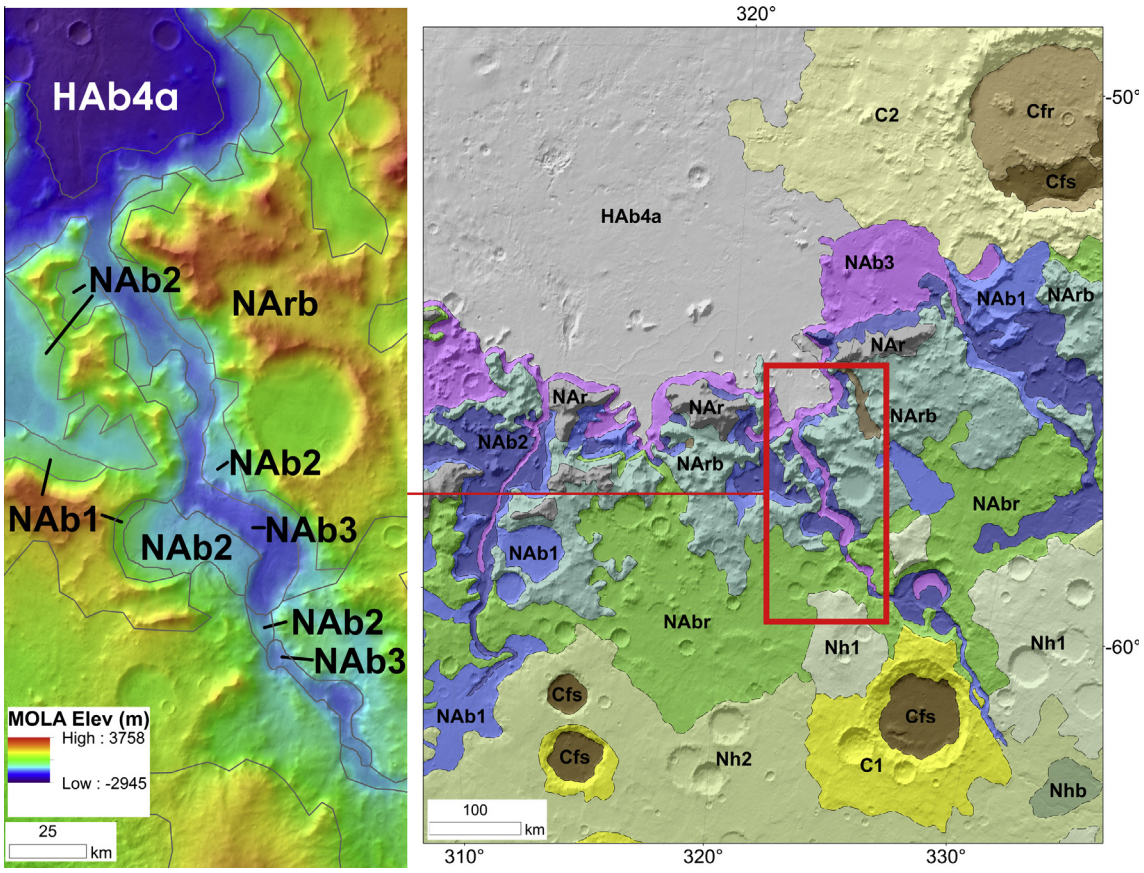

Fig. 6. Merged daytime THEMIS with MOLA topography using Geographic Information Systems with approximate geologic contacts delineating distinct stratigraphic relations highlighted in and surrounding Dzigai Vallis (left), as portrayed in the geologic map of Fig. 3 (right; part of the geologic map shown at the right; note the structure symbols are not shown), one of three distinct valleys that debouch into the Argyre basin (the other two being western Surius Vallis and eastern Nia Vallis). Note the spatial correlations among the map units, scarps, and distinct elevation ranges generally highlighted by the topographic-based color scheme with (from young to old generally with increasing mean elevations shown in Fig. 5): dark blue to violet demarking the lowest and youngest basin materials—unit HAb4a (gray on geologic map), dark blue to light blue—unit Nab3 (violet on map), light blue—unit NAb2 (dark blue on map), and light green delineating the oldest and highest standing—unit Nab1 (light blue on map). These stratigraphic sequences, which generally occur at elevational ranges, are consistently observed around the basin, interpreted to mark changing hydraulic head and associated major changes in basin conditions such as related to Tharsis magmatic-driven pulses. (For interpretation of the references to color in this figure legend, the reader is referred to the web version of this article.)

impact event among other activity would have contributed to the resurfacing of extremely ancient terrains, which includes destruction of part of the global crater population. Barlow (1990, 2004, 2005) reported greater confidence using larger impact craters (>5 km) for relative-age dating, also because of the recognized major resurfacing. Here, we have compiled cumulative crater densities for 3-km-diameter, 5-km-diameter, and 16-km-diameter impact craters (Table 3). Kargel et al. (1995) considered the crater population in southern Argyre Planitia larger than 4 km diameter to be indicative of the basement rock materials or early massive basin deposits, whereas the crater population between 1.0 and 1.41 (square-root of 2) km to be indicative of modification (e.g., by glacial and lacustrine processes). Similar to those findings, 2 km-diameter and smaller diameter impact craters have been shown to be useful in analyzing resurfacing ages (Platz and Michael, 2011; Platz et al., 2013). In a study related to this geologic investigation, detailed analysis using HiRISE and CTX images of parts of the basin included counts down to 50-m-diameter craters (El Maarry et al., 2013).

The crater statistics consist of total crater populations (including partly buried, degraded, and pristine impact craters), which may indicate minimum emplacement ages (since part of the population is destroyed due to resurfacing through time). The crater statistics also include pristine craters only (i.e., craters and their associated ejecta blankets that have not been visibly resurfaced at resolution, which includes dissection, tectonic deformation, or partial burial by lava flows and fluvial, alluvial, and colluvial deposits), which indicate ages of Hesperian and Amazonian resurfacing depending on the particular map unit and estimated absolute chronology systems (Table 3). A similar approach proved to be useful in unraveling the geologic evolution of the Thaumasia region (Dohm et al., 2001a). In addition, our approach of defining primary depositional and modification ages based on total crater populations and pristine-only crater counts is somewhat similar to that employed by Kargel et al. (1995). Though, here we have much more robust results afforded through the combined comprehensive mapping, GIS-based area calculations of the map units for compiling crater statistics, and usage of THEMIS, CTX, and MOLA data, in addition to Viking data.

Cumulative size–frequency diagrams (SFDs) were created (Crater Analysis Techniques Working Group, 1979) and isochrons were fitted from both the Hartmann (2005) and Neukum et al. (2001) production functions (Table 3). Estimated absolute ages are based on the Hartmann (2005) and Neukum et al. (2001) chronology systems. These ages were assigned a range of chronostratigraphic epochs based on the boundaries defined in Neukum et al. (2001), Hartmann (2005), and Werner and Tanaka (2011), and compared with that shown in Tanaka et al. (2014) (Table 3). This range of assignments is an attempt to encompass the uncertainty and error inherent in the varied models, conservatively. As

with all crater counts, these should be treated as an approximate guide, and the relative differences between each unit are more certain than the actual model ages (for more discussion, see Section 4.2 of Robbins et al. (2013)). Also, a part of the crater populations of the ancient terrains (particularly Early Amazonian or older) have been destroyed, and thus the range of chronostratigraphic epochs for a specific unit includes the rock materials with estimated minimum age of emplacement and subsequent modification.

Using THEMIS, CTX, and MOLA data, a total of 82 impact craters (Table 4) were either deleted from the total count of a specific geologic unit (if embayed or buried by the geologic-unit materials) or added to older adjacent polygons (if they formed part of the basement of an adjacent unit). For example, an impact crater that forms part of the floor of a glaciated valley but is embayed and partly buried by valley-fill materials was not included in the valley-fill materials; instead, it was compiled with the valley-forming materials. The valley infill deposits would otherwise be errantly

Table 4
Locations and diameters of impact craters that were subtracted from unit polygons and either deleted (if embayed or buried by the geologic-unit materials) or added to older adjacent polygons, if the impact craters were insufficient in size to map at scale (impact craters <50 km were not mapped) and that form part of the basement of an adjacent unit.

Crater latitude	Crater longitude	Crater diameter	Original unit	New unit
−40.305	−28.184	9.75	NAb1	NAbr
−36.638	−44.771	14.79	NAb1	NAbr
−39.801	−30.932	18.02	NAb1	NAbr
−37.044	−44.678	25.36	NAb1	NAbr
−53.828	−60.247	26.26	NAb1	NAbr
−54.075	−60.848	33.1	NAb1	NAbr
−51.854	−56.198	32.57	NAb2	NAb1
−36.417	−34.001	13.33	NAb2	NAbr
−49.567	−57.932	15.36	NAb2	NAbr
−47.44	−56.569	19.99	NAb2	NAbr
−39.722	−50.336	20.18	NAb2	NAbr
−38.712	−36.819	21.86	NAb2	NAbr
−40.061	−50.62	30	NAb2	NAbr
−47.25	−51.091	30.31	NAb2	NAr
−55.86	−28.366	17.63	NAb2	NAbr
−45.429	−51.322	21.64	NAb2	NAbr
−55.077	−28.822	29.97	NAb2	NAbr
−58.758	−37.004	31.71	NAb2	NAbr
−54.424	−30.015	40.3	NAb2	NAbr
−60.278	−31.703	34.99	NAb2	C1
−59.801	−32.414	88.48	NAb2	C1
−57.532	−47.336	15.77	NAb2	DELETED
−57.321	−47.132	22.4	NAb2	DELETED
−57.711	−47.689	23.27	NAb2	DELETED
−37.414	−45.548	65.84	NAb2	Nh2
−37.663	−44.297	24.88	NAb3	NAb1
−41.183	−44.762	10.88	NAb3	NAb2
−36.456	−40.301	12.41	NAb3	NAb2
−41.452	−45.804	26.73	NAb3	NAb2
−43.959	−35.512	37.55	NAb3	NAb4b
−38.684	−40.428	7.07	NAb3	NAbr
−59.475	−34.64	13.25	NAb3	NAbr
−38.493	−40.22	17.02	NAb3	NAbr
−38.617	−40.194	18.65	NAb3	NAbr
−44.446	−50.275	19.05	NAb3	NAbr
−42.065	−42.51	19.53	NAb3	NAbr
−42.374	−40.675	22.18	NAb3	NAbr
−40.849	−45.449	22.76	NAb3	NAbr
−37.562	−40.259	24.17	NAb3	NAbr
−35.936	−39.94	39.08	NAb3	NAbr
−56.377	−48.634	33.93	NAb3	NAbr
−44.244	−47.438	44.76	NAb3	NAbr
−45.635	−53.679	55.35	NAb3	NAbr
−48.295	−51.868	12.25	HAb4a	NAb3
−45.997	−45.204	17.43	HAb4a	NAb3
−45.164	−48.919	21.76	HAb4a	NAb3
−44.109	−43.14	25.08	HAb4a	NAb3
−49.686	−51.647	41.16	HAb4a	NAb3
−50.331	−52.102	50.74	HAb4a	NAb3
−44.555	−44.613	61.66	HAb4a	NAb3
−44.921	−44.396	137.65	HAb4a	NAb3
−44.662	−41.999	13.39	HAb4a	NAb4b
−44.655	−42.172	31.36	HAb4a	NAb4b
−56.185	−38.817	16.12	HAb4a	NAbr
−58.668	−43.38	40.02	NAbr	NAbr
−37.595	−48.313	16.77	NAbr	C1
−38.721	−51.999	9.75	NAbr	NH1
−46.861	−59.793	46.16	NAbr	NH1
−35.02	−38.202	29.98	NAbr	NH2
−51.892	−25.252	5.65	NAb1	NAbr
−52.208	−25.259	18.01	Nab1	NAbr

(*continued on next page*)

Table 4 (*continued*)

Crater latitude	Crater longitude	Crater diameter	Original unit	New unit
−43.181	−27.659	18.88	NArsp	NAbr
−43.062	−21.139	31.6	NArsp	NAbr
−41.351	−21.413	37.88	NArsp	NAbr
−42.975	−24.089	92.95	NArsp	NAbr
−57.411	−41.322	16.92	NArsp	NAbr
−44.129	−32.156	79.2	Cfs	NAbr
−37.056	−60.805	30.2	Nh2	Nh1
−64.622	−24.344	30.95	Nh2	Nh1
−63.796	−20.772	50.89	Nh2	Nh1
−64.161	−24.627	52.77	Nh2	Nh1
−63.402	−22.169	65.09	Nh2	Nh1
−38.218	−61.205	105.4	HNh4	Nh1
−57.335	−60.314	34.04	Nhb	Nh1
−57.532	−61.383	36.48	Nhb	Nh1
−37.224	−47.579	27.2	Nhb	Nh2
−51.377	−64.965	30.86	Nhb	Nh2
−51.692	−65.646	34.66	Nhb	Nh2
−49.95	−67.362	36.85	Nhb	Nh2
−35.987	−47.608	47.77	Nhb	Nh2
−50.833	−68.723	101.32	Nhb	Nh2

given older ages. Such a revision to crater populations of specific unit polygons is unique from existing geologic mapping investigations, as the total number of impact craters are normally tallied for determining the relative age of the rock materials without scrutiny of whether they are associated with underlying materials.

The geologic information was critical for estimating ages of several of the units. For example, unit HAb4a includes major emplacement of materials within the primary Argyre basin from Late Hesperian activity, with underlying basin materials extending at depth to the basin floor emplaced by earlier post-Argyre-impact activity, including Argyre-impact-related lake formation and subsequent climate/environmental conditions detailed below; i.e., part of the impact population includes exposed parts of the underlying craters and their rims. Coupled with the stratigraphic and cross-cutting relations, identification of the superposed (i.e., pristine and not visibly resurfaced; Table 3) >3-km-diameter impact craters using CTX data clearly indicates that a late stage of major resurfacing occurred during the Late Hesperian and Early Amazonian epochs, corresponding to Stages 4–5 (Late Hesperian–Early Amazonian) Tharsis development (Fig. 4).

4. Discussion

Here we give a brief overview of pre-Argyre and Argyre impact activity in the Argyre province. We then discuss: (1) the stratigraphic record of the Argyre province; (2) the basin conditions through time since the Argyre impact event, such as ancient surface modification including the timing and origin of the putative eskers located in the southeast part of the basin floor, new evidence for a paleolake within the Argyre basin that sourced Uzboi Vallis, and geologically-recent surface modification; and (3) the extent of Argyre-related tectonism and its influence on the surrounding regions, which includes a geophysical perspective.

4.1. Overview of pre-Argyre and Argyre impact activity

The giant Argyre impact event led to major resurfacing of the extremely ancient cratered highlands in the Argyre province, which includes destruction of the remanent magnetic signatures (Acuña et al., 1999, 2001; Connerney et al., 1999, 2001; Arkani-Hamed, 2003, 2004; Roberts et al., 2009; Roberts and Arkani-Hamed, 2012). Pre-Argyre deformation and uplift of the extremely ancient crustal materials included the formation of extremely ancient mountain ranges (e.g., the Thaumasia highlands and Coprates rise; Figs. 1 and 2), marking a dynamic ancient phase (i.e., during an active dynamo (Baker et al., 2007; Dohm et al., 2013; Ruiz, 2014)) of Mars. This includes major crustal contraction and shortening exemplified by thrust faults (Schultz and Tanaka, 1994; Dohm et al., 2001a, 2002a; Nahm and Schultz, 2011) and other prominent features (Dohm and Maruyama, 2014a; Dohm et al., 2014a,b).

The Argyre impact resulted in the formation of the primary Argyre basin, rim materials, deep-seated basement structures including faults, and structurally-controlled valleys and basins which have routed subsurface and surface water and rock materials. In addition, the impact event appears to have deformed the Thaumasia highlands mountain range and the southeast part of the Thaumasia plateau, as their southeast margins parallel the shape of the basin and outer ring structures (Dohm et al., 2001a) (Figs. 1 and 2). The Thaumasia highlands comprise distinct remanent magnetic signatures, large tectonic structures, and a relatively high density of impact craters distinct from the younger Tharsis lavas to the north–northwest and Argyre impact basins and mesas to the south–southeast.

4.2. Overview of the stratigraphic record

The oldest units of Early–Middle Noachian age consist of ancient, heavily cratered rock materials that form plateaus, hills, rugged mountains such as of the Thaumasia highlands mountain range which extend west to east for nearly 2400 km, approximately the length of the Himalayas, prominent ridges, and highly degraded crater rims (unit Nh1; see Tables 1–3 and Fig. 3 for this and other units) away from the Argyre basin and rim. A relatively small part of the Thaumasia highlands, located in the northwest part of the map region, is composed of mountain-range-forming materials, which have been highly modified by water-, wind-, gravity- magmatic-, and tectonic-driven activity and impact cratering. These materials have been mapped as unit HNTh, and interpreted as highly resurfaced basement complex, among other materials associated with the formation of an orogenic complex (Table 2).

This varied landscape was likely blanketed by ejecta from the Argyre impact event, at least within the Argyre province. Complex modification of these ancient rock materials due to cratering, tectonic deformation, erosional processes, and volcanic and sedimentary burial has degraded or destroyed many of the older morphologic features. This includes a substantial proportion

of the superposing crater populations, which makes it difficult to constrain the onset of unit formation (see Section 3.2). Thus, in many cases, morphologic features and rocky mantles postdating the rock-unit materials characterize the surfaces of these ancient units.

The giant Argyre impact event created distinct rim materials, mapped as units NAr, NArb, NAbr, and NArsp, likely excavated from deep within the mantle, and/or including primordial lower crustal materials transferred at and near the martian surface by the impact event and associated overturn and inversion of stratigraphy. Subsequently, they have been sculpted by liquid water, water–ice, wind, and mass wasting. The impact also formed a primary basin, which has served as a catchment of rock materials and water since the event. Source regions of the materials and water include the nearby rim materials to at least as far away as Tharsis to the northwest and the South Pole to the south.

There are several indications of a high-standing lake that fed the Uzboi system, supportive of the original hypothesis presented through the multiple Parker et al. (Parker, 1985, 1989, 1994; Parker and Gorsline, 1991, 1992, 1993; Parker et al., 2000). Distinct from this original hypothesis, which includes the system having formed at a time when there reportedly was change from a warm/wet climate to a drier climate that allowed surface water (channels and lakes) during the Late Noachian (see Parker, 1996), this geologic investigation points to the Argyre lake-Uzboi system having formed much earlier due to the giant Argyre impact event and the associated regional melting of ice (water inundation in the Argyre province maps out at least within the dark blue regions shown in Fig. 1). The indications include impact-crater retention ages of the high-standing materials in the primary basin identified, mapped, and interpreted to be the oldest basin-filling materials emplaced through major hydrological and environmental change directly associated with the giant impact event, which includes lake formation (i.e., member 1 of the Argyre basin infill materials designated as unit NAb1; Fig. 3 and Tables 1–3). Also, there are spatial associations (including stratigraphic and elevation) among the source region of Uzboi Vallis, terraces, benches, a possible spillway of a local basin shown in Figs. 7 and 8, and the mean elevation of unit NAb1 (Fig. 5), all of which near an elevation of 0 km (as a potential equipotential surface (compare Figs. 5–9)). The close timing of the Argyre impact event and lake formation is corroborated by similar crater retention ages amongst the Argyre-rim materials (e.g., units NAbr and NArb) and the older, higher-standing unit Nab1 materials. An older retention age of the latter (see Table 3) could be explained by the rim-forming materials having undergone greater erosion due to their greater relief. An extensive impact-associated lake could have existed well above 0 km, nearing an elevation of 1.5 km. This is particularly evident when using GIS to visualize the potential water extent beyond the primary Argyre basin, which includes mapped elongated basins with valley networks along their margins and dendritic valleys (Fig. 9), further detailed in Section 4.3.2.

In addition to the primary basin resulting from the Argyre impact event, local structurally-controlled basins also formed

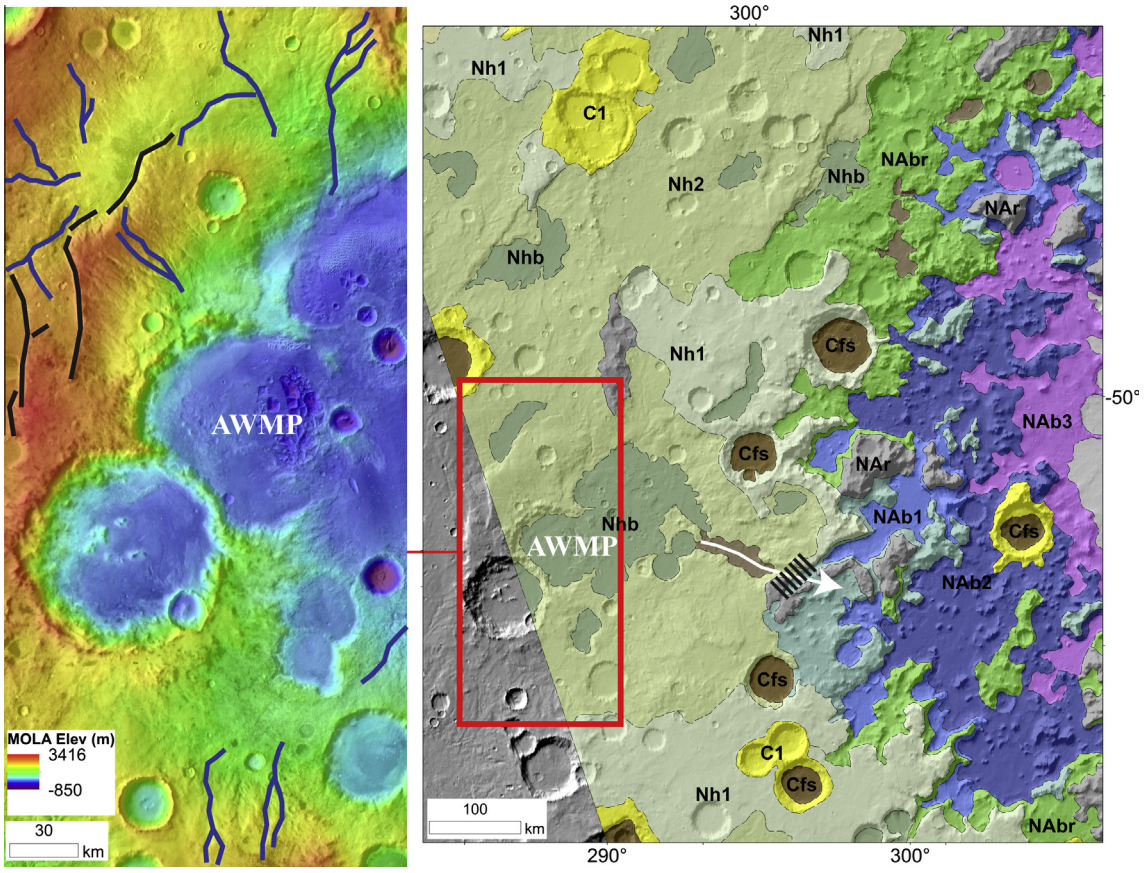

Fig. 7. Based on Dohm et al. (2011a), MOLA color shaded relief map coupled with a THEMIS IR daytime mosaic highlighting the western part of the Argyre western margin paleolake (AWMP, left) and its location with respect to the Argyre basin as shown on part of the geologic map of Fig. 3 (right). Argyre-induced tectonic structures (left, black lines), drainage systems that debouched into the basin (left, representative drainages highlighted by blue lines), and a possible spillway (right, white arrow which also marks a graben-like structure that may have influenced water flow or later deformed the possible spillway). Note that the drainage systems terminate within a contour interval generally ranging from 0 to 1.5 km (within the green-highlighted topography, which could mark a topographic bench and once associated high-standing lake); the latter elevation occurs at a possible spillway divide (right, dashed black line) at present-day topography (see Fig. 8). (For interpretation of the references to color in this figure legend, the reader is referred to the web version of this article.)

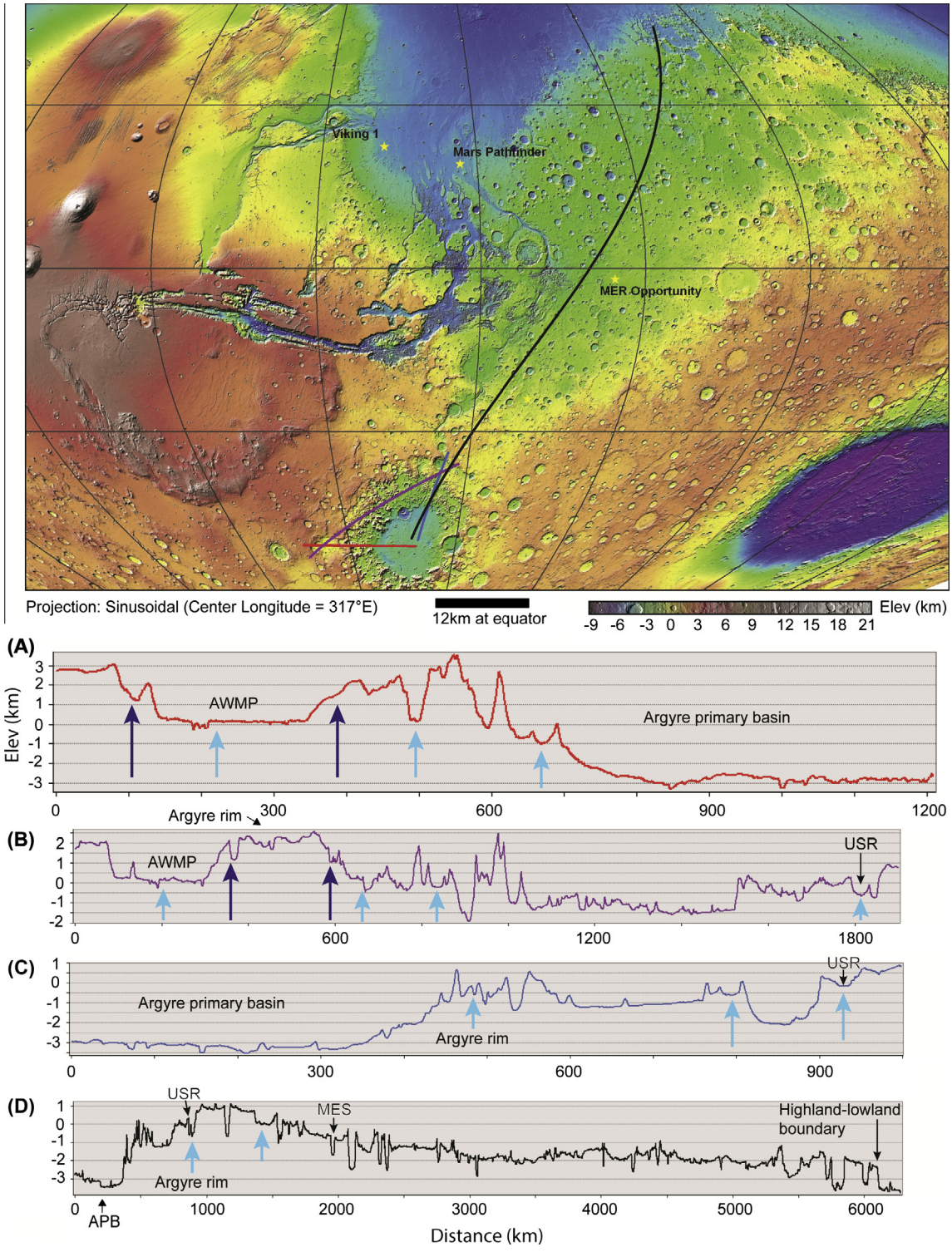

Fig. 8. Topographic profiles (A. red, B. violet, C. blue, and D. black) and associated transects annotated on a MOLA map (top) through the Argyre west margin paleolake (AWMP), Uzboi spillway (USR), Argyre primary basin (APB), and Argyre rim materials. Note the potential equipotential surface of the highest standing Argyre lake, AWMP, and USR, and the mean elevation of the highest occurring and oldest member/sequence of the basin infilling materials (unit NAb1) at a similar elevation shown in Fig. 5 (hovering around an elevation of zero (light blue arrows)), as well as an even higher potential equipotential surface indicated by benches, terraces, possible spillway of AWMP into the primary Argyre impact basin, and higher reaches of unit NAb1 (nearing 1.5 km (dark blue arrows)). Hydrologic activity would have involved the margins at higher reaches, and the Uzboi drainage system would have cut into the impact crater rim materials. (For interpretation of the references to color in this figure legend, the reader is referred to the web version of this article.)

among rim materials and adjacent to the primary basin and its rim, as well as served as catchments for liquid water, water–ice, and sediments. For example, drainages, which include valley networks, mark the margins of and debouch into many of the local basins indicating that many contain sedimentary, lacustrine, and evaporite deposits, mapped as units NHb and NArsp (e.g., Figs. 3, 7 and 8;

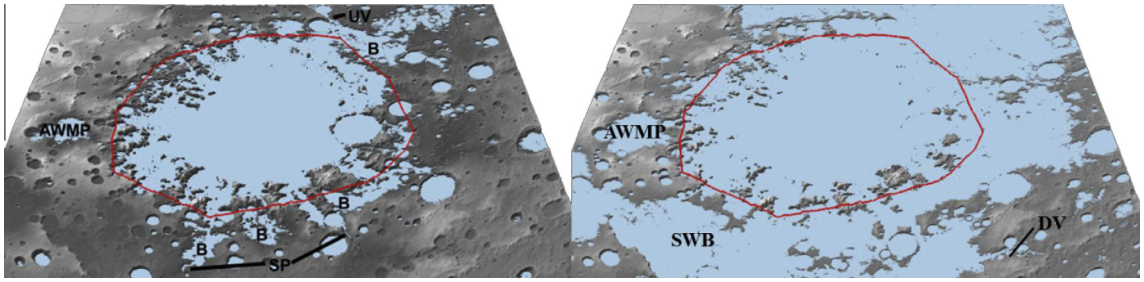

Fig. 9. (Left) Based on Dohm et al. (2011a), schematic paleolake map of the Argyre basin using a maximum topographic elevation of 0 km based on MOLA topography (regions in blue). An estimated extent of the hypothesized Argyre lake based on geomorphologic and topographic analyses, as well as detailed geologic mapping is also shown (red line). In addition to the estimated extent, dendritic channel systems (SP), local basins (B) which occur among the crater rim materials, and the Uzboi Vallis system (UV) correspond to the blue-highlighted region. Also shown is a small extent (near base level) of AWMP. The volumes of the hypothesized AWMP and Argyre lakes are estimated to be 1.6×10^4 and 1.9×10^6 km^3, respectively, using MOLA. There is significant evidence of water–ice modification (e.g., glaciation) as shown by e.g., Hiesinger and Head (2002). Ever changing conditions in the Argyre basin includes a possible interplay among lakes, ice sheets, and glaciers through time, including waning water bodies. Also compare with Figs. 3 and 5–8. (Right) Similar to left, but at 1 km with an estimated volume of 3.1 million km^3, nearing that of the Mediterranean Sea. Note that the potential water extent maps to a greater extent of the AWMP lake, the drainage basin located to the southwest of the Argyre basin (SWB), which displays drainage networks along its margins, and a distinct dendritic valley located to the southeast of the primary Argyre basin (DV). (For interpretation of the references to color in this figure legend, the reader is referred to the web version of this article.)

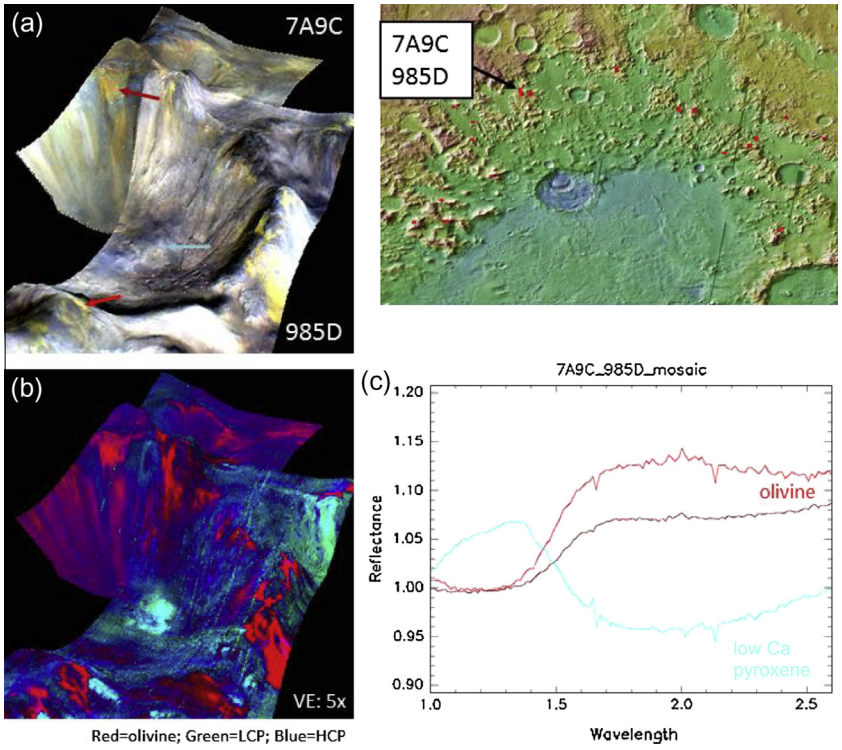

Fig. 10. CRISM-based information combined with the MOLA data and geologic map of this investigation and for spectroscopic/stratigraphic investigation (spectroscopic information corresponds with unit NAbr—Argyre basin and rim materials; see location on geologic map of Fig. 3). Example of olivine and low-calcium pyroxene outcrops in the Nereidum Montes; these are mountainous highly degraded Argyre rim materials mapped as unit NAbr materials. (a) Mosaic of CRISM FRT observations 7A9C and 985D, with location shown on a MOLA map (top right), draped over MOLA topography (vertical exaggeration x5). (b) Mosaic of summary parameters of FRT 7A9C and 985D. Red indicates olivine, green indicates low-calcium pyroxene and blue indicates high-calcium pyroxene. (c) Sample ratioed spectra from FRT 7A9C and 985D. Location of where each spectrum was acquired is indicated by arrows in part (a). Dark red arrow indicates location of dark red olivine spectrum, bright red arrow indicates location of bright red olivine spectrum, teal arrow indicates location of teal low-calcium pyroxene spectrum. The CRISM data corroborates the Argyre-rim materials in part being uplifted ancient upper mantle materials, and that the terrains, which are distinctly hydrologically modified, contain magnesian lithologies such as olivine-dominated rocks (Buczkowski et al., 2008a,b, 2010). (For interpretation of the references to color in this figure legend, the reader is referred to the web version of this article.)

See also Section 4.3). Hydrothermal deposits related to the Argyre impact event, eolian deposits sourcing from nearby (rim materials) and distant provenances (e.g., Tharsis), and lower crustal materials and/or upper mantle materials also likely contribute to the rim materials and basin infill deposits of the basins structurally controlled by the Argyre impact. Consistent with this is the CRISM-based identification of olivine, prehnite, chlorite, low-calcium pyroxene, high-calcium pyroxene, and phyllosilicates such as iron–magnesium smectite among some of the local basins and rim materials, as well as parts of the primary basin margin (Figs. 10 and 11; also see Poulet et al., 2007; Buczkowski et al., 2008a,b, 2010; Lane and Goodrich, 2010; Ody et al., 2012). In addition, phyllosilicates are relatively common in the cratered highlands as observed by both Omega instrument onboard the Mars Express spacecraft (e.g., Bibring et al., 2004, 2005; Poulet et al., 2005, 2007) and CRISM instrument onboard the Mars

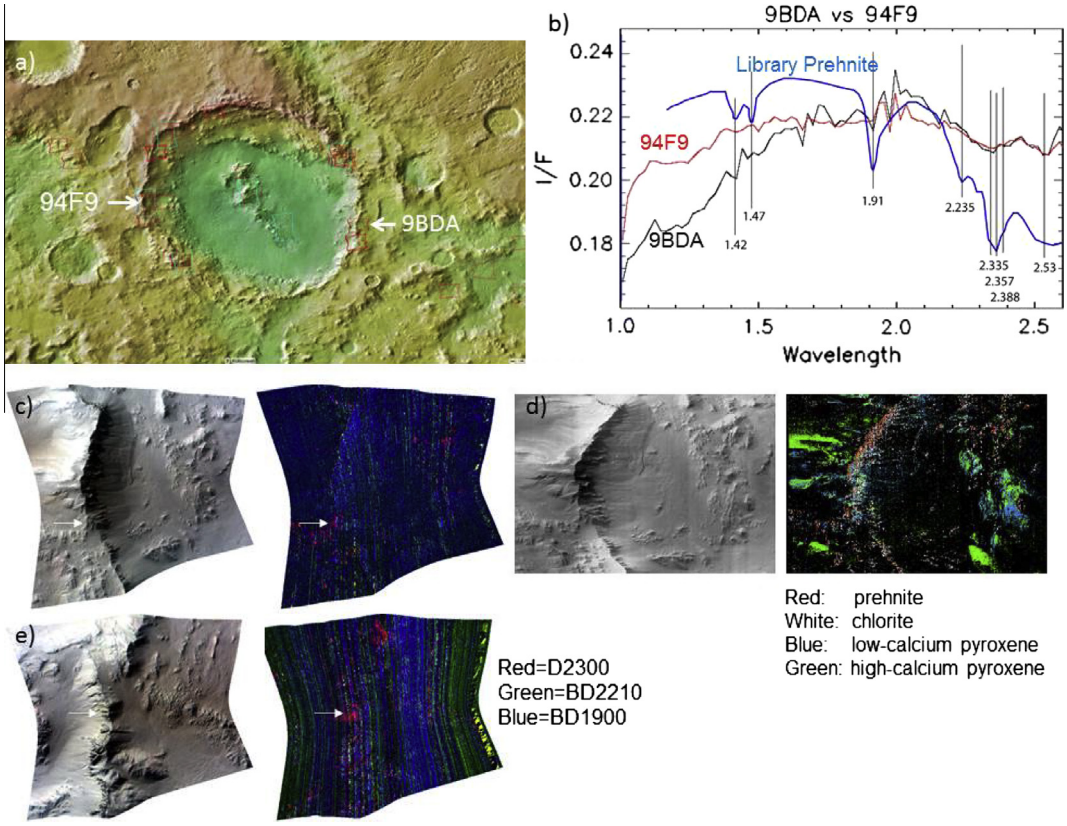

Fig. 11. CRISM-based information combined with the MOLA data and geologic map of this investigation for spectroscopic/stratigraphic investigation (spectroscopic information corresponds with unit C1—old crater materials; see location on geologic map of Fig. 3). Location of CRISM images FRT94F9 and FRT 9BDA observations covering parts of the rim and floor materials of Hale crater shown on a MOLA map ((a) white arrows). (b) Sample spectra from CRISM FRT 9BDA (black line) and 94F9 (red line). Blue spectrum is of a library prehnite (USGS spectral library splib06a). Black vertical lines mark out wavelengths of interest. (c) Geo-referenced CRISM image FRT 94F9 (left) and summary parameter image (right). Arrows point to location where spectrum in part (b) was sampled. (d) Tetracorder analysis of FRT 94F9 indicates that chlorite and prehnite are common on the Hale crater rim, while both low- and high-calcium pyroxenes are present both on the crater floor and outside the crater. (e) Geo-referenced CRISM image FRT 9BDA (left) and summary parameter image (right). Arrows point to location where spectrum in part (b) was sampled. These minerals are consistent with Argyre-impact-modified terrain, including the excavation of relatively olivine-rich, deep mantle and/or primordial crustal materials transferred at or near the martian surface by the impact event and associated overturn and inversion of stratigraphy, as well as hydrothermal activity possibly persisting for millions of years following the Argyre impact event. The Hale-crater-forming impact event occurred near the spillway of Uzboi Vallis, and thus possible water enrichment of the Hale target materials may have contributed to hydrothermal activity related to the Hale impact event subsequent to the relatively long-lived Argyre-driven hydrothermal activity (estimated to have persisted for 10 Ma (Abramov and Kring, 2005) following the ~3.93 Ga Argyre impact event (based from Robbins et al., 2013). (For interpretation of the references to color in this figure legend, the reader is referred to the web version of this article.)

Reconnaissance Orbiter (Murchie et al., 2007, 2009a,b; Mustard et al., 2008), and in particular, exemplified in structurally-controlled basins such as in Terra Sirenum (e.g., Davila et al., 2011) and those Argyre-impact-induced in the Argyre province (e.g., Buczkowski et al., 2008b).

Following the Argyre impact event, climatic perturbations away from the prevailing cold and dry conditions (Fairén et al., 2003; Baker et al., 2007; Hynek et al., 2010; Rossi et al., 2011), related to the major stages of growth of the Tharsis superplume such as exemplified by the opening of Valles Marineris, major activity at Syria Planum, and the uplift of Thaumasia plateau and associated circum-Chryse and putative northwestern slope valleys development (Stages 1–3 of Tharsis evolution as shown in Fig. 4) (Dohm et al., 2001b, 2007a, 2009a), resulted in transient hydrological cycling and related dynamic landscape modification of the Argyre province. This included major etching of the rim materials, units NAr, NArb, NAbr, NArsp, as well as resurfacing of the cratered highlands away from the Argyre rim materials, such as the rock materials of unit Nh1 which includes extremely ancient crustal materials which were blanketed by extensive Argyre impact ejecta in the Argyre province. Resurfacing of the ancient cratered highland materials included erosion and the emplacement of deposits on the Argyre-impact-controlled landscape well into the Hesperian Period, contributing to units Nh1–Nh3, HNh4, Nhb, HNTh, AHTp. Both endogenic and exogenic activity contributed to the resurfacing of the terrains within and marginal to the Agyre basin and rim materials, including precipitation and the growth of glaciers and the formation of gullies within impact craters, even into the very Late Amazonian epoch (El Maarry et al., 2013; Soare et al., 2014a,b).

Associated with the major resurfacing described above are Argyre basin infill deposits (units NAb2, NAb3, NAb4b, and HAb4a) which overly unit NAb1 materials, as the Argyre basin has served as a large repository of the eroded Argyre rim materials and cratered highland materials away from the rim materials following the Argyre impact event. The spiked hydrologic activity related to Tharsis activity resulted in the migration of groundwater and surface water and the eventual formation of ice-covered lakes which would wane in volume and transition into frozen ice bodies, as well as the growth of glaciers, but to a lesser extent than the former impact-induced lake. Pronounced growth of Argyre's neighboring prominent martian feature, Tharsis superplume, during the Middle Noachian to Early Hesperian, had accompanying flooding, ocean formation, hydrological cycling, and dissection of the martian landscape which included the rugged rim materials. This Tharsis-driven resurfacing shed materials into the basin distinctly recorded in units Nab2, Nab3, and Nab4b (see Table 2 for details, including descriptions and interpretations).

Near the upper left corner of the geologic map shown in Fig. 3, at an apparent break between the Thaumasia highlands and the Coprates rise mountain ranges near the southeastern margin of the Thaumasia plateau, networking troughs source from a rift system. The troughs appear to dissect friable materials interpreted to be ignimbrites (unit HNplt of Dohm et al., 2001a—see Fig. 9a), mapped and identified here as unit AHtp of the Thaumasia plateau. Such geologic and hydrologic activity (including fluvial, alluvial, colluvial, and glacial), which includes the formation of the troughs, resulted in a transferal of water and rock materials from the Thaumasia highlands and Coprates rise mountain ranges and the Thaumasia plateau to the transition zone at lower elevations (Figs. 1 and 2). The emplacement of the materials along the break in slope is evident by partial burial of wrinkle ridges, with only ridge crest exposed in places.

Major Tharsis activity during the Late Hesperian (Stage 4) included major outgassing associated with the development of the Tharsis Montes shield volcanoes, Olympus Mons, and Alba Mons, as well as rapid emplacement of circum-Chryse floodwaters and sediments to form an ocean inset within the extent of the previous larger ocean and associated hydrological cycling (Baker et al., 1991; Fairén et al., 2003). This would have driven environmental change in the giant catchment basin, resulting in the emplacement of fluvial, lacustrine, and glacial deposits on the basin floor, mapped and defined as unit HAb4a. Unit HAb4a records the final major sedimentary sequence in the Argyre basin, with the deeper floor deposits underlying this unit likely to be related to the initial Argyre-impact-related lake (unit Nab1) and Stages 1–3 (Noachian–Early Hesperian) of Tharsis development (Fig. 4), correlating in age with units Nab2, NAb3, and NAb4b (unit NAb4b occurs along a part of the northern and northeastern margins of the central basin floor materials, being distinctly embayed by unit HAb4a). This final sequence included flooding and emplacement of sediments and burial of volatiles and eventual release to form vent structures. For example, related to this geologic investigation, Argyre Mons is a newly identified feature interpreted to have formed from subterranean gas releases (e.g., mud volcanoes), magmatic-driven activity, or an impact event, with gas release being the favored

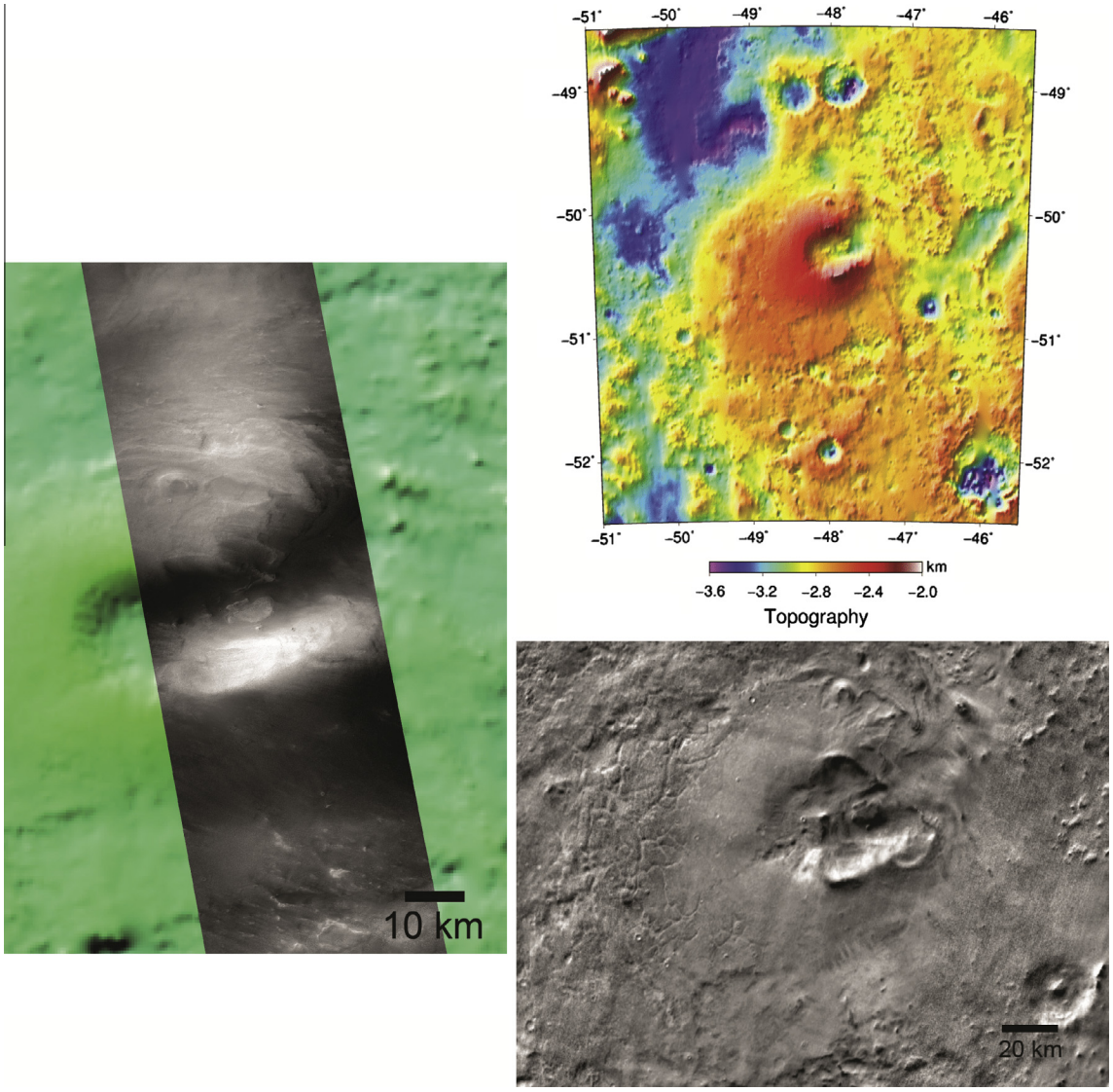

Fig. 12. Based on Williams et al. (2014), possible vent structure at the floor of Argyre basin (see location on geologic map of Fig. 3). The landform could be a sedimentary (e.g., mud volcano), volcanic (e.g., cinder cone or maar), or impact-related feature, either formed before (i.e., now exhumed through differential erosion), during emplacement of unit HAb4a, or following emplacement of unit HAb4a; high-standing 'rim' is ~1 km higher than interior and surrounding terrain. (Top) MOLA DEM and (bottom) THEMIS daytime IR (middle) CTX superposed on MOLA. Late Hesperian (or younger) venting of volatiles during the emplacement of unit HAb4a sediments, which includes flooding, ponding to form a lake, and rapid sedimentation during the final sequence of the basin infill deposits, could have resulted in mud volcanism along the floor of the basin.

hypothesis (Fig. 12; Williams et al., 2014). Numerous and widespread vent structures in the northern plains, interpreted to be mud volcanoes, are likely the result of rapid emplacement of circum-Chryse floodwaters and sediments and associated ocean formation (Skinner and Tanaka, 2007; Skinner and Mazzini, 2009; Oehler and Allen, 2010; Komatsu et al., 2011, 2012), related to Stage-4 Tharsis-driven activity.

The emplacement of unit HAb4a is coincident with the development of equatorial glacial landscapes in the Aeolis Mensae region (Davila et al., 2013) and possibly along parts of Mount Sharp (Fairén et al., 2014), all of which could be tied to Stage-4, Tharsis-driven environmental change (Fig. 4). Magmatism and associated flooding sourcing from the Tharsis superplume, with floodwaters more acidic and briny at the source of the superplume-driving heat engine, included ponding of sediment-laden floodwaters in the northern plains (Dohm et al., 2009b). We hypothesize here that the Tharsis-induced transient hydrological cycling included precipitation over the promontories of Tharsis and away from Tharsis such as at the south pole and Argyre with the concentration of more neutral water; i.e., the initial water outbursts were more acidic due to its magmatic source resulting in magma-water-related deposits such as sulfates vs. latter phases of the magmatic-induced transient hydrological cycle such as snowfall and related ice sheet, glacial, and ground ice accumulations. Such relatively cold hydrological cycling beyond the Tharsis superplume may have contributed to the growth of glaciers in Gale Crater and elsewhere (Davila et al., 2013; Fairén et al., 2014).

In addition to late-stage Tharsis superplume activity, but to a lesser extent, the growth of Elysium superplume (e.g., Baker et al., 2007) and changes in obliquity and eccentricity (e.g., Touma and Wisdom, 1993; Laskar et al., 2004), may have also contributed to the youngest mapped basin unit (member HAb4a), as well as resurfacing of most of the surfaces within and outside of the Argyre basin. This includes the partial infill of topographic lows of the modified highlands terrain largely through sedimentary processes, as well as rock materials being shed from the Thaumasia highlands into the transition zone (Figs. 1 and 2). Corroborating this, the superposed-only crater statistics point to final major resurfacing during the Late Hesperian/Early Amazonian for most of the geologic units (i.e., that which could destroy crater populations exceeding 3 km; Table 3).

Basin-forming events are not limited to the Early–Middle Noachian, as there were impact events such as the formation of Lowell Crater (Late Hesperian and possibly much more recent) that post-dated the Argyre basin-forming one; this would have resulted in local to regional deformation and flooding (Lias et al., 1997). Another example includes Galle Crater. Not only does it deform the southeast part of the Argyre basin, but also appears to have contributed to the formation of valleys that debouch into the southeast part of the basin (south of the impact crater; see the features mapped as troughs in Fig. 3 located along the southern margin of the central part of the ejecta blanket of Galle) and disrupted floor deposits.

The volatile enrichment of the Argyre basin and its associated structures and rock materials, resulting from the climatic perturbations and environmental changes discussed above, largely shielded from atmospheric conditions by dry mantles similar to ancient glacial ice in Antarctica, would play a significant role in shaping a dynamic landscape in geologically recent time, and possibly presently. Relatively recent atmospheric precipitation is likely to have played a role in the modification of the regional landscape, including the flow of materials from high reaches towards the basin floor pronounced in the basin materials (El Maarry et al., 2013). Such evidence, possibly indicative of glacial, colluvial, and/or alluvial activities, corroborates earlier investigations that indicated widespread glacial activity in martian history, some of it comparatively recent, perhaps as late as the Middle or even Late Amazonian (Kargel et al., 1995; Head et al., 2003; Kargel, 2004; Madeleine et al., 2009).

Periglacial activity, climate-controlled and influenced by such long-term (i.e., since the Argyre impact event), water-enrichment in the basin and surroundings, has been and continues to be a major resurfacing agent (El Maarry et al., 2013; Soare et al., 2014a,b). The primary basin, local basins, and structurally-controlled valleys may contain Antarctic-like paleosols that record far-reaching environmental information dating back billions of years (Mahaney et al., 2001, 2009, 2011). In addition, internal heat and volatiles migrating along basement structures may contribute to geologically recent and even possibly present-day modification of parts of the basin, expressed in the form of fault and fracture systems, gullies, and open-system-pingo-like structures (Soare et al., 2014b). Characteristics of multiple Argyre gullies are consistent with an origin involving liquid water (Conway and Soare, 2013), which could involve brines, a hypothesis consistent with features elsewhere on Mars interpreted to involve brines such as dark slope streaks (Ferris et al., 2002; Miyamoto et al., 2004) and slope linea (McEwen et al., 2013). The impact-influenced dynamic landscape during ancient and geologically recent times is further discussed in Section 4.3.

4.3. Basin conditions from impact to today

Ancient (Argyre impact and post-impact) and geologically recent activity induced by magmatic-, orbital-, impact-, weathering-, and climatic-driven phenomena (some of which are often interlinked) are recorded in the fluvial-, lacustrine-, glacial-, and periglacial-sculpted terrains of the Argyre province. For example, there is a wide array of landforms suggestive of a dynamic landscape modified by wind, liquid water, water ice, and gravity-driven processes. This includes dune deposits in topographic lows, valleys that dissect the Argyre basin rim materials and the margins of local basins, alluvial fans, valley-filling deposits with flow features, crevasse-like fractures, tarns, cirques, megaflutes, drumlins, eskers, gullies, and terraces, and small-scale polygonal-patterned ground comprising high and low-centered polygons (e.g., Hiesinger and Head, 2002; Kargel, 2004; Banks et al., 2008, 2009; Soare et al., 2014a,b). The polygons mark relatively young and possibly ice-rich mantled terrain that is extant in wide-ranging and pristine in some instances and truncated and/or dissected in others (see discussion in Section 4.3.3).

During ancient times (Noachian–Early Amazonian: ~>1.23 Ga based on the model of Hartmann and Neukum (2001)), hydrological cycling due to major geologic activity outside of the Argyre province, following the Argyre-basin-filling lake (Argyre-impact induced, as further discussed below), exchanged water from both the atmosphere and groundwater. This is exemplified by sharp, transient climatic changes triggered by igneous activity of the Tharsis superplume (Baker et al., 1991, 2000, 2002; Dohm et al., 2000, 2007a, 2009b; Fairén et al., 2003; Kargel, 2004) (Fig. 4). This water cycling in the Argyre basin could have included south-to-north hydraulic gradients in the groundwater system built up over time by south polar glacial activity (e.g., Head and Pratt, 2001).

Other geologic activities outside of the Argyre province, such as the growth of Elysium and impacts events such as Lowell and Galle would have also influenced hydrological and environmental conditions in the deep Argyre impact basin. Lowell crater, a relatively pristine, double-ring impact crater, located to the west of the Argyre basin, is interpreted to have formed during the Late Hesperian–Early Amazonian. This crater in particular may have contributed to environmental change in and surrounding Argyre

basin following its formation. The diameters of the outer and inner rings are about 195 km and 85 km, respectively, comparable to the 180-km-diameter Chicxulub crater, which is associated with profound global-scale environmental changes that most likely contributed to the demise of the dinosaurs at the boundary of the Cretaceous and Tertiary Periods (Alvarez et al., 1980). The Lowell impact triggered a series of events: (1) formation of secondary craters on surrounding rock outcrops in the Lowell and Thaumasia regions as much as 800 km from the rim of the impact crater, (2) production of meltwater and associated channel dissection of rock outcrops to the northeast and southwest, indicating ice-enriched target materials, and (3) a massive debris flow, which embayed and partly buried structures to the southeast (Lias et al., 1997).

Depending on climatic conditions and the nature of the cycling processes, whether endogenic or exogenic, the cycling may have involved groundwater discharges into an ice-covered lake, spring-fed activity, catastrophic outburst floods, ponding to form lakes in the primary basins that would eventually freeze, gelifluction of rock materials, debris flow and alluvial fan development, and glacier accumulation and inflow into the basin. The water reservoirs would eventually ablate and be mantled and shielded from atmospheric conditions.

During geologically recent times, the atmospheric cycling of water through late-stage volcanism, such as from the Tharsis/Elysium corridor region (Dohm et al., 2008 and the references therein), may have contributed to environmental changes in the Argyre basin and surrounding regions as well, especially when considering the physiographic setting of the deep Argyre basin and the adjacent Tharsis. In addition, variations in orbital and spin parameters within the last tens of millions of years, and associated hydrological cycling, may be responsible for the development of glacial deposits down to the mid latitudes (Head et al., 2003), and potentially would have had a bearing on changing environmental conditions of the Argyre basin and surrounding regions.

Orbital and spin parameters have been invoked by numerous authors to explain various sets of features on the surface of Mars. These include the presence of debris aprons and potential dust-covered glaciers at the mid-latitudes, latitude-dependent mantling, and aureole deposits associated with Olympus Mons and other volcanoes in the Tharsis region, as well as very recent (i.e., within thousands of years) landscape changes putatively ascribed to periglacial processes and freeze–thaw cycling (e.g., Costard et al., 2002; Banks et al., 2008, 2009; Fastook et al., 2008; Raack et al., 2012). The first comprehensive solutions for the variation in obliquity and eccentricity for Mars were presented by Laskar et al. (2004) and remain the most accurate solutions for the last ~20 myr.

Periods of high obliquity (>30°) are usually invoked in order to trigger the sublimation of ice deposits at the poles into the atmosphere and their deposition at the mid-latitudes (e.g., Laskar et al., 2004). Such periods of high obliquity would have affected environmental conditions in the Argyre basin including possibly allowing the melting of ice-rich materials (i.e., interstitial ice in the pore space of sediments, lenses of ground ice, and mantled covered glaciers and ice) (Kargel, 2004). Contributions in geologically recent times from precipitation, and possibly present-day fog (Neumann et al., 2003) and snow, all may have contributed to surface modification, including periglacial activity, as well as life if existing. The above conditions make the Argyre province a prime astrobiologic target on Mars, but due to its vastness, new mission designs will likely be required to optimize the search for life (Fink et al., 2005, 2007a,b, 2008; Schulze-Makuch et al., 2012).

4.3.1. Ancient surface modification

On Earth, large and often structurally-controlled basins act as catchments for volatiles and sediments. They record geologic and hydrologic activity including environmental changes and perturbations in climate at local and global scales. Basement structures, including faults, fractures, and joints, often serve as conduits for the movement of volatiles in both the subsurface and surface environments. Even in arid deserts on Earth water can be routed along basement structures at depth, as occurs in the Atacama Desert; here, water runoff from the Andes is channeled to the Pacific Ocean along deep-seated basement structures in which microbial life may thrive (Dohm et al., 2011b).

In the case of the Argyre impact event that resulted in a complex of basement faults, fractures, and joints, including deep-seated and shallow faults concentric and radial about the basin, the structural control of volatile migration likely played a significant role in the hydrogeologic history of the Argyre province. This includes the formation of the hypothesized Argyre impact-induced lake and linked Uzboi Vallis, as well as subsequent hydrogeologic activity such as related to major pulses of Tharsis-driven activity (Fig. 4). Groundwater models by Harrison and Grimm (2009) corroborate structurally-controlled migration of groundwater into the Argyre basin highlighted by this geologic investigation.

If the basin filled during a glacial climate period, ice accumulation and glacial inflow into an ice-covered lake or sea may have taken place (Kargel and Strom, 1992; Kargel, 2004). The ice cover may have acted to dam the Uzboi outlet, but periodic disruptions of the dam may have generated megafloods, which helped to carve Uzboi Vallis and could have contributed to environmental and marine depositional changes in the northern plains (Parker and Gorsline, 1991; Dohm et al., 2011a).

The influence of the Argyre impact extends well beyond the basin, rim, and adjoining cratered plateau regions. For example, impact-influenced terrain and regional drainage is observed along the southeastern margin of the Thaumasia plateau and the transitional zone that separates the Thaumasia plateau from the Argyre basin and rim regions (Dohm et al., 2001a). Also, major drainages originate on plateaus 1600 km to the south (to Dorsa Argentea's system of sinuous ridges; Kargel and Strom (1990, 1992)), over 700 km to the southeast, and 900 km east of Argyre; these ancient valley systems incise the Charitum Montes and terminated near the margin of the primary basin near sinuous ridges in the southern Argyre Planitia.

Deposits, which partly infill the impact-derived structurally-controlled primary and secondary basins and modified valleys, record surface modification in the Argyre province resulting from major changes in environmental and hydrological conditions detailed above. These include the initial Argyre impact event and associated lake formation followed by endogenic activity largely related to major stages of growth of the Tharsis superplume (Fig. 4), with lesser activity such as related to other volcanic provinces such as Elysium, the Tharsis/Elysium corridor, impact events such as Lowell and Galle, and changes in obliquity and eccentricity. Possible lake formation in the immediate aftermath of the Argyre impact event may have been followed by progressive deep freezing of the lake as hydrothermal activity decreased over time, as radiogenic heat flow then also declined, and sublimation of ice gradually thinned the frozen lake until the cold climate froze it completely to its base. Climatic oscillations may have caused debris-covered glaciers to wax and wane episodically and gradually erode the rim mountains and transfer sediment deeper into the basin.

Detailed topographic analysis of the sinuous ridges located in the southern Argyre basin was completed for three of the main ridges of the southeast part of the Argyre basin (Fig. 3): Cleia Dorsum, Pasithea Dorsum, and Charis Dorsum (Banks et al., 2009). Results of this analysis indicated that the Argyre sinuous ridges cross topography and that the ridges tend to have sharper

crested shapes and increasing ridge heights on descending slopes, and low, broad, and more rounded shapes and decreasing ridge heights on ascending slopes (see Fig. 5 of Banks et al. (2009) for location within basin and profiles). These results indicated that the Argyre sinuous ridges may have been formed by a pressurized flow as opposed to an open air, gravity-driven flow such as in an open river channel (Banks et al., 2009). The characteristics of the southern Argyre sinuous ridges are therefore consistent with those of terrestrial eskers and are related to flow processes associated with meltwater flowing in tunnels beneath or within a large ice deposit (Shreve, 1985). Terrestrial eskers commonly climb and cross topographic divides because water flowing within or beneath a large ice mass is under hydraulic pressure. In descending ice tunnels, viscous heat produced by flow of meltwater causes melting of the tunnel walls increasing the height of the tunnel and the resulting, sharper esker ridge. Meltwater flowing in ascending tunnels has less viscous energy resulting in freezing of water onto the walls and particularly the top of the tunnel and, consequently, the formation of shorter, broader, and more rounded ridge heights (Shreve, 1985). Conversely, the ascending and descending undulations of the sinuous ridges appear to be inconsistent with the shoreline origins hypothesized by Parker (1994) and Parker and Gorsline (1992). However, some local ponding of water may have contributed to the layering observed in terrain surrounding many of these ridges (Kargel and Strom, 1992; Kargel, 2004; Banks et al., 2009). Altogether, these observations support the hypothesis that the Argyre sinuous ridges are eskers that formed from meltwater flowing at times in tunnels beneath a large ice deposit and at times in open channels within the ice deposit in the southern Argyre basin (Kargel and Strom, 1992; Hiesinger and Head, 2002; Kargel, 2004; Banks et al., 2009).

Mapping efforts of this geologic investigation indicate that the esker-like narrow ridges would have been associated with the late-stage emplacement of basin sediments mapped as unit HAb4a, which is interpreted to be related to Stage-4 Tharsis (Late Hesperian–Early Amazonian) development (Fig. 4), or the last major stratigraphic sequence of the basin infill deposits (NAb1, Nab2, Nab3, NAb4b, HAb4a) discussed above.

4.3.2. New evidence for a lake within the Argyre basin that sourced Uzboi Vallis

Did a large Argyre lake source the Uzboi Vallis drainage system during the Noachian Period, as hypothesized during a Viking-era investigation (Parker and Gorsline, 1991)? This very important question, being a main focus of this geologic investigation, is addressed through comparative analysis among the stratigraphic, geomorphologic, structural, and MOLA topographic information. For example, spatial and temporal relations amidst the possible equipotential surface of the Uzboi spillway (Fig. 8) can be readily compared to features around the basin. These features include high-standing unit NAb1 materials, which are mapped as the oldest valley- and basin-filling materials (member 1 of the Argyre basin sequence; Tables 1–3, Figs. 3, 5, and 6), terraces and benches (Figs. 7 and 8), and valleys incised into existing valleys at certain elevations (Figs. 3 and 6). There is a direct correlation between these feature types, indicating that the base level of a water body played a significant role in resurfacing the basin. The base level hovers around the zero-elevation level (Fig. 5) due to a likely change in a fluctuating hydraulic head following the formation of the Argyre lake, as well as extensive resurfacing (i.e., both erosional and depositional processes) since the lake formed directly following the impact event (~3.93 Ga), and isostatic adjustment since the impact event interpreted based on stratigraphy and impact crater statistics.

A possible key piece of evidence that the base level of the putative Argyre lake may have reached the height of the spillway of Uzboi Vallis (including the surface of the lake and associated groundwater system) is a recently identified lake basin located on the western margin of the Argyre impact basin (Figs. 1, 7, and 8); this is referred to as the Argyre western-margin-paleolake basin (AWMP; Dohm et al., 2011a). A paleolake is inferred by the series of distinct drainage systems that debouch into the basin (Fig. 7). Drainage systems terminate near a possible bench that occurs at a topographic interval ranging from 1 to 1.5 km, an elevation range which corresponds with a possible spillway that separates the paleolake basin from the Argyre basin (Fig. 8). The spillway divide occurs at an elevation of ~1.5 km. It must be noted that paleotopography may vary significantly from the present-day topography due to factors such as post-impact isostatic adjustment, which includes tectonic uplift or subsidence, and erosion.

The paleolake, alternatively, may be independent of the Argyre lake, having formed later in time and with no link to an Argyre-lake-related hydrologic system. But if the water was as high as 1 km as shown in Fig. 9, or more, or ranging between 0 km and 1 km, then a linkage is possible. In addition to the high-standing unit Nab1 materials and terraces and benches in part formed by valleys that dissect these oldest basin infill deposits within existing valleys (Figs. 3 and 6), by considering a water column of the lake that would reach the 0 km contour interval (Figs. 5 and 7–9) – a conservative value (nearly the base of AWMP) based on geomorphic and topographic analysis of different parts of the Argyre basin – the extent of the lake would link to distinct dendritic valley systems, broad valley systems, and local basins that occur among the basin rim materials, as well as the Uzboi drainage system (Fig. 9—left). If the hypothesized Argyre lake reached an elevation of 1.0 km, then it would have an estimated volume of 3.1 million km^3. For comparison, this closely approximates the volume of the Mediterranean Sea, estimated to be 3.75 million km^3 (Fig. 9—right; also compare with the dark blue region of Fig. 1). Such a relatively high-standing water body makes sense when compared to other topographic basins outside of the Argyre basin, including the basin in the bottom-left part of Fig. 9 (compare left and right scenes with the latter highlighting a lake, marked as SWB, that would infill the basin), which displays drainages along its margin. But where did water come from to form such a large water body? One plausible explanation is that an impact event generated hydrogeologic conditions that would have resulted in the formation of the relatively large water body, such as the melting of surface and subsurface ice, migration of surface and subsurface water from great distances, and impact-induced precipitation.

A figure of merit regarding the impact-melting hypothesis can be obtained by considering some basic energy considerations. The estimated volume of water—3.05×10^6 km^3, would require about 1.0×10^{24} J of thermal energy to produce the water by melting ice, or a bit more if the ice was initially much colder than the freezing point. For an Argyre impact energy of around 6×10^{25} J (Williams and Greeley, 1994), only about 1.7% of the Argyre impactor's kinetic energy is needed to melt ice to make a sea the size of Argyre's. For comparison, Braslau (2012) found that 26% of a 6 km/s bolide impact's kinetic energy was transferred into heating of a granular target. The energy partitioning varies depending on details of the impact and target. Most partitioning relations require <10% of the Argyre impact's heat energy going into melting ice in order to generate the Mediterranean Sea-size quantity of liquid water. Thus, from an energy perspective melting the needed amount of melted ice is entirely plausible. Of course it would require the target to be extremely ice-rich, for example, an ice sheet or polar layered deposit or ice-rich permafrost extending kilometers deep. This calculation raises a possibility that Argyre's glacial and lacustrine history may have started immediately upon impact into an icy region. The geomorphology and crater counts

further require that renewed glacial and lake processes then continued afterward in much more recent times.

This geologic mapping investigation and geomorphic analysis of the Argyre province, therefore, ties the lake that formed shortly following the Argyre impact event with Uzboi Vallis and the northern plains, which includes a possible northern plains ocean, and thus pointing to an extensive hydrological system. The putative existence of a giant lake indicates that Mars was a highly water-enriched planet at the time of the ~3.93 Ga Argyre impact event, supported by the stratigraphy and accompanying crater statistics such as the relatively high-standing oldest basin unit (unit Nab1) (Table 3 and Figs. 3 and 6). Thus, we provide strong support for and add new details to the hypothesis of Parker and Gorsline (1991).

The source of water of the initial highest-standing lake is hypothesized to be from the Argyre impact event, an event which would have induced major environmental change in the Argyre province and surroundings, including the melting of ice, as well as the formation of a complex of basement faults, fractures, and joints, including deep-seated and shallow faults concentric and radial about the basin. These structures controlled the migration of water in the subsurface as conduits and surface as structurally-controlled valleys, focusing water migration to the basin from great distances (thousands of kilometers) from the impact site.

4.3.3. Geologically-recent surface modification

At HiRISE resolution (~25–50 cm/pixel), the terrain in parts of the Argyre province often appears mantled by material that exhibits a high albedo, is relatively smooth (although meter-sized boulders often overlie it), and varies in ground coverage from continuous to dissected to discontinuous. This type of terrain is ubiquitous at the middle to high latitudes in both hemispheres and commonly is referred to as the latitude-dependent mantle (*LDM*) (i.e., Mustard et al., 2001; Milliken et al., 2003; Morgenstern et al., 2007; Lefort et al., 2009, 2010; Madeleine et al., 2009; Zanetti et al., 2010; Mangold, 2011; Raack et al., 2012; Wilmes et al., 2012). The *LDM* is hypothesized to be water–ice rich and either comprised uniquely of ice–dust accumulated by air-fall deposition (i.e., Morgenstern et al., 2007; Levy et al., 2009, 2011; Lefort et al., 2009, 2010; Madeleine et al., 2009; Zanetti et al., 2010; Wilmes et al., 2012) or of ice–dust and loess that is transformed epigenetically into ground ice (Mustard et al., 2001; Soare et al., 2012b; Skinner et al., 2012). Based on age estimates derived from crater-retention rates, the *LDM* could have been emplaced during the very Late Amazonian Epoch, in response to changes of obliquity and eccentricity (i.e., Mustard et al., 2001; Milliken et al., 2003; Madeleine et al., 2009; Mangold, 2011; Wilmes et al., 2012).

Recent water-related modifications (Figs. 13 and 14) of the landscape putatively comprise three assemblage types: (1) glacial; (2) periglacial; and (3) crater-wall "wet-debris" flows. The glacial assemblages comprise landforms whose shape, size, and geological traits, i.e. terminal and recessional lobes, lateral and medial ridges, slope-side location, and esker-like lineations, would be indicative of glaciation were they collectively observed on Earth (i.e. Kargel and Strom, 1990, 1992; Baker, 2001; Baker et al., 2001; Kargel, 2004; Banks et al., 2008; El Maarry et al., 2013). See Kargel et al. (2014) for a thorough review of glaciation on Earth as viewed from space, with field validations.

Possible periglacial landforms include: multi-metre and non-sorted polygons with high and low-centers, formed by thermal-contraction cracking and possibly underlain at the margins by water ice; multi-metre and sorted polygons that are the work of freeze–thaw cycling and cryoturbation; and, decametre-scale mounds whose shape, height, occasional summit-depressions and slope-side location coincide with the traits of open-system pingos on Earth, i.e. perennial (water) ice-cored mounds formed by hydrostatic pressure (Seibert and Kargel, 2001; Kargel, 2004; Soare et al., 2014a,b, 2015; Banks et al., 2008; Raack et al., 2012). Lineaments, which we interpret to be faults and fractures, also are commonly observed at OSP locations (Fig. 15). Based on field investigation of pingos on Earth, Soare et al. (2014b) propose that the candidates could be the result of a glacially-driven hydraulic gradient (e.g., Liestol, 1975), a topographically-driven hydraulic gradient (e.g., Müller, 1959), and a tectonic hydraulic gradient (i.e., regional faults and structural-discontinuities which channel and concentrate groundwater, possibly deeply-seated water, to form a pingo (e.g.,

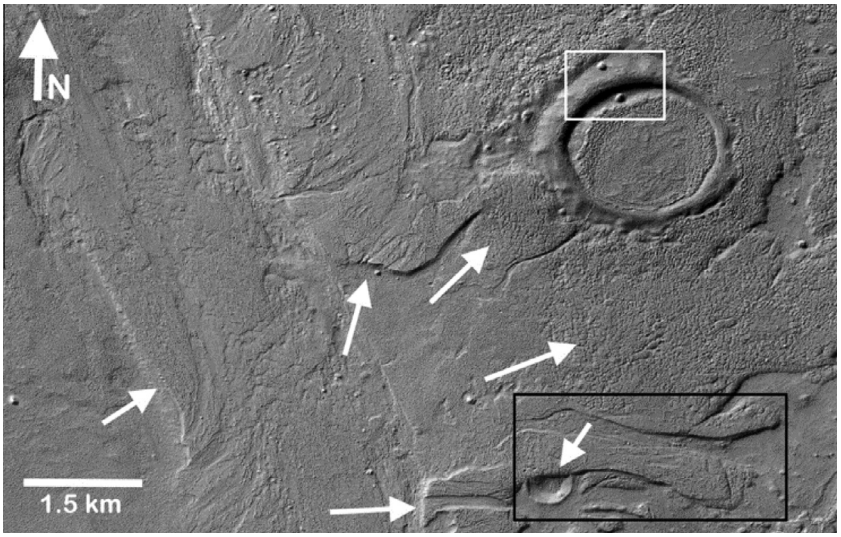

Fig. 13. Based on El Maarry et al. (2013), CTX image of the Moanda crater–valley system (MCVS) deposits (see location on geologic map of Fig. 3) showing several stages of environmental change and associated surface modification (white arrows point to multiple resurfacing events by varying processes, including possible glacial, alluvial, periglacial, fluvial, among others). Several small valleys dissect the MCVS deposits, which may have covered the whole region after their emplacement, as is evident from the deposits filling a 1.5-km-wide impact crater at the upper right of the view. Note the circular hills (white box) and flow materials partly covering the impact crater (black box) which may yet contain significant amounts of volatiles beneath a dry mantle (El Maarry et al., 2013). Part of image ID: P17_007745_1410_XN_39S040W.

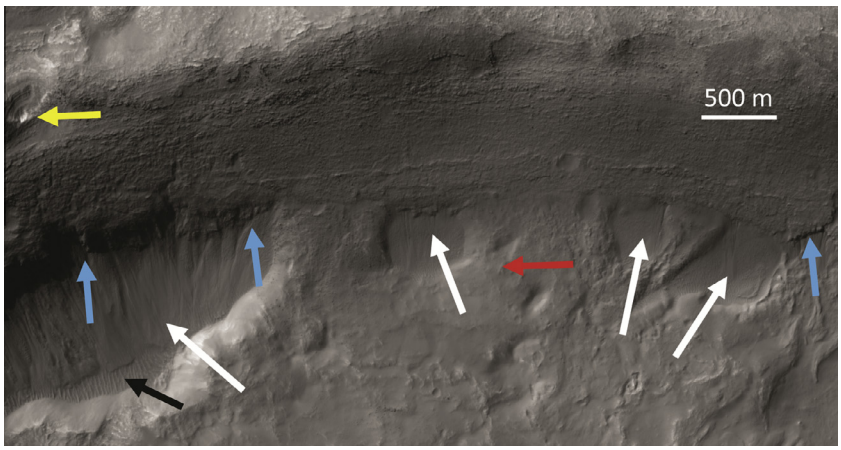

Fig. 14. The northern part of HiRISE image PSP_006888_1410 (see location on geologic map of Fig. 3) clearly shows gullies that source at a geologic contact (blue arrows), which separates the overlying layered deposits (yellow arrow) from more massive-appearing deposits (red arrow). The gullies occur within distinct topographic depressions (terrestrial thermokarst- or karst-like; white arrows) with associated debris aprons partly infilling the depressions, as well as partly burying dune deposits (black arrow). Groundwater and stratigraphic control appear influential on gully formation. (For interpretation of the references to color in this figure legend, the reader is referred to the web version of this article.)

Müller, 1959)). The third possibility could indicate flow along deep-seated basement structures associated with the ancient giant impact basin and possibly internal heat flow of Mars vented through the structural conduits.

Throughout the region gully-like landforms observed on crater-walls exhibit significant channel sinuosity, braiding and benches or levees. The depositional fans show multiple superpositions (Fig. 14) and often are incised by channels or channel segments (Soare et al., 2014a,b, 2015; Conway et al., 2015). On Earth, these traits would be markers of "wet-debris" flows.

4.4. Impact-induced tectonism and geophysical assessment

The Argyre impact event excavated a broad, deep basin and produced small and large extensional and compressional structures; these include structurally controlled fault scarps, broad ridges, valleys, and mountain ranges within several hundred kilometers of the basin margin which are generally oriented radially and concentric to the basin. Farther away, toward the Thaumasia plateau, more subtle basins and broad rises may in part have resulted from Argyre-related deformation (also compare with Craddock et al.

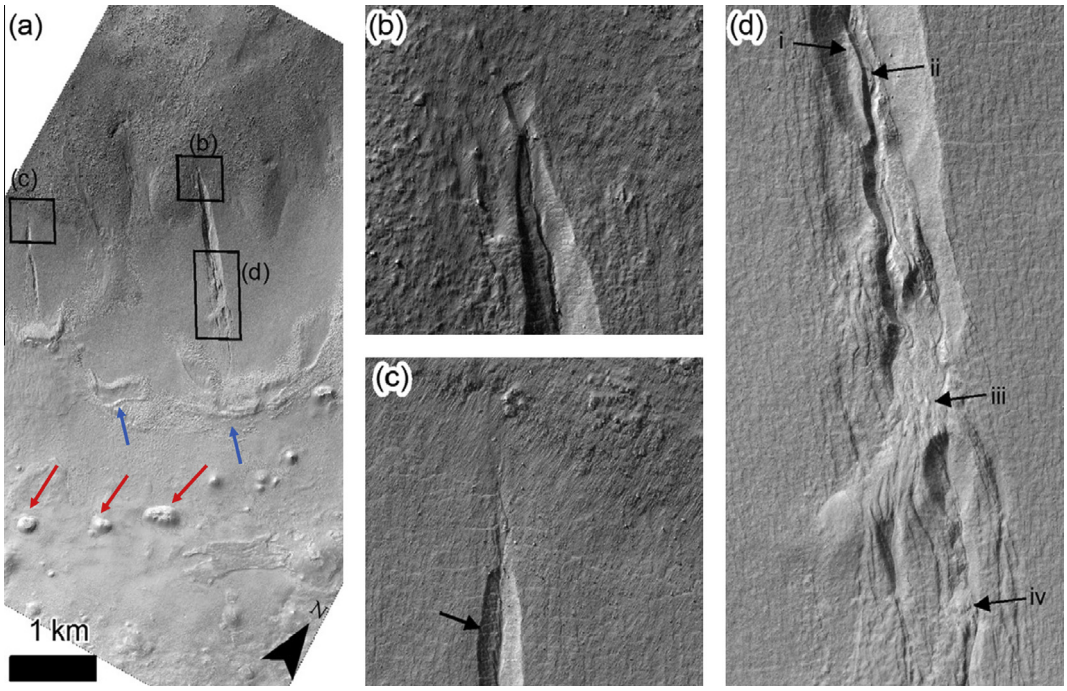

Fig. 15. Based on Soare et al. (2014b), gullies and graben-like cavities upslope of candidate open system pingos (OSP, red arrows), with arcuate ridges in between, interpreted to be moraines (blue arrows) (see location on geologic map of Fig. 3). HiRISE image ESP_020720_1410. (a) Overview of the site, showing the locations of insets (b–d) and the downslope position of the putative OSPs relative to the gullies and arcuate ridges. (b) Top of the alcove of the eastern gully, showing an abrupt start of the channel embedded in the graben-like elongated depression. A possible landslide scar is located at the northern tip of the cavity. (c) Top of the alcove of the western gully, with rill-like features running into the graben-like cavity; the features seem to originate upslope from the non-polygonised terrain. Note the polygonal network within the cavity and in the surrounding terrain; black arrow points to location with low-centered polygons. (d) Mid-part of the eastern gully, with multiple terraces (i and ii) and multiple self-blocking digitate deposits (iii and iv), as indicated by black arrows. Note the distinct lineaments, which we interpret to be fractures and faults, as well as a polygonal network within the cavity and in the surrounding terrain. Image credits: NASA/JPL/University of Arizona. (For interpretation of the references to color in this figure legend, the reader is referred to the web version of this article.)

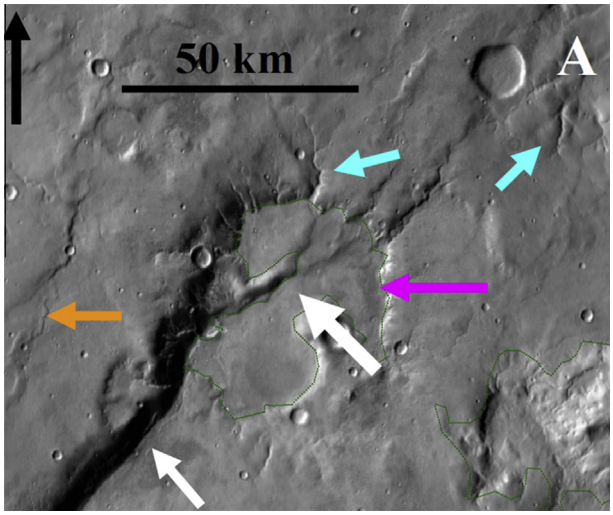

Fig. 16. THEMIS IR daytime images showing an Argyre impact-induced prominent fault (narrow white arrow) that splays out to the north–northeast (broad white arrow), deforming a drainage basin (violet arrow) (see location on geologic map of Fig. 3); this indicates post-Argyre-impact isostatic adjustment of basement structures. Also shown are drainages (blue arrows) and a wrinkle ridge (orange arrow), some of which appear to be controlled by underlying faults generated by the Argyre impact event. The structural feature is identified as a macrostructure (a structure reaching 100s of kilometers in length) on the geologic map, which locates roughly concentric about and to the northwest of the Argyre basin. Phyllosilicate has been identified in the basin through CRISM-based (Buczkowski et al., 2008a,b). (For interpretation of the references to color in this figure legend, the reader is referred to the web version of this article.)

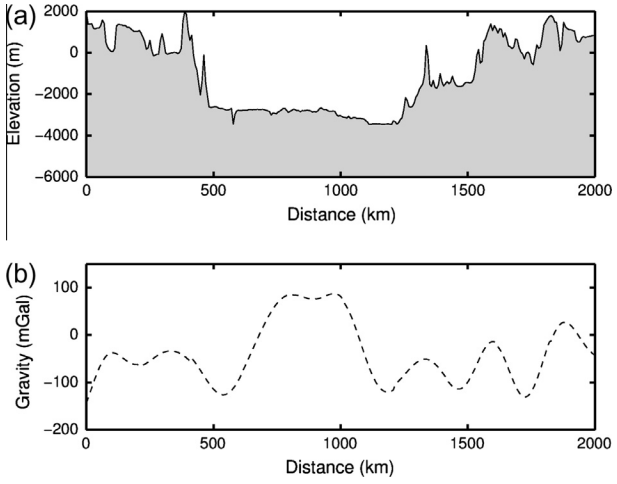

Fig. 18. (a) Topography and (b) free-air gravity anomaly profiles through the center of the Argyre basin.

(1990)). Some 2000 km away from the basin, the outline of the southeast margin of the Thaumasia plateau is roughly concentric with the Argyre basin, suggesting that the margin could be controlled by the impact-related crustal structure (Figs. 1 and 2) (e.g., Dohm et al., 2001a; Yin, 2012a).

Structurally-controlled local basins among the rim material and outside of the primary Argyre basin also resulted from the large impact event. These small exterior basins served as local catchments for water and sediments. Isostatic adjustments following the formation of the Argyre basin (Thomas and Masson, 1984; Wichman and Schultz, 1989; Dohm et al., 2001a) include normal faulting possibly related to the reactivation of some of the impact-induced older basement structures. An example is the deformation of a structurally-controlled basin and its sedimentary deposits (Fig. 16).

Argyre-induced basement structures have not only controlled major watersheds, but also have influenced the geometric patterns of some subsequent impact craters, i.e. the observed polygonal impact craters (Öhman et al., 2008). The simple polygonality of craters is formed early in the cratering process and is somewhat similar to the structure-controlled square planview shape of Meteor Crater, Arizona (Shoemaker, 1963; Quaide et al., 1965), whereas the complex craters' polygonal planview forms later in the cratering process (Öhman et al., 2008, and references therein). The Argyre impact-resulting structures are distinct in the MOLA map (Fig. 17a) and topographic profile (Fig. 18a), and their general signatures can be observed in the gravity map data as gravity highs and lows (Fig. 17b).

The interior of the Argyre basin, for example, is characterized by a positive free-air gravity anomaly (mascon) with a magnitude

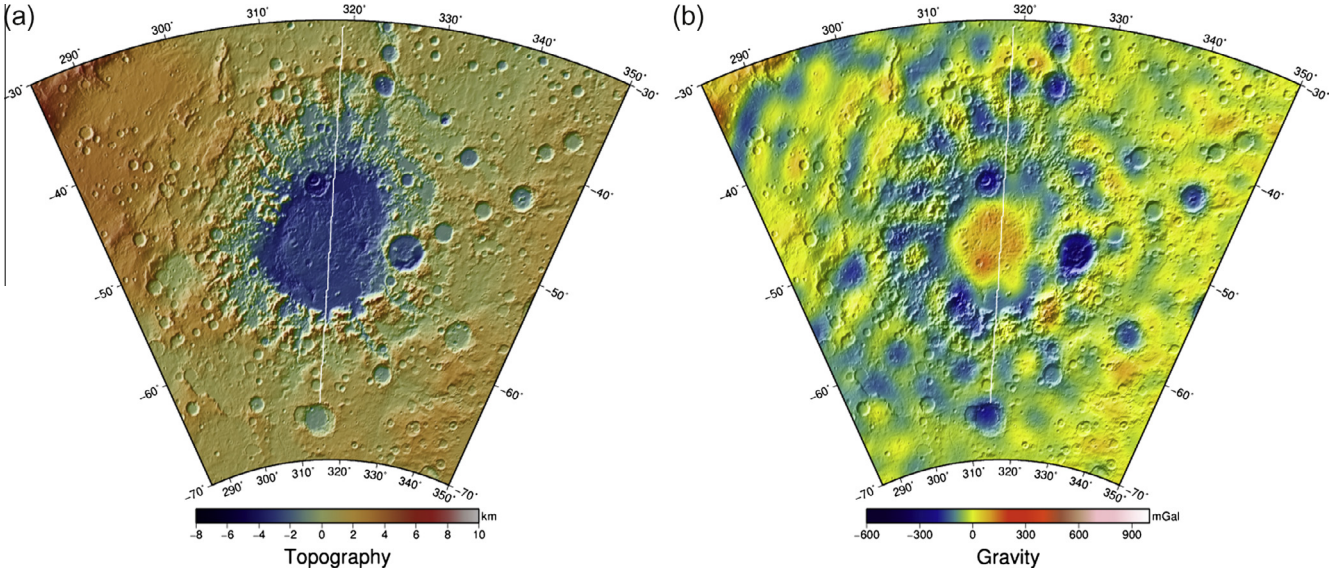

Fig. 17. (A) MOLA topography (B) and free-air gravity derived from the Mars gravity field MRO110B2 (Konopliv et al., 2011) of Argyre province. Lines show ground tracks of profiles in Fig. 18.

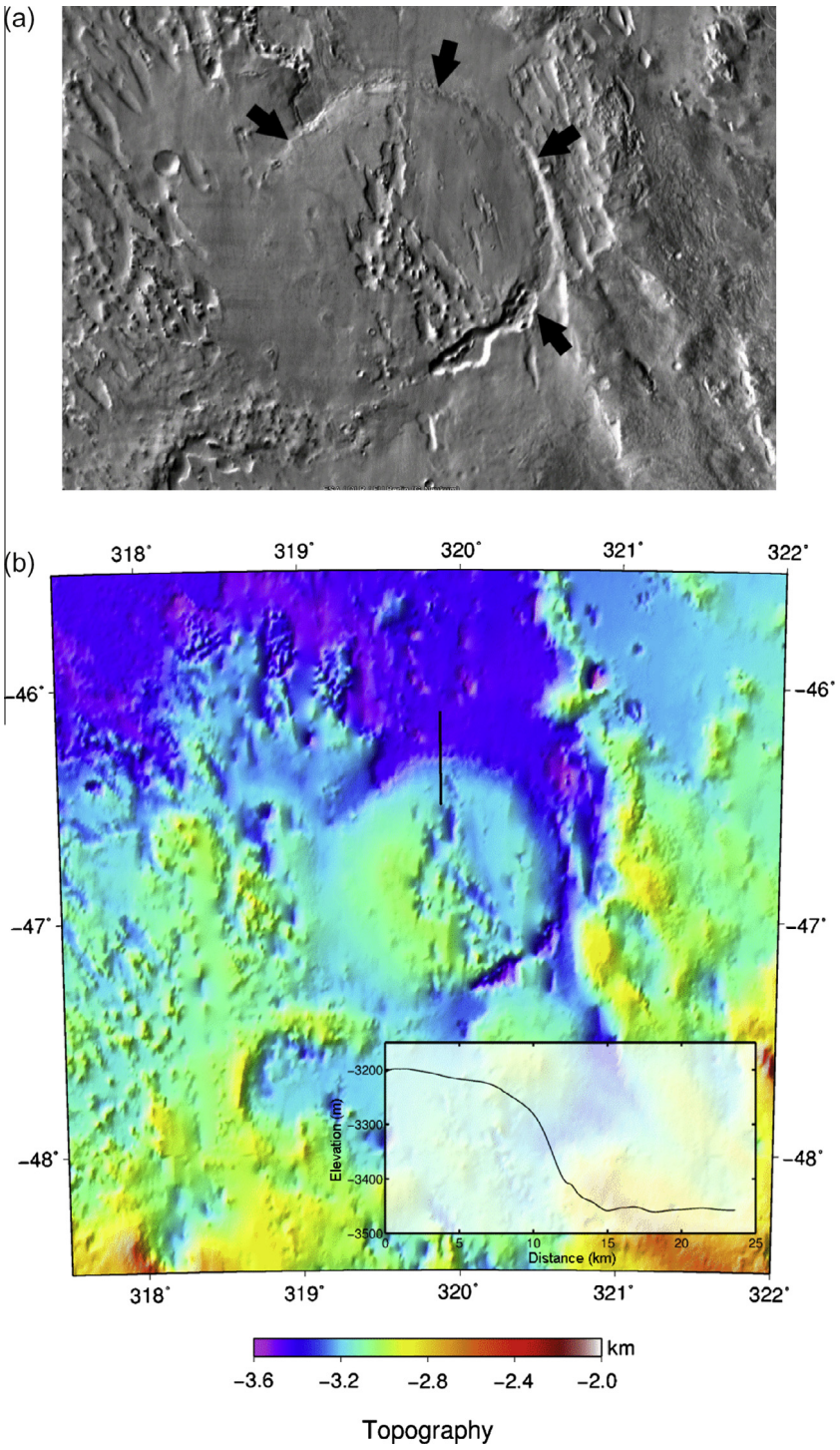

Fig. 19. (a) THEMIS daytime IR image of the floor of Argyre basin. The quasi-circular feature (black transect line highlighting the northern part) is interpreted to be a ~60 km diameter buried crater. (b) Topography of the putative buried impact structure. The northern edge appears to have been exhumed creating a nearly 300 m arcuate scarp seen in the inset profile (location shown with black line).

~140 mGal surrounded by an annulus of low gravity at the basin's inner periphery (Figs. 17b and 18b). This is observed for the Isidis basin and commonly observed for lunar impact basins (Muller and Sjogren, 1968; Konopliv et al., 2001; Matsumoto et al., 2010). Such mascons have been attributed to the super-isostatic uplift of the Moho beneath the basin (Neumann et al., 1996; Wieczorek and Phillips, 1999) and/or the infilling and partial burial of the basins by material, such as flood basalts and sediments, that are at least partially flexurally supported (Solomon and Head, 1980).

The floor deposits of the Argyre basin are comprised of sedimentary rocks that, depending on their thickness, porosity, and state of compensation, may contribute to the gravity anomaly if accumulation occurred without complete isostatic compensation. Based on the observed relation between crater depth to diameter for large crater basins (Howenstine and Kiefer, 2005), the inner basin diameter of Argyre, ~915 km, implies an unfilled basin depth of ~6 km. The actual basin depth of ~4 km suggests ~2 km of burial if flexure of the basin floor is minimal. Several quasi-circular

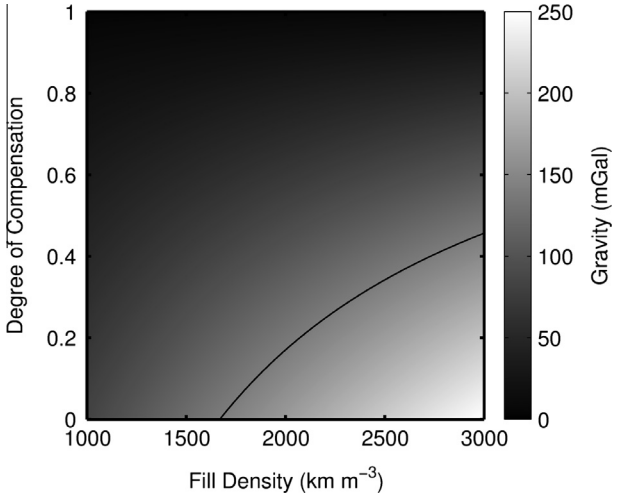

Fig. 20. The free-air gravity anomaly for a slab of material 2 km thick as a function of material density and degree of compensation. The 140 mGal contour (black curve), the approximate magnitude of the mascon within the basin interior, is shown for reference.

features are apparent on the interior floor of Argyre basin and are likely buried impact craters. The largest of these features has a diameter of ~60 km (Fig. 19). The crater depth to diameter power law fit to craters between 7 and 110 km in diameter (Garvin et al., 2002) yields a depth of ~2 km indicating at least 2 km of material filling this crater to its rim. Taking $h = 2$ km as the thickness of deposits in the basin, the magnitude of the resulting gravity anomaly is estimated assuming a simple slab model (Schubert and Turcotte, 2002):

$$\Delta g = 2\pi G\rho h[1 - C(r_p/(r_p + t_c))^2],$$

where G is the gravitational constant, ρ is the fill density, h is the thickness of deposits in the basin, r_p is the radius of Mars, t_c is the crust thickness assumed to be 50 km, and C is the degree of compensation which is zero for a completely rigid lithosphere and approaches unity for Airy isostasy. The resulting gravity anomaly is shown in Fig. 20. The ~140 mGal mascon within the basin can be explained by post-impact deposition alone if the compensation of the load is no greater than ~45%. A fill density <1670 kg m^{-3} results in a gravity anomaly <140 mGal for any compensation state suggesting this is an approximate lower bound on the fill density.

5. Conclusions

Detailed geologic investigation using Viking and post-Viking data has revealed the evolutional history of the Argyre province. This includes distinct basin units most likely marking a lake that formed as a result of the Argyre impact event, as well as subsequent perturbations in environmental conditions (climate, surface, and subsurface) associated with major stages of Tharsis superplume development among other lesser endogenic-driven activity such as Elysium rise. It has also revealed newly identified lake-containing basins, mapped the extent of Argyre-related tectonism and the influence of the giant impact on the surrounding regions, corroborated the esker hypothesis, with details on the timing of formation being the Late Hesperian, and highlighted ancient, geologically-recent, and possibly present-day surface modification. Examples of geologically-recent landforms and possible present-day activity include polygonal-patterned ground, gullies, open-system pingos, and flow-like features of the valley-fill materials, including glacier-like landforms. Possible contributors to the water enrichment and remobilization of water and sediment in Argyre in geologic recent time could include local precipitation related to atmospheric cycling of water vapor such as from the south pole into the deep basin and an intrabasinal water cycle including fog.

A hypothesized generalized summary of the geologic evolution of the Argyre province based on this geologic investigation includes: (1) the Argyre impact event and related formation of the Argyre basin, rim materials, ejecta blanket, basement structures (faults and structurally-controlled valleys, basins, and mesas) radial and concentric about the basin, and lake and associated sedimentation (marked by unit Nab1) with connecting Uzboi Vallis, (2) waning and eventually frozen Argyre lake with associated glaciers extending away from the lake, (3) mantling of basin and rim materials including the ice bodies due primarily to wind- and gravity-driven processes, (4) Stages 1–3 Tharsis-driven activity and associated transient hydrological cycling and major environmental change and landscape modification in and surrounding the Argyre basin, including melt and associated flooding and spring activity, gelifluction, and alluvial, colluvial, lacustrine, glacial, and periglacial activity (recorded by units Nab2, Nab3, Nab4b), (5) Stage 4 Tharsis-driven activity and related hydrological cycling and major environmental change and landscape modification, including lake formation and associated sedimentation (marked by unit HAb4a), though much less in extent when compared to the Argyre-impact-related lake that sourced Uzboi Vallis, and subsequent freezing and esker development distinct in the southeast part of the Argyre basin, as well as the development of glaciers such as those that were directed through Surius Vallis, Dzigai Vallis, and Nia Vallis and that linked to the basin environment, (6) impact events such as Lowell, Galle, and Hale contributed to environment change and surface modification, and (7) ice enrichment of the rock materials of the Argyre province, environmental changes related to changes in orbital parameters (spin axis and orbital eccentricity) and endogenic activity such as in the Tharsis/Elysium corridor region, relatively steep slopes, and Agryre-impact-induced structures as conduits for the transferal of heat and volatiles also has contributed to surface modification in geologic recent times. This history points to Argyre as a prime target for the search for life on Mars.

Acknowledgments

J.M. Dohm was supported by the National Aeronautics and Space Administration (NASA) Planetary Geology & Geophysics Program. Professors Dohm and Miyamoto express their gratitude to the Tokyo Dome Corporation for their support of the TeNQ exhibit and the branch of Space Exploration Education & Discovery, the University Museum, the University of Tokyo. Work by A.G. Fairén was supported by the European Research Council under the European Union's Seventh Framework Programme (FP7/2007-2013), ERC Grant agreement No. 307496. We are grateful for the thoughtful reviews by T. Öhman and an anonymous reviewer which ultimately resulted in an improved manuscript.

References

Abramov, O., Kring, D.A., 2005. Impact-induced hydrothermal activity on early Mars. J. Geophys. Res. 110, E12S09. http://dx.doi.org/10.1029/2005JE002453.
Acuña, M.H. et al., 1999. Global distribution of crustal magnetization discovered by the Mars Global Surveyor MAG/ER experiment. Science 284, 790–793.
Acuña, M.H. et al., 2001. Magnetic field of Mars: Summary of results from the aerobraking and mapping orbits. J. Geophys. Res. 106, 23403–23417.
Alvarez, L.W. et al., 1980. Extraterrestrial cause for the Cretaceous–Tertiary extinction. Science 208, 1095–1108.
Anderson, R.C. et al., 2001. Significant centers of tectonic activity through time for the western hemisphere of Mars. J. Geophys. Res. 106, 20563–20585.
Anguita, F. et al., 2001. Tharsis dome, Mars: New evidence for Noachian–Hesperian thick-skin and Amazonian thin-skin tectonics. J. Geophys. Res. 106, 7577–7589.
Archinal, B.A. et al., 2002. A MOLA-controlled RAND-USGS control network for Mars. Lunar Planet. Sci. XXXIII. Abstract #1632.

Archinal, B.A. et al., 2003. Mars Digital Image Model (MDIM) 2.1 control network. ISPRS Working Group IV/9 Workshop "Advances in Planetary Mapping 2003", Houston, March 2003.
Arkani-Hamed, J., 2003. Thermoremanent magnetization of the martian lithosphere. J. Geophys. Res. 108. http://dx.doi.org/10.1029/2003JE002049.
Arkani-Hamed, J., 2004. Timing of the martian core dynamo. J. Geophys. Res. 109. http://dx.doi.org/10.1029/2003JE002195.
Baker, V.R., 2001. Water and the martian land-scape. Nature 412, 228–236.
Baker, V.R. et al., 1991. Ancient oceans, ice sheets and the hydrological cycle on Mars. Nature 352, 589–594.
Baker, V.R. et al., 2000. Mars' Oceanus Borealis, ancient glaciers, and the MEGAOUTFLO hypothesis. Lunar Planet. Sci. XXXI. Abstract 1863.
Baker, V.R., Maruyama, S., Dohm, J.M., 2001. Tharsis superplume (3): Implications on the role of water, environmental change and life. Geol. Soc. Am. Abstr. Progr. 33 (7). Abstract A432.
Baker, V.R., Maruyama, S., Dohm, J.M., 2002. A theory of plate tectonics and subsequent long-term superplume activity on Mars. International Workshop: Role of Superplumes in the Earth System, Electronic Geosciences, pp. 312–316.
Baker, V.R., Maruyama, S., Dohm, J.M., 2007. Tharsis superplume and the geological evolution of early Mars. In: Yuen, D.A., Maruyama, S., Karato, S.-I., Windley, B.F. (Eds.), Superplumes: Beyond Plate Tectonics. Springer, pp. 507–523.
Banks, M.E. et al., 2008. High Resolution Imaging Science Experiment (HiRISE) observations of glacial and periglacial morphologies in the circum-Argyre Planitia highlands. J. Geophys. Res. 113, E12015. http://dx.doi.org/10.1029/2007JE002994.
Banks, M.E. et al., 2009. An analysis of the sinuous ridges in the southern Argyre Planitia, Mars using HiRISE and CTX images and MOLA data. J. Geophys. Res. 114, E09003. http://dx.doi.org/10.1029/2008JE003244.
Barlow, N.G., 1990. Constraints on early events in martian history as derived from the cratering record. J. Geophys. Res. 95, 14191–14201.
Barlow, N.G., 2004. Martian subsurface volatile concentrations as a function of time: Clues from layered ejecta craters. Geophys. Res. Lett., 31 http://dx.doi.org/10.1029/2003GL019075.
Barlow, N.G., 2005. A review of martian impact crater ejecta structures and their implications for target properties. In: Kenkmann, T., Hörz, F., Deutsch, A. (Eds.), Large Meteorite Impacts III. Geological Society of America Special Paper 384, pp. 433–442.
Bibring, J.-P. et al., 2004. OMEGA: Observatiore pour la Minéralogie, l'Eau, les Glaces et l'Activité. In: Wilson, A. (Ed.), Mars Express: The Scientific Payload. ESA, Noordwijk, Netherlands, pp. 37–49.
Bibring, J.-P. et al., 2005. Mars surface diversity as revealed by the OMEGA/Mars Express observations. Science 307 (5715), 1576–1581.
Braslau, D., 2012. Partitioning of energy in hypervelocity impact against loose sand targets. J. Geophys. Res.: Atmos. 75 (2), 3987–3999.
Buczkowski, D.L. et al., 2008a. CRISM analyses of Argyre basin. Lunar Planet. Sci. XXXIX. Abstract 1030.
Buczkowski, D.L. et al., 2008b. Mineralogic and morphologic signatures of Noachian water in the Argyre impact basin. EOS Trans., American Geophysical Union (Fall).
Buczkowski, D.L. et al., 2010. Investigation of an Argyre basin ring structure using Mars Reconnaissance Orbiter/Compact Reconnaissance Imaging Spectrometer for Mars. J. Geophys. Res. 115, E12011. http://dx.doi.org/10.1029/2009JE003508.
Christensen, P.R. et al., 2004. The Thermal Emission Imaging System (THEMIS) for the Mars 2001 Odyssey mission. Space Sci. Rev. 110, 85–130.
Condit, C.D., 1978. Geologic map of the Mare Australe area of Mars. US Geol. Survey Map Misc. Invest. Ser. Map I-1076, Scale 1:5,000,000.
Connerney, J.E.P. et al., 1999. The global magnetic field of Mars and implications for crustal evolution. Science 284, 790–793.
Connerney, J.E.P. et al., 2001. The global magnetic field of Mars and implications for crustal evolution. Geophys. Res. Lett. 28, 4015–4018.
Connerney, J.E.P. et al., 2005. Tectonic implications of Mars crustal magnetism. Science 102, 14970–14975.
Conway, S.J., Soare, R.J., 2013. Gully morphometrics as indicators of degradation intensity around the Argyre basin. Lunar Planet. Sci. 44. Abstract #2488.
Conway, S.J., Balme, M.R., Soare, R.J., 2015. Using gullies to estimate the thickness of the latitude-dependent mantle. Lunar Planet. Sci. XXXXVI. Abstract #2964.
Costard, F. et al., 2002. Formation of recent martian debris flows by melting of near-surface ground ice at high obliquity. Science 295 (5552), 110–113. http://dx.doi.org/10.1126/science.1066698.
Craddock, R.A., Greeley, R., Christensen, P.R., 1990. Evidence of an ancient impact basin in Daedalia Planum, Mars. J. Geophys. Res. 95, 10729–10740.
Crater Analysis Techniques Working Group, 1979. Standard techniques for presentation and analysis of crater size–frequency data. Icarus 37, 467–474.
Crown, D.A., Price, K.H., Greeley, R., 1992. Geologic evolution of the east rim of the Hellas basin, Mars. Icarus 100, 1–25.
Davila, A.F. et al., 2011. A large sedimentary basin in the Terra Sirenum region of the southern highlands of Mars. Icarus 212, 579–589.
Davila, A.F. et al., 2013. Evidence for Hesperian glaciation along the martian dichotomy boundary. Geology 41, 755–758. http://dx.doi.org/10.1130/G34201.1.
Dohm, J.M., Maruyama, S., 2014a. New evidence for plate tectonism on Mars: Accreted terrains. Japan Geoscience Union Meeting, April 28–May 2, 2014, PPS02-02, #418.
Dohm, J.M., Maruyama, S., 2014b. Habitable trinity. J. Geosci. Front. http://dx.doi.org/10.1016/j.gsf.2014.01.005.
Dohm, J.M., Tanaka, K.L., 1999. Geology of the Thaumasia region, Mars: Plateau development, valley origins, and magmatic evolution. Planet. Space Sci. 47, 411–431.
Dohm, J.M. et al., 2000. Pulses of magmatic activity through time: Potential triggers for climatic variations on Mars. Lunar Planet. Sci. XXXI. Abstract #1632.
Dohm, J.M., Tanaka, K.L., Hare, T.M., 2001a. Geologic map of the Thaumasia region of Mars. US Geol. Survey Map I-2650.
Dohm, J.M. et al., 2001b. Ancient drainage basin of the Tharsis region, Mars: Potential source for outflow channel systems and putative oceans or paleolakes. J. Geophys. Res. 106, 32943–32958.
Dohm, J.M., Maruyama, S., Baker, V.R., 2001c. Mars plate tectonics: Surface geology and analyses of topographic and geophysical data. American Geophysical Union 82 (47), F713.
Dohm, J.M. et al., 2001d. Earth-like evolution of the Tharsis magmatic complex: Traits of a terrestrial superplume (2). Geol. Soc. Am. Abstr. Progr. 33 (7). Abstract A309.
Dohm, J.M. et al., 2002a. Plate tectonism on early Mars: Diverse geological and geophysical evidence. Lunar Planet. Sci. XXXIII. Abstract #1639.
Dohm, J.M. et al., 2002b. Evolution and traits of Tharsis superplume, Mars. Superplume International Workshop, Abstracts with Programs, Tokyo, pp. 406–410.
Dohm, J.M. et al., 2005. Mars geological province designations for the interpretation of GRS data. Lunar Planet. Sci. XXXVI. Abstract #1567.
Dohm, J.M. et al., 2007a. Traits and evolution of the Tharsis superplume, Mars. In: Yuen, D.A., Maruyama, S., Karato, S.-I., Windley, B.F. (Eds.), Superplumes: Beyond Plate Tectonics. Springer, pp. 523–537.
Dohm, J.M. et al., 2007b. Possible ancient giant basin and related water enrichment in the Arabia Terra province, Mars. Icarus 190, 74–92. http://dx.doi.org/10.1016/j.icarus.2007.03.006.
Dohm, J.M. et al., 2008. Recent geological and hydrological activity on Mars: The Tharsis/Elysium Corridor. Planet. Space Sci. 56, 985–1013.
Dohm, J.M. et al., 2009a. New evidence for a magmatic influence on the origin of Valles Marineris, Mars. J. Volcanol. Geotherm. Res. 185, 12–27. http://dx.doi.org/10.1016/j.jvolgeores.2008.11.029.
Dohm, J.M. et al., 2009b. GRS evidence and the possibility of ancient oceans on Mars. Planet. Space Sci. 57, 664–684.
Dohm, J.M. et al., 2011a. Did a large Argyre lake source the Uzboi Vallis drainage system?: Post-Viking-era geologic mapping investigation. Lunar Planet. Sci. XXXIII. Abstract #2255.
Dohm, J.M. et al., 2011b. An inventory of potentially habitable environments on Mars: Geological and biological perspectives. In: Garry, W.B., Bleacher, J.E. (Eds.), Analogs for Planetary Exploration. Geological Society of America Special Paper 483, pp. 317–347, http://dx.doi.org/10.1130/2011.2483(21).
Dohm, J.M. et al., 2013. Mars evolution. In: Fairén, A.G. (Ed.), Mars: Evolution, Geology, and Exploration. Nova Science Publishers Inc., pp. 1–33.
Dohm, J.M. et al., 2014a. Accretionary complexes: Recorders on Earth and possibly Mars. 2014 GSA Annual Meeting in Vancouver, British Columbia, Paper No. 25-9.
Dohm, J.M. et al., 2014b. Accretionary complexes: Recorders on Earth and possibly Mars. American Geophysical Union (Fall). Paper No. P33E-07.
El Maarry, M.R., Dohm, J.M., 2013. Regional morphologies of the smooth deposits in the mountainous regions of Argyre, Mars: Results from high resolution mapping. Lunar Planet. Sci. XXXXIV. Abstract #2806.
El Maarry, M.R. et al., 2013. Morphology and evolution of the ejecta of Hale crater in Argyre basin, Mars: Results from high resolution mapping. Icarus 226, 905–922.
Fairén, A.G., Dohm, J.M., 2004. Age and origin of the lowlands of Mars. Icarus 168, 277–284. http://dx.doi.org/10.1016/j.icarus.2003.11.025.
Fairén, A.G., Ruiz, J., Anguita, F., 2002. An origin for the linear magnetic anomalies on Mars through accretion of terranes: Implications for dynamo timing. Icarus 160, 220–223. http://dx.doi.org/10.1006/icar.2002.6942.
Fairén, A.G. et al., 2003. Episodic flood inundations of the northern plains of Mars. Icarus 165, 53–67. http://dx.doi.org/10.1016/S0019-1035(03)00144-1.
Fairén, A.G. et al., 2014. A cold hydrological system in Gale Crater, Mars. Planet. Space Sci. 93, 101–118.
Fastook, J.L. et al., 2008. Tropical mountain glaciers on Mars: Altitude-dependence of ice accumulation, accumulation conditions, formation times, glacier dynamics, and implications for planetary spin-axis/orbital history. Icarus 198, 305–317.
Ferris, J.C. et al., 2002. Dark slope streaks on Mars: Are aqueous processes involved? Geophys. Res. Lett. 29. http://dx.doi.org/10.1029/2002GL014936.
Fink, W. et al., 2005. Next-generation robotic planetary reconnaissance missions: A paradigm shift. Planet. Space Sci. 53, 1419–1426.
Fink, W. et al., 2007a. Tier-scalable reconnaissance missions for the autonomous exploration of planetary bodies. In: IEEE Aerospace Conference Proceedings, Paper #1199. http://dx.doi.org/10.1109/AERO.2007.352715.
Fink, W., George, T., Tarbell, M.A., 2007b. Tier-scalable reconnaissance: The challenge of sensor optimization, sensor deployment, sensor fusion, and sensor interoperability. Proc. SPIE 6556, 655611. http://dx.doi.org/10.1117/12.721486.
Fink, W., Tarbell, M.A., Jobling, F.M., 2008. Tier-scalable reconnaissance – A paradigm shift in autonomous remote planetary exploration of Mars and beyond. In: Costas, L.A. (Ed.), Planet Mars Research Focus. Nova Science Publishers, Hauppauge, NY, ISBN: 1-60021-826-1 (Chapter 1).
Frey, H.V. et al., 2002. Ancient lowlands on Mars. Geophys. Res. Lett. 29. http://dx.doi.org/10.1029/2001GL013832.

Garvin, J.B. et al., 2002. Global geometric properties of martian impact craters. Lunar Planet. Sci. XXXIII. Abstract 1255.
Glamoclija, M., Marinangeli, L., Komatsu, G., 2011. Harmakhis Vallis Source Region, Mars: Insights into the recent geothermal history based on geological mapping. Planet. Space Sci. 59, 1179–1194. http://dx.doi.org/10.1016/j.pss.2010.09.017.
Harrison, T.M., 2009. The Hadean crust: Evidence from >4 Ga zircons. Annu. Rev. Earth Planet. Sci. 37, 479–505.
Harrison, K.P., Grimm, R.E., 2009. Regionally compartmented groundwater flow on Mars. J. Geophys. Res. 114. http://dx.doi.org/10.1029/2008JE003300.
Hartmann, W.K., 2005. Martian cratering 8: Isochron refinement and the chronology of Mars. Icarus 174, 294–320.
Hartmann, W.K., Neukum, G., 2001. Cratering chronology and the evolution of Mars. Space Sci. Rev. 96, 165–194.
Head, J.W., Pratt, S., 2001. Extensive Hesperian-aged south polar ice sheet on Mars: Evidence for massive melting and retreat, and lateral flow and ponding of meltwater. J. Geophys. Res. 106, 12275–12299.
Head, J.W. et al., 2003. Recent ice ages on Mars. Nature 426, 797–802.
Hiesinger, H., Head, J.W., 2002. Topography and morphology of the Argyre basin, Mars: Implications for its geologic and hydrologic history. Planet. Space Sci. 50, 939–981.
Hodges, C.A., 1980. Geological map of the Argyre quadrangle of Mars. U.S. Geol. Sur. Misc. Inv. Series Map I-1181, Scale 1:500,000.
Howenstine, J.B., Kiefer, W.S., 2005. Morphometry of large martian impact craters. Lunar Planet. Sci. XXXVI. Abstract 1742.
Hynek, B.M., Beach, M., Hoke, R.T., 2010. Updated global map of martian valley networks and implications for climate and hydrologic processes. J. Geophys. Res. 115. http://dx.doi.org/10.1029/2009JE003548.
Irwin III, R.P., Tanaka, K.L., Robbins, S.J., 2013. Distribution of Early, Middle, and Late Noachian cratered surfaces in the martian highlands: Implications for resurfacing events and processes. J. Geophys. Res.: Planets 118, 278–291. http://dx.doi.org/10.1002/jgre.20053.
Ivanov, B.A., 2001. Mars/Moon cratering rate ratio estimates. Space Sci. Rev. 96, 87–104.
Jones, A.P. et al., 2011. A geomorphic analysis of Hale crater, Mars: The effects of impact into ice-rich crust. Icarus 211, 259–272.
Kargel, J.S., 2004. Mars: A Warmer Wetter Planet. Praxis-Springer, 557p.
Kargel, J.S., Strom, R.G., 1990. Ancient glaciation on Mars. Lunar Planet. Sci., 597–598
Kargel, J.S., Strom, R.G., 1992. Ancient glaciation on Mars. Geology 20, 3–7.
Kargel, J.S. et al., 1995. Evidence of ancient continental glaciation in the martian northern plains. J. Geophys. Res. 100, 5351–5368.
Kargel, J.S. et al. (Eds.), 2014. Global Land Ice Measurements from Space. Springer-Praxis, Heidelberg (e-book and hard-cover print publication, LXXIX, 876p., 409 illus., 336 illus. in color. With extra online material).
Kasting, J.F., Whitmire, D.P., Reynolds, R.T., 1993. Habitable zones around main sequence stars. Icarus 101, 108–128.
Komatsu, G. et al., 2011. Roles of methane and carbon dioxide in geological processes on Mars. Planet. Space Sci. 59, 169–181. http://dx.doi.org/10.1016/j.pss.2010.07.002.
Komatsu, G. et al., 2012. Small mounds in Chryse Planitia, Mars: Testing a mud volcano hypothesis. Lunar Planet. Sci. XXXXIII. Abstract #1103.
Konopliv, A.S. et al., 2001. Recent gravity models as a result of the lunar prospector mission. Icarus 150, 1–18.
Konopliv, A.S. et al., 2011. Mars high resolution gravity fields form MRO, Mars seasonal gravity, and other dynamical parameters. Icarus 211, 401–428.
Lane, M.D., Goodrich, C.A., 2010. High-magnesian olivine in the Argyre rim: Derived from a primitive magma? Lunar Planet. Sci. XLI. Abstract 2094.
Laskar, J. et al., 2004. Long term evolution and chaotic diffusion of the insolation quantities of Mars. Icarus 170, 343–364.
Lefort, A. et al., 2009. Observations of periglacial landforms in Utopia Planitia with the High Resolution Imaging Science Experiment (HiRISE). J. Geophys. Res. 114, E04005. http://dx.doi.org/10.1029/2008JE003264.
Lefort, A. et al., 2010. Scalloped terrain in the Peneus and Amphritrites Paterae region of Mars as observed by HiRISE. Icarus 205 (1), 259–268. http://dx.doi.org/10.1026/j.icarus.2009.06.005.
Leonard, G.J., Tanaka, K.L., 2001. Geologic map of the Hellas region of Mars. US Geol. Survey Map I-2694.
Levy, J., Head, J., Marchant, D., 2009. Thermal contraction crack polygons on Mars: Classification, distribution and climatic implications from HiRISE observations. J. Geophys. Res. 114, E01007. http://dx.doi.org/10.1029/2008JE003273.
Levy, J.S., Head, J.W., Marchant, D.R., 2011. Gullies, polygons and mantles in martian permafrost environments: Cold desert landforms and sedimentary processes during recent martian geological history. In: Martini, I.P., French, H.M., Perez Alberti, A. (Eds.), Ice Marginal and Periglacial Processes and Sediments. Geological Society of London 354, pp. 167–182, http://dx.doi.org/10.1144/SP35410 0305-8719.
Lias, J.H., Dohm, J.M., Tanaka, K.L., 1997. Geologic history of Lowell impact. Lunar Planet. Sci. XXVIII. Abstract #1650.
Liestol, O., 1975. Pingos, springs, and permafrost in Spitsbergen. Nor. Polar Årbook, 7–29.
Lillis, R.J. et al., 2008. An improved crustal magnetic field map of Mars from electron reflectometry: Highland volcano magnetic history and the end of the martian dynamo. Icarus 194, 575–596. http://dx.doi.org/10.1016/j.icarus.2007.09.032.
Madeleine, J.B. et al., 2009. Amazonian northern mid-latitude glaciation on Mars: A proposed climate scenario. Icarus 203, 390–405. http://dx.doi.org/10.1016/j.icarus.2009.04.037.
Mahaney, W.C. et al., 2001. Morphogenesis of Antarctic paleosols: Martian analog. Icarus 154, 113–130.
Mahaney, W.C. et al., 2009. Secondary Fe and Al in Antarctic paleosols: Correlation to Mars with prospect for the presence of life. Icarus 203, 320–330. http://dx.doi.org/10.1016/j.icarus.2009.05.007.
Mahaney, W.C. et al., 2011. Aluminum extracts in Antarctic paleosols: Proxy data for organic compounds and bacteria and implications for martian paleosols. Sediment. Geol. 237, 84–94.
Malin, M.C. et al., 2007. Context Camera investigation on board the Mars Reconnaissance Orbiter. J. Geophys. Res. 112. http://dx.doi.org/10.1029/2006JE002808.
Mangold, N., 2011. Ice sublimation as a geomorphic process: A planetary perspective. Geomorphology 126, 1–17. http://dx.doi.org/10.1016/2010.11.009.
Maruyama, S., 1997. Pacific-type orogeny revisited: Miyashiro-type orogeny proposed. The Island Arc 6, 91–120. http://dx.doi.org/10.1111/j.1440-1738.1997.tb00042.x.
Maruyama, S. et al., 1997. Paleogeographic maps of the Japanese Islands: Plate tectonic synthesis from 750 Ma to the present. The Island Arc 6, 121–142.
Maruyama, S., Dohm, J.M., Baker, V.R., 2001a. Mars plate tectonics (1): An Earth prospective. American Geophysical Union (Fall) 82(47), Suppl. Abstract P32C-0565.
Maruyama, S., Dohm, J.M., Baker, V.R., 2001b. Tharsis superplume (1): Why superplume? Geol. Soc. Am. Abstr. Progr. 33 (7). Abstract A310.
Maruyama, S., Baker, V.R., Dohm, J.M., 2008. Life and Land of Mars, 4.6 Billion Years. Koudansha, Tokyo, 256p. (in Japanese).
Maruyama, S. et al., 2013. The naked planet Earth: Most essential pre-requisite for the origin and evolution of life. Geosci. Front. 4, 141–165.
Maruyama, S. et al., 2014. Initiation of leaking Earth: An ultimate trigger of the Cambrian explosion. Gondwana Res. 25, 910–944.
Matsumoto, K. et al., 2010. An improved lunar gravity field model from SELENE and historical tracking data: Revealing the farside gravity features. J. Geophys. Res. 115 (E6), E06007.
McCauley, J.F., 1978. Geologic map of the Coprates quadrangle of Mars. US Geol. Survey Map Misc. Invest. Ser. Map I-897, Scale 1:5,000,000.
McEwen, A.S., Eliason, E.M., Bergstrom, J.W., 2007. Mars Reconnaissance Orbiter's High Resolution Imaging Science Experiment (HiRISE). J. Geophys. Res. 112. http://dx.doi.org/10.1029/2005JE002605.
McEwen, A.S. et al., 2013. Recurring slope lineae (RSL) in equatorial Mars. European Planetary Science Congress 2013. Abstract #846.
McGill, G.E., 1978. Geologic map of the Thaumasia quadrangle of Mars. US Geol. Survey Misc. Invest. Ser. Map I-1077, Scale 1:5,000,000.
McGill, G.E., 1989. Buried topography of Utopia, Mars: Persistence of a giant impact depression. J. Geophys. Res. 94, 2753–2759.
Mest, S.C., Crown, D.A., 2001. Geology of the Reull Vallis region, Mars. Icarus 153, 89–110.
Milliken, R.E., Mustard, J.F., Goldsby, D.L., 2003. Viscous flow features on the surface of Mars: Observations from high-resolution Mars Orbiter Camera (MOC) images. J. Geophys. Res. 108 (E6), 5057. http://dx.doi.org/10.1029/2002JE002005.
Miyamoto, H. et al., 2004. Fluid dynamical implications of anastomosing slope streaks on Mars. J. Geophys. Res. 109, E06008. http://dx.doi.org/10.1029/2003JE002234.
Moore, J.M., Wilhelms, D.E., 2007. Geologic map of part of western Hellas Planitia, Mars. US Geol. Survey Map SIM-2953, 2007.
Morgenstern, A. et al., 2007. Deposition and degradation of a volatile-rich layer in Utopia Planitia, and implications for climate history on Mars. J. Geophys. Res. 112, E06010. http://dx.doi.org/10.1029/2006JE002869.
Müller, F., 1959. Beobachten über pingos (Observations on pingos). Medd. Grønl. 153 (3), 127 (Reprinted as Technical Translation 1073 by National Research Council of Canada, Ottawa, Canada, 1963).
Muller, P.M., Sjogren, W.L., 1968. Mascons: Lunar mass concentrations. Science 161, 680–684.
Murchie, S. et al., 2007. CRISM (Compact Reconnaissance Imaging Spectrometer for Mars) on MRO (Mars Reconnaissance Orbiter). J. Geophys. Res. 112, 1–57.
Murchie, S.L. et al., 2009a. A synthesis of martian aqueous mineralogy after one Mars year of observations from the Mars Reconnaissance Orbiter. J. Geophys. Res. 114, E00D06. http://dx.doi.org/10.1029/2009JE003342.
Murchie, S.L. et al., 2009b. The Compact Reconnaissance Imaging Spectrometer for Mars investigation and data set from the Mars Reconnaissance Orbiter's primary science phase. J. Geophys. Res. 114, E00D07. http://dx.doi.org/10.1029/2009JE003344.
Mustard, J.F., Cooper, C.D., Rifkin, M.R., 2001. Evidence for recent climate change on Mars from the identification of youthful near-surface ground ice. Nature 412, 411–414. http://dx.doi.org/10.1038/35086515.
Mustard, J. et al., 2008. Hydrated silicate minerals on Mars observed by the CRISM instrument on MRO. Nature 454, 305–309.
Nahm, A.L., Schultz, R.A., 2011. Magnitude of global contraction of Mars from analysis of surface faults: Implications for martian thermal history. Icarus 211, 389–400.
Neukum, G., Ivanov, B.A., Hartmann, W.K., 2001. Cratering records in the inner Solar System in relation to the lunar reference system. In: Kallenbach, R., Geiss, J., Hartmann, W.K. (Eds.), Chronology and Evolution of Mars. Kluwer Academic Publishers, pp. 55–86.
Neumann, G.A. et al., 1996. The lunar crust: Global structure and signature of major basins. J. Geophys. Res. 101, 16841–16863.

Neumann, G.A., Smith, D.E., Zuber, M.T., 2003. Two Mars years of clouds detected by the Mars Orbiter Laser Altimeter. J. Geophys. Res.: Planets 108, 5023. http://dx.doi.org/10.1029/2002JE001849.
Ody, A. et al., 2012. Global maps of anhydrous minerals at the surface of Mars from OMEGA/MEx. J. Geophys. Res. 117, E00J14. http://dx.doi.org/10.1029/2012JE004117.
Oehler, D.Z., Allen, C.C., 2010. Evidence for pervasive mud volcanism in Acidalia Planitia, Mars. Icarus 208, 636–657. http://dx.doi.org/10.1016/j.icarus.2010.03.031.
Öhman, T. et al., 2008. Polygonal impact craters in Argyre region, Mars: Implications for geology and cratering mechanics. Meteorit. Planet. Sci. 43, 1605–1628.
Parker, T.J., 1985. Geomorphology and Geology of the Southwestern Margaritifer Sinus – Northern Argyre Region of Mars. Master's Thesis, Geology Department, California State University, Los Angeles. 165pp.
Parker, T.J., 1989. Channels and valley networks associated with Argyre Planitia, Mars. Lunar Planet. Sci. XX, 826–827.
Parker, T.J., 1994. Martian Paleolakes and Oceans. Ph.D. Dissertation, Geological Sciences, University of Southern California. 200pp.
Parker, T.J., 1996. Highlights from 1:500K geologic mapping of central and southern Argyre Planitia. Lunar Planet. Sci. XXVII, 1003–1004.
Parker, T.J., Gorsline, D.S., 1991. Where is the source for Uzboi Vallis, Mars? Lunar Planet. Sci. XXII, 1033–1034.
Parker, T.J., Gorsline, D.S., 1992. Preliminary geologic mapping of the MTM-55036 and -55043 quadrangles, southern Argyre Planitia, Mars (abs.). Lunar Planet. Sci. 23, 1031–1032.
Parker, T.J., Gorsline, D.S., 1993. Extent and timing of fluvial and lacustrine events in Argyre Planitia, Mars. American Geophysical Union (Spring). 1pp.
Parker, T.J., Clifford, S.M., Banerdt, W.B., 2000. Argyre Planitia and the Mars global hydrologic cycle. Lunar Planet. Sci. 31. Abstract 2033.
Platz, T., Michael, G.G., 2011. Eruption history of the Elysium Volcanic Province, Mars. Earth Planet. Sci. Lett. 312, 140–151. http://dx.doi.org/10.1016/j.epsl.2011.10.001.
Platz, T. et al., 2013. Crater-based dating of geological units on Mars: Methods and application for the new global geological map. Icarus 225, 806–827. http://dx.doi.org/10.1016/j.icarus.2013.04.021.
Poulet, F. et al., 2005. Phyllosilicates on Mars and implications for early martian climate. Nature 438, 623–627.
Poulet, F. et al., 2007. Martian surface mineralogy from Observatoire pour la Minéralogie, l'Eau, les Glaces et l'Activité on board the Mars Express spacecraft (OMEGA/MEx): Global mineral maps. J. Geophys. Res. 112, E08S02. http://dx.doi.org/10.1029/2006JE002840.
Quaide, W.L., Gault, D.E., Schmidt, R.A., 1965. Gravitative effects on lunar impact structures. Ann. N.Y. Acad. Sci. 123, 641–655.
Raack, J., Reiss, D., Heisinger, H., 2012. Gullies and their relationship to the dust–ice mantle in the northwestern Argyre basin, Mars. Icarus 219, 129–141. http://dx.doi.org/10.1016/j.icarus.2012. 02.0125.
Robbins, S.J., Hynek, B.M., 2012. A new global database of Mars impact craters ⩾1 km: 1. Database creation, properties, and parameters. J. Geophys. Res. 117. http://dx.doi.org/10.1029/2011JE003966.
Robbins, S.J. et al., 2013. Large impact crater histories of Mars: The effect of different model crater age techniques. Icarus 225, 173–184. http://dx.doi.org/10.1016/j.icarus.2013.03.019.
Roberts, J.H., Arkani-Hamed, J., 2012. Impact-induced mantle dynamics on Mars. Icarus 218, 278–289.
Roberts, J.H., Lillis, R.J., Manga, M., 2009. Giant impacts on early Mars and the cessation of the martian dynamo. J. Geophys. Res. 114, E04009. http://dx.doi.org/10.1029/2008JE003287.
Rodriguez, J.A.P. et al., 2011. Secondary chaotic terrain formation in higher outflow channels of southern circum-Chryse, Mars. Icarus 213, 150–194.
Rodriguez, J.A.P. et al., 2014. Evidence for Middle Amazonian catastrophic flooding and glaciation on Mars. Icarus 242, 202–210.
Rossi, A.P. et al., 2011. Evolution of periglacial landforms in Thaumasia highland, Mars. In: Balme, M.R., Bargery, A.S., Gallagher, C.J., Gupta, S. (Eds.), Geomorphology on Mars and Other Planets. Geological Society, London, Special Publications 356, pp. 69–85.
Rotto, S.L., Tanaka, K.L., 1995. Geologic/geomorphologic map of the Chryse Planitia region of Mars. US Geol. Survey Map I-2441 (1:5,000,000).
Ruiz, J., 2014. The early heat loss evolution of Mars and their implications for internal and environmental history. Sci. Rep. 4. http://dx.doi.org/10.1038/srep04338.
Saunders, R.S., 1979. Geologic map of the Margaritifer Sinus quadrangle of Mars. US Geol. Survey Map Misc. Invest. Ser. Map I-1144, Scale 1:5,000,000.
Schubert, G., Turcotte, D.L., 2002. Geodynamics. Cambridge University Press.
Schubert, G. et al., 1992. Origin and thermal evolution of Mars. In: Mars. University of Arizona Press, Tucson, pp. 147–183.
Schultz, R.A., Tanaka, K.L., 1994. Lithospheric-scale buckling and thrust structures on Mars: The Coprates rise and south Tharsis ridge belt. J. Geophys. Res. 99, 8371–8385.
Schulze-Makuch, D. et al., 2012. The biological oxidant and life detection (BOLD) mission: A proposal for a mission to Mars. Planet. Space Sci. 67, 57–69.
Scott, D.H., Carr, M.H., 1978. Geologic map of Mars. US Geol. Survey Map I-1083.
Scott, D.H. et al., 1986–1987. Geologic maps of the western and eastern equatorial and polar regions of Mars. US Geol. Survey Map Misc. Inv. Ser. Map I-1802-A, B, C.
Segura, T.L. et al., 2002. Environmental effects of large impacts on Mars. Science 298, 1977–1980.
Seibert, N.M., Kargel, J.S., 2001. Small-scale martian polygonal terrain: Implications for liquid surface water. Geophys. Res. Lett. 28, 899–903.
Shoemaker, E.M., 1963. Impact mechanics at Meteor crater, Arizona. In: Middlehurst, B.M., Kuiper, G.P. (Eds.), The Moon, Meteorites, and Comets. University of Chicago Press, Chicago, pp. 301–336.
Shreve, R.L., 1985. Esker characteristics in terms of glacier physics, Katahdin esker system, Maine. Geol. Soc. Am. Bull. 96, 639–646.
Skinner, J.A., Mazzini, A., 2009. Martian mud volcanism: Terrestrial analogs and implications for formational scenarios. Mar. Petrol. Geol. 26, 1866–1878.
Skinner, J.A., Tanaka, K.L., 2007. Evidence for and implications of sedimentary diapirism and mud volcanism in the southern Utopia highland-lowland boundary plain, Mars. Icarus 186, 41–59.
Skinner Jr., J.A., Tanaka, K.L., Platz, T., 2012. Widespread loess-like deposit in the martian northern lowlands identifies Middle Amazonian climate change. Geology 40, 1127–1130. http://dx.doi.org/10.1130/G33513.1.
Sleep, N.H., 1994. Martian plate tectonics. J. Geophys. Res. 99, 5639–5655.
Smith, D.E. et al., 1999. The global topography of Mars and implications for surface evolution. Science 284, 1495–1503.
Soare, R.J., Conway, S.J., Dohm, J.M., 2012a. Evidence of landscape modification in and around the Argyre impact basin, Mars, by "wet" periglacial processes. 2012 GSA Annual Meeting and Exposition, Charlotte, North Carolina, 44, 7, 64.
Soare, R.J. et al., 2012b. Climate-change and the origin of ice-rich permafrost in mid Utopia Planitia, Mars. Mars Recent Climate Change Workshop, Ames Research Center, Moffett Field, California.
Soare, R.J. et al., 2014a. Possible ice-wedge polygons and recent landscape modification by "wet" periglacial processes in and around the Argyre impact basin, Mars. Icarus 233, 214–228.
Soare, R.J. et al., 2014b. Possible open-system (hydraulic) pingos in and around the Argyre impact regions of Mars. Earth Planet. Lett. 398, 25–36.
Soare, R.J. et al., 2015. Pre- and post-glacial periglaciation in Argyre Planitia, Mars. Lunar Planet. Sci. XXXXVI. Abstract #1218.
Solomon, S., Head, J.W., 1980. Lunar mascon basins: Lava filling, tectonics, and evolution of the lithosphere. Rev. Geophys. Space Phys. 18, 107–141.
Spagnuolo, M.G., Dohm, J.M., 2004. Triggering the end of plate tectonics by forced climate changes. Workshop on Martian Hemispheres, Lunar Planetary Institute. Abstract #4001.
Tanaka, K.L., 1986. The stratigraphy of Mars. J. Geophys. Res. 91 (Suppl.), E139–E158 (Proc. Lunar Planet. Sci. Conf. 17th, Part 1).
Tanaka, K.L. et al., 1988. The resurfacing history of Mars: A synthesis of digitized, Viking-based geology. Proc. Lunar Sci. Conf. 18, 665–678.
Tanaka, K.L., Skinner, J.A., Hare, T.M., 2005. Geologic map of the northern plains of Mars. USGS Misc. Scientific Investigations. Map 2888, Scale 1:15,000,000.
Tanaka, K.L. et al., 2014. Geologic map of Mars. US Geol. Survey Map Scientific Investigations Map 3292.
Thomas, G., Masson, H., 1984. Geology and tectonics of the Argyre area on Mars: Comparisons with other basins in the Solar System. Earth Moon Planets 31, 25–42.
Touma, J., Wisdom, J., 1993. The chaotic obliquity of Mars. Science 259, 1294–1296.
Werner, S.C., Tanaka, K.L., 2011. Redefinition of the crater-density and absolute-age boundaries for the chronostratigraphic system of Mars. Icarus 215, 603–607.
Wichman, R.W., Schultz, P.H., 1989. Sequence and mechanisms of deformation around the Hellas and Isidis impact basins on Mars. J. Geophys. Res. 94, 17333–17357.
Wieczorek, M.A., Phillips, R.J., 1999. Lunar multiring basins and the cratering process. Icarus 139, 246–259.
Wilhelms, D.E., 1987. The geologic history of the Moon. US Geol. Survey Prof. Pap. 1348.
Williams, D.A., Greeley, R., 1994. Assessment of antipodal-impact terrains on Mars. Icarus 110, 196–202.
Williams, J.-P. et al., 2014. A large vent structure within Argyre basin, Mars. Lunar Plant. Sci. XXXXV. Abstract 2807.
Wilmes, M. et al., 2012. Surface age of the ice–dust mantle deposit in Malea Planum, Mars. Planet. Space Sci. 60, 199–206. http://dx.doi.org/10.1016/j.pss.2011.08.006.
Yin, A., 2012a. An episodic slab-rollback model for the origin of the Tharsis rise on Mars: Implications for initiation of local plate subduction and final unification of kinematically linked global plate-tectonic network on Earth. Lithosphere 4, 553–593. http://dx.doi.org/10.1130/L195.1.
Yin, A., 2012b. Structural analysis of the Valles Marineris fault zone: Possible evidence for large-scale strike-slip faulting on Mars. Lithosphere. http://dx.doi.org/10.1130/L192.
Zanetti, M. et al., 2010. Distribution and evolution of scalloped terrain in the southern hemisphere, Mars. Icarus 206, 691–706. http://dx.doi.org/10.1016/j.icarus.2009.09.010.